DEVELOPMENT OF CHLOROPHYLL-A AND TOTAL SUSPENDED SOLIDS ALGORITHMS FOR MONITORING WATER QUALITY IN THE INANDA DAM, KWA-ZULU NATAL, USING REMOTELY SENSED LANDSAT 8 AND SENTINEL 2 IMAGERY

By

Vadhini Moodley

A dissertation submitted in fulfilment of the academic requirements for the Master of Science degree in the School of Agricultural, Earth and Environmental Sciences, at the University of KwaZulu-Natal.

Durban

South Africa

July 2023

ABSTRACT

Freshwater is a crucial resource necessary for the survival of all life on earth. Globally, freshwater resources only comprise two percent of all available water on the planet, however it is utilized in various ways that include agriculture, industries, socio-economic development, domestic purposes, drinking water, recreational purposes, and energy production. On a much larger scale, inland water bodies also aid in climate regulation, carbon cycling, habitat provision for various organisms and ensure the maintenance and balance of ecosystems. Despite the many uses and services provided by these freshwater systems, they have been negatively affected by anthropogenic activities and climate change, leading to the deterioration of their quality. It has therefore become imperative to monitor these inland water bodies to ensure the sustainability of these resources for current and future generations. Traditionally, water quality monitoring is done by collecting in-situ water samples which are then analysed in a laboratory. This method, while extremely accurate, is time-consuming, labour-intensive, expensive, and does not capture the variations of water quality parameters in a water body. Recent advancements in the field of remote sensing have now made it possible to monitor water quality remotely using satellite imagery. The launch of Landsat 8 and Sentinel 2, with improved specifications compared to prior satellites, makes it possible to retrieve water quality parameters remotely via the use of algorithms. There are many water quality parameters measured to determine the quality of an inland water body, however chlorophyll-a (chl-a) and total suspended solids (TSS) are among the most retrieved parameters using remote sensing methods. This is due to their ability to influence the spectral signature of water and their importance in determining the quality of a water body. This study attempted to develop algorithms to monitor chl-a and TSS in the Inanda Dam, KwaZulu-Natal using Landsat 8 and Sentinel 2 imagery. In-situ water samples were collected from the Inanda Dam and the corresponding Landsat 8 and Sentinel 2 satellite imagery were downloaded. The water samples were analysed to determine chl-a and TSS concentrations and the satellite imageries were pre-processed to obtain radiance and reflectance values. The radiance and reflectance values for individual bands and band combinations were correlated with in-situ chl-a and TSS using a Pearson correlation to determine which band/band ratios can be used to retrieve chl-a and TSS. The band/band ratios which obtained a correlation of 0.8 and more were then used to develop the algorithms to retieve the water quality parameters. The results indicate that Landsat 8 B1 to B5 radiance and reflectance, either individually or as part of a band ratio, obtained high correlations with in-situ chl-a, and the band/band ratios of Landsat 8 B1 to B5 radiance and B1 to B7 reflectance correlated with in-situ TSS. Successful correlations were found between in-situ chl-a and Sentinel 2 B1, B3, B4, B5, B6 and B10 TOA reflectance and B1 to B5 BOA reflectance band/band combinations, and in-situ TSS correlated well with band/band combinations of Sentinel 2 B1, B3 to B8a and B10 TOA reflectance and B1 to B5, B7, B11, B12 BOA reflectance. Algorithms were then developed using SPSS with all band/band combinations which obtained a correlation of 0.8 and higher with in-situ chl-a and TSS, however the most accurate algorithms, after validation, were those developed with highest correlated band/band combinations. The Landsat 8 B4:B2 radiance algorithm and B4:B1 reflectance algorithm obtained R^2-values of 0.869 and 0.842, and the Sentinel 2 B3 TOA reflectance algorithm and B1 BOA reflectance algorithm achieved R^2-values of 0.828 and 0.816 respectively when retrieving chl-a remotely. In terms of TSS estimation from satellite imagery, the Landsat 8 B1 radiance and reflectance algorithms acquired R^2-values of 0.955 and 0.966 respectively, and the Sentinel 2 B1:B3 TOA reflectance and B1 BOA reflectance algorithms obtained R^2-values of 0.790 and 0.902. These algorithms were then used to produce surface distribution maps of chl-a and TSS for the Inanda Dam. The Landsat 8 B4:B2 radiance algorithm most accurately mapped chl-a distributions and the Landsat 8 B1 radiance algorithm mapped TSS distributions with a high level of accuracy, however all algorithms were found capable of chl-a and TSS retrieval from Landsat 8 and Sentinel 2 imagery. While the empirical algorithms developed in this study proved viable in the estimation of chl-a and TSS from Landsat 8 and Sentinel 2 imagery for the Inanda Dam, it must be noted that the algorithms are time and site specific. Therefore, more research must be conducted in the field of remote water quality

monitoring across South Africa to develop algorithms independent of location and time that can be used to aid in water quality monitoring.

Keywords: remote sensing, water quality monitoring, Landsat 8, Sentinel 2, chlorophyll-a, total suspended solids, algorithm development

PREFACE

The work described in this dissertation was carried out in the School of Agricultural, Earth and Environmental Sciences, University of KwaZulu-Natal, Durban, from January 2018 to July 2023, under the supervision of Dr. Silas Njoya Ngetar.

This study represents original work by the author and has not otherwise been submitted in any form for any degree or diploma to any tertiary institution. Where use has been made of the work of others, it is duly acknowledged in the text.

Vadhini Moodley Signed[redacted] Date: 10/07/2023

As the candidate's supervisor I have approved this dissertation for submission.

Dr. Njoya S. Ngetar Signed: ______ [redacted] _______ Date: 10/07/2023

DECLARATION 1 - PLAGIARISM

I, Vadhini Moodley, declare that:

1. The research reported in this dissertation, except where otherwise indicated, is my original research.

2. This dissertation has not been submitted for any degree or examination at any other university.

3. This dissertation does not contain other persons' data, pictures, graphs, or other information, unless specifically acknowledged as being sourced from other persons.

4. This dissertation does not contain other persons' writing, unless specifically acknowledged as being sourced from other researchers. Where other written sources have been quoted, then:

   a. Their words have been re-written, but the general information attributed to them has been referenced.

   b. Where their exact words have been used, then their writing has been placed in italics and inside quotation marks and referenced.

5. This dissertation does not contain text, graphics or tables copied and pasted from the Internet, unless specifically acknowledged, and the source being detailed in the dissertation and in the References sections.

Signed: [redacted]...........

DECLARATION 2 - PUBLICATIONS AND MANUSCRIPTS

1. **Chapter 2 is based on**: Moodley, V. and Ngetar, N.S. (Submitted for publication). The use of Landsat 8, Sentinel 2, and related algorithms in monitoring inland water quality. A review. **(Submitted to** *Earth Science Informatics)*

2. **Chapter 3 is based on**: Moodley, V. and Ngetar, N.S. (Submitted for publication). Chlorophyll-a and total suspended solids algorithms for monitoring water quality in the Inanda Dam, Kwa-Zulu Natal, using remotely sensed Landsat 8 and Sentinel 2 imagery. **(Submitted to the** *Journal of Spatial Science)*

Signed: [redacted]

ACKNOWLEDGEMENTS

The completion and submission of this dissertation would not have been possible without the assistance of various personnel and organizations. I would like to sincerely thank the following people and organizations for their contribution to this research, without which this study would not have been possible.

To my supervisor, Dr Silas Ngetar Njoya, there is so much to thank you for that it is near impossible to note your various contributions in a paragraph. You have guided and assisted me through the entire research process, helping me to secure funding, travelling to Pietermaritzburg and Johannesburg for meetings and to acquire equipment for data collection, accompanying me to the Inanda Dam to collect water samples, and ensuring I stayed motivated for the duration of my research. I thank you for being unbelievably patient with me, and continuously reading through the various drafts of my journal articles and reports until they were of an academic standard. The skills I have acquired through your supervision and mentorship, both academic and professional, are innumerable and I humbly thank you for everything you have done for me and taught me during this journey.

I would like to express my gratitude to my family, who have made countless sacrifices to ensure I can achieve such a milestone in my life. To my mother, Linda Moodley, who would transport me to Howard campus daily, to my father, Asogan Moodley, who took the time to transport me to Inanda Dam and Talbot and Talbot laboratories, and to my sister, Yakshapriya Moodley, for her continual support and motivation throughout my research, I would like to thank you. You have all assisted me with logistical arrangements, sample collection, emotional support and were pillars of strength during this study.

A huge thank you to my extended family and my friends for all the support and encouragement they have given me. To Charity Cele, I thank you for taking time out of your schedule to assist me with data collection and to my colleagues at Howard College, I thank you for all the help you have given me over the years.

This research would not have been possible without the finance provided by the Water Research Commission of South Africa. Thank you to Dr. E Ubomba-Jaswa for providing the funding for this study and for organizing the reference group who provided suggestions and feedback on a continual basis which assisted in shaping my research.

I would like to thank Mr Viktor Hlope of Inanda Dam for granting me permission to collect water samples and the members of the Inanda Dam for always accommodating my many requests.

Special thanks must be given to the National Aeronautics and Space Administration United States Geological Survey for making Landsat 8 satellite imagery freely available and the European Space Agency for making Sentinel 2 satellite data and SNAP software freely available, all of which were utilized in this study.

Gratitude must be given to Brice Gijsbertsen for the provision of access to ENVI software and the assistance provided in the installation of the software.

I would also like to thank the University of Kwa-Zulu Natal, in particular Howard College, for providing me with the facilities and software needed to complete this study and the fee remission granted for the first year of study. I would also like to thank Susan Sheriff for always assisting with administrative affairs whenever needed.

If I have left out any person or organizations erroneously, I humbly ask for your forgiveness and I thank you for the assistance and motivation you have shown me throughout my research journey.

TABLE OF CONTENTS

LIST OF FIGURES

LIST OF TABLES

CHAPTER 1

GENERAL INTRODUCTION

1.1. Water quality monitoring

Inland water bodies, often consisting of lakes, dams, and reservoirs, are vital for the survival of all organisms on Earth. These waters are important for aquatic life, provision of ecosystem services, recreational activities, climate regulation, economic and sustainable development, and are a source of drinking water globally (Soomets et al., 2020; Bonansea et al., 2019a; Lee et al., 2016; Lim and Choi, 2015; Hu et al., 2021). Despite their importance, anthropogenic factors such as urbanization, industrialization, sewage, climate change, eutrophication, together with natural factors have led to the deterioration of inland waters worldwide (Prasad, Saluja and Garg, 2020; Guo et al., 2021; Lim and Choi, 2015; Ouma, Noor and Hebert, 2020; Hu et al., 2021). It is therefore imperative to continuously monitor these water sources to ensure effective water resource management (Bonansea et al., 2019a). Traditional water quality monitoring methods include the collection and analysis of in-situ water samples, which while accurate, are expensive, time-consuming, labour-intensive, and often unable to capture the variations of water quality parameters over a water body (Guo et al., 2021; Prasad, Saluja and Garg, 2020; Lim and Choi, 2015). Remote sensing, with its ability to cover entire water bodies and assess spatial and temporal variations in a more economic, quick, and effective manner, positions itself as a complementary and alternative tool that can be used to monitor water quality (Guo et al., 2021; Lim and Choi, 2015; Bonansea et al., 2019a; Zhang, Huang and Wang, 2020). Multiple studies have explored the use of remote sensing to monitor water quality, however, previously launched satellites had low spatial, temporal, and radiometric resolutions, making it difficult to retrieve water quality parameters from small water bodies (Li et al., 2021; Grendaitė et al., 2018; Guo et al., 2021). Recent advancements such as the launch of Landsat 8 and Sentinel 2, with its improved specifications and free data dissemination have made it possible to monitor the water quality of small inland water bodies (Li et al., 2021; Peterson, Sagan and Sloan, 2020).

1.2. Landsat 8 and Sentinel 2

Previously, remote water quality monitoring was done for large water bodies or oceanic waters, as satellites such as MERIS and MODIS were designed for ocean applications and the poor spatial resolution and signal-to-noise ratio (SNR) made it difficult to monitor smaller water bodies (Chen et al., 2017a; Malahlela et al., 2018; Li et al., 2021; Guo et al., 2021; Fadel, Faour and Slim, 2016; Hu et al., 2021). The launch of Landsat 8 and Sentinel 2, with their improved specifications, now makes monitoring smaller water bodies a possibility. Landsat 8 was launched on the 11th of February 2013 and the Sentinel 2 constellation, made up of Sentinel 2A and Sentinel 2B, was launched on the 23rd of June 2015 and the 7th of March 2017 respectively (Bonansea et al., 2019a). Landsat 8 consists of eleven bands, eight of which are visible, near-infrared (NIR), or shortwave-infrared (SWIR) bands at a spatial resolution of 30 m, one panchromatic band at 15 m and two thermal infrared (TIR) bands with a spatial resolution of 100 m. Sentinel 2 is made up of 13 bands which have varying spatial resolutions of 10 m, 20 m, and 60 m across all the bands (Fadel, Faour and Slim, 2016; Lim and Choi, 2015; Toming et al., 2016; Vanhellemont and Ruddick, 2014). Landsat 8 and each Sentinel 2 satellite have a temporal resolution of 16 days and 10 days, respectively, however when all three satellites are used in tandem the revisit time decreases to two to three days (Toming et al., 2016; Ouma, Noor and Herbert, 2020). Both satellites have improved specifications, namely the 12-bit radiometric resolution which allows for better detection in changes on the Earth's surface, improved SNR allowing for water reflectance to be estimated and in turn water quality parameters, and an increased number of bands which provides users with more information and allows features to be seen more clearly (Fadel, Faour and

Slim, 2016; Ouma, Noor and Herbert, 2020; Vanhellemont and Ruddick, 2016; González-Márquez et al., 2018). The above-mentioned factors, coupled with the free dissemination of Landsat 8 and Sentinel 2 data, make both satellites a viable option for the monitoring of water quality in smaller water bodies.

1.3. Remote monitoring of water quality

Water quality parameters can be derived quantitatively from satellite imagery using algorithms. There are various algorithms that can be used to monitor water quality, such as analytical algorithms, semi-analytical algorithms and machine learning algorithms, however empirical methods are mostly used (Matthews, 2011; Ritchie, Zimba and Everitt, 2003; Gholizadeh, Melesse and Reddi, 2016). The empirical method, which is easier to understand and implement, will be used in this study, and utilizes statistical relationships to relate spectral properties and water quality parameters (Ritchie, Zimba and Everitt, 2003). Studies which attempt to monitor water quality using remote sensing make use of some generic steps, namely pre-processing of satellite imagery, the correlation of bands/band ratios with in-situ water quality parameters and the development of algorithms (Matthews, 2011). Often, monitoring water quality with remote rensing mainly uses optically active water quality parameters, which are those parameters capable of influencing satellite signals (Markogianni et al., 2017). These water quality parameters include chlorophyll-a (chl-a), total suspended solids (TSS), coloured dissolved organic matter (CDOM), and secchi disk depth (SDD). This study will focus on the remote monitoring of chl-a and TSS in the Inanda Dam.

1.4. Chl-a and TSS

Chl-a and TSS are the most commonly monitored water quality parameters due to their ability to influence the spectral signature of water (Markogianni et al., 2017) and their importance in the management of freshwater resources (Elangovan and Murali, 2020; Manuel et al., 2020; Ciancia et al., 2020). Chl-a is a pigment found in phytoplankton species which can be used as an indicator of the trophic status of water bodies and is a marker of possible algal blooms and eutrophication, which makes it an important water quality parameter to monitor when determining the health of an inland water body (Markogianni et al., 2017; Soomets et al., 2020; Ledesma et al., 2019; Li et al., 2021, Matthews, 2011; Gurlin, Gitelson and Moses, 2011). The Inanda Dam, which is classified as an eutrophic water body, is known for having high chlorophyll levels which negatively impact the dam (Hart, 2011). An increased amount of chl-a can lead to biodiversity loss, increased cyanobacteria, the death of fish and turbid water conditions, making it a very important parameter to monitor in the Inanda Dam (Matthews and Bernard, 2015). TSS consists of organic and mineral suspended solids derived from many sources such as rivers, coasts, and catchment areas and comprises clay minerals, detritus, and living and dead phytoplankton (Soomets et al., 2020). TSS is often used as a proxy for pollutants entering a water body and increased amounts of TSS can cause algal blooms, affect dissolved oxygen levels, increase sediment discharge into a water body and increase turbidity (Ciancia et al., 2020; Peterson et al., 2018; Soomets et al., 2020; Yanti, Susilo and Wicaksono, 2016). The presence of too much sediment negatively affects the water quality, functionality, and storage capacity of dams (Jaiyeola, 2016). The Inanda Dam is impacted by upstream activities which release sediment-laden water that then flows into the dam and sand mining that occurs near the dam leading to an increase in the suspended sediment entering the dam, hence monitoring TSS in the Inanda Dam is vital in protecting and managing this water resource (Jaiyeola, 2016). The above-mentioned characteristics make it vital to monitor both parameters as they can be used to determine the quality of a water body.

1.5. Aim

The aim of this study was to develop algorithms for monitoring water quality in the Inanda Dam using Landsat 8 and Sentinel 2 satellite imagery.

1.6. Objectives

The objectives of this study were:

1. To develop algorithms for monitoring chl-a in the Inanda Dam using Landsat 8 and Sentinel 2 and produce maps showing the surface distribution of chl-a in the Inanda Dam.
2. To develop algorithms for monitoring TSS in the Inanda Dam using Landsat 8 and Sentinel 2 and produce maps showing the surface distribution of TSS in the Inanda Dam.

1.7. Study Area

The Inanda Dam (Figure 1.1), located in the Valley of a Thousand Hills, started operations in 1989, and forms part of the uMgeni catchment (Tinmouth, 2009; Jaiyeola, 2016). The dam is approximately 23 km in length, 50 m in depth, with a surface area of 1440 hectares (Jaiyeola, 2016). The temperature of this area ranges from 25˚C to 38˚C during summer and 9˚C to 19˚C during winter (Jaiyeola, 2016). Average rainfall ranges from from 800 mm to 1125mm, with most of the rain falling during the summer months (Jaiyeola, 2016; Tinmouth, 2009; Ngetar, 2002; Namugize, Jewitt and Graham, 2018). The dam is surrounded by hilly, undulating landscapes in which rural communities practice agriculture (Nkoana, 2014; Rangeti, 2014) and is a vital source of drinking water for the surrounding communities and the people of Durban, South Africa (Fischer et al., 2019).

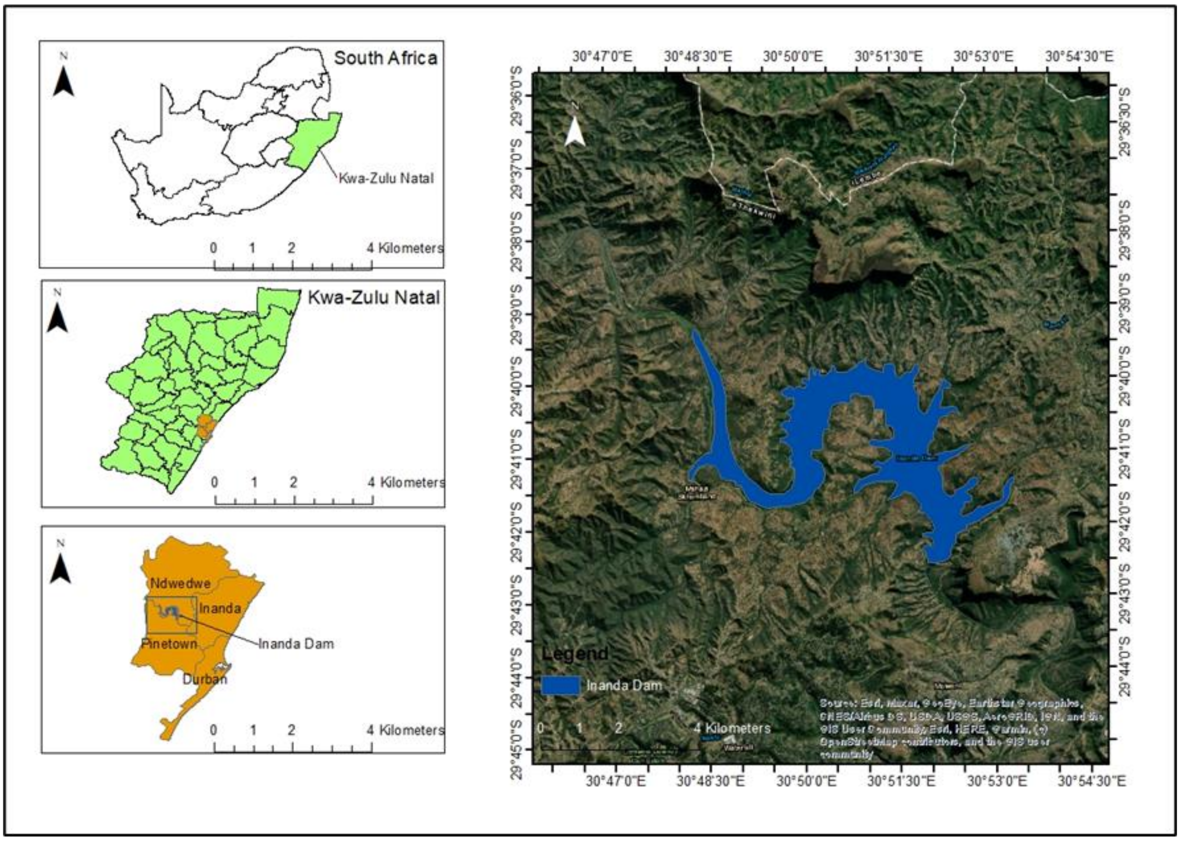

Figure 1.1: Map of Inanda Dam and its surrounding locations in Kwa-Zulu Natal Province, South Africa.

1.8. Dissertation Outline

This dissertation consists of four chapters, beginning with chapter one which is an introductory chapter and concluding with chapter four which consists of an overview of the findings and directions for future research. Chapters two and three are presented as journal articles which include a literature review, aim, objectives, methodology, results and discussion of this study. Chapters two and three have been written as journal articles and were submitted for publication to the Department of Higher Education and Training (DHET) accredited peer-reviewed journals. Even though chapters two and three have been written as individual manuscripts, which can be read independently, both chapters are linked to the aims and objectives of this study. It must, however, be noted, that there is some repetition and overlap between the chapters due to the chosen format of this dissertation. Listed below is an overview of each chapter.

Chapter 1 presents a general introduction to the research conducted, inclusive of aims, objectives and study area.

Chapter 2 is a literature review on the use of Landsat 8, Sentinel 2, and algorithms for monitoring various water quality parameters.

Chapter 3 explores the use of Landsat 8, Sentinel 2, and empirical algorithms for retrieving chl-a and TSS from the Inanda Dam using remote sensing.

Chapter 4 provides a synthesis of all the chapters, highlighting the key findings in relation to the aims and objectives of the dissertation, and the scholarly contributions of this research, while also providing recommendations for future studies.

CHAPTER 2

LITERATURE REVIEW

This chapter is based on Moodley, V. and Ngetar, N.S. The use of Landsat 8, Sentinel 2, and related algorithms in monitoring inland water quality. A review. (Submitted to *Earth Science Informatics*)

Abstract

Freshwater resources are currently threatened by numerous factors, including, negative impacts of climate change, land-use changes, nutrient enrichment, organic and inorganic pollution, acidification and brownification. Attempts to redress these threats using methods such as monitoring in-situ water quality, are expensive, time-consuming and do not often capture the spatio-temporal variations of the problem. Remote sensing is not only a cost and time-effective tool for assessing and monitoring water quality but also a tool for assessing the spatial distribution of water quality parameters in water bodies. The development of algorithms for extracting water quality parameters from satellite imagery has become a practice in the remote sensing community. Landsat 8 and Sentinel 2 are satellites that offer free data with spatial, radiometric, and temporal resolutions capable of monitoring small to large inland water bodies. Several studies have been conducted to determine the capabilities of Landsat 8 and Sentinel 2 imagery for monitoring water quality, considering their improved signal-to-noise ratio (SNR), 12-bit quantization, and increased bands. A literature review presented in this paper shows that despite existing challenges, Landsat 8 and Sentinel 2 could be successfully used to monitor water quality parameters such as chlorophyll-a (chl-a), total suspended solids (TSS), coloured dissolved organic matter (CDOM) and secchi disk depth (SDD) provided the imageries have undergone atmospheric corrections and are cloud-free. However, internationally, there is still a need for more research on the use of Landsat 8 and Sentinel 2 for monitoring other water quality parameters like total phosphorous (TP), total nitrogen (TN), dissolved organic carbon (DOC) and ammonia.

Keywords: water quality, Landsat 8, Sentinel 2, algorithm development

2.1. Introduction

Freshwater resources are vital to all life on Earth (Markogianni et al., 2017; Bonansea et al., 2019a; Lim and Choi, 2015; Pahlevan et al., 2019; Pu et al., 2019). Inland water bodies provide multiple services such as drinking water, recreational activities, tourism, habitats for biodiversity, climate regulation, carbon cycling and energy production (Pirasteh et al., 2020; Pahlevan et al., 2019; Markogianni et al., 2017; Li et al., 2017; Karaoui et al., 2019; Dörnhöfer et al., 2016). Despite the provision of these services by inland freshwater bodies, they have been negatively affected by human activities and climate change (Pu et al., 2019; Huangfu et al., 2020; Pahlevan et al., 2019), which in turn have deteriorated their quality (Markogianni et al., 2017; Li, Ding and Ilyas, 2021; Sharaf El Din, Zhang and Suliman, 2017). It is therefore imperative to monitor water bodies periodically and efficiently (Huangfu et al., 2020; Li, Ding and Ilyas, 2021) to determine their water quality status, which enables scientists, decision-makers, and governments to adopt strategies to deal with current water quality challenges and model future changes (Palmer, Kutser and Hunter, 2015; Markogianni et al., 2017; Sharaf El Din, Zhang and Suliman, 2017).

Water quality generally describes the physical, chemical, and biological properties of water (Ritchie, Zimba and Everitt, 2003; Mushtaq and Nee Lala, 2017), and is traditionally monitored using in-situ measurements and laboratory analysis. These methods are expensive, labour-intensive, time-consuming, inaccessible in certain areas, and does not allow for the identification of spatial-temporal variations in water quality, which is necessary for a comprehensive assessment of the water quality of an area (Gholizadeh, Melesse and Reddi, 2016; Mushtaq and Nee Lala., 2017; Dörnhöfer et al., 2016; Sòria-Perpinyà et al., 2021; Huangfu et al., 2020). Remote sensing presents itself as an alternative and complementary approach to in-situ water quality monitoring (Boucher et al., 2018). The advancements in satellite technology, together with the development of water quality algorithms, have made remote sensing a valuable tool for detecting water quality parameters over large surface areas in space and time (Buma and Lee, 2020; Boucher et al., 2018). The launch of Landsat 8 in 2013 (Loveland and Irons, 2016) and Sentinel 2A in 2015 and Sentinel 2B in 2017 (Toming et al., 2016) offer new opportunities for water quality monitoring, despite both satellites being designed for land applications (Ciancia et al., 2020).

This paper reviews the capabilities of Landsat 8 and Sentinel 2 and the development of algorithms for monitoring various water quality parameters, their strengths, and areas that require further research.

2.2. Landsat 8 and Sentinel 2 background and their capabilities in water quality monitoring

The use of satellites for monitoring water quality is not new; however, these satellites were predominantly designed for ocean applications, hence it was only possible to monitor large inland water bodies and not medium to small-sized inland water bodies due to the poor spatial resolution and low SNR of the satellites (Chen et al., 2017a; Malahlela et al., 2018; Li et al., 2021; Guo et al., 2021; Fadel, Faour and Slim, 2016; Hu et al., 2021). The launch of Landsat 8 and the Sentinel 2 constellation, with their improved specifications (improved signal-to-noise ratio (SNR), 12-bit radiometric resolution, and increased number of bands), has made it possible to monitor small to medium-sized water bodies (Fadel, Faour and Slim, 2016; Ouma, Noor and Herbert, 2020). Landsat 8 was launched on the 11th of February 2013, ensuring the continuation of the Landsat data record, which began in 1972 with Landsat 1 (Loveland and Irons, 2016). Sentinel 2 is a constellation made up of two satellites, Sentinel 2A, launched on the 23rd of June 2015, and Sentinel 2B, launched on the 7th of March 2017 (Ouma, Noor and Herbert, 2020). Landsat 8 has a spatial resolution of 30 m for eight bands in the visible, near-infrared (NIR) and shortwave-infrared (SWIR) sections of the electromagnetic spectrum (EMS), one panchromatic band at a spatial resolution of 15 m, and two thermal infrared (TIR) bands that have a spatial resolution of 100 m (Table 2.1). Sentinel 2 has spatial resolutions of 10 m, 20 m, and 60 m varying across 13 bands in the EMS's visible, NIR and SWIR sections (Table 2.2). Both satellite systems have a 12-bit radiometric resolution which allows for the retrieval of water quality parameters from small to medium water bodies, provided atmospheric correction has been applied (Loveland and Irons, 2016; Toming et al., 2016). The temporal resolution of Landsat 8 is 16 days, and each Sentinel 2 satellite has a temporal resolution of 10 days; however, when Sentinel 2A and Sentinel 2B are used in combination, the temporal resolution decreases to five days. Furthermore, when Landsat 8, Sentinel 2A and 2B are used in tandem, the temporal resolution decreases to two or three days (Toming et al., 2016; Ouma, Noor and Herbert, 2020), suggesting satellite imagery will be available every two to three days for a specific area to allow for continuous monitoring to take place. The coupling of these factors and the free dissemination of data from both satellite systems make them useful for water quality analysis (Vanhellemont and Ruddick, 2014), enabling the spatio-temporal variations of water quality to be monitored on a continuous surface compared to manual point-sampling methods (Kim, Ko and Nam, 2016).

Table 2.1: Landsat 8 bands and its characteristics (Fadel, Faour and Slim, 2016; Lim and Choi, 2015)

Sensor types	Band	Wavelengths (µm)	Resolution (m)
OLI (Operational Land Imager)	Band 1 (B1) – Coastal aerosol	0.43-0.45	30
	Band 2 (B2) – Blue	0.45-0.51	30

	Band 3 (B3) – Green	0.53-0.59	30
	Band 4 (B4) – Red	0.64-0.67	30
	Band 5 (B5) – NIR	0.85-0.88	30
	Band 6 (B6) – SWIR 1	1.57-1.65	30
	Band 7 (B7) - SWIR 2	2.11-2.29	30
	Band 8 (B8) – Panchromatic	0.50-0.68	15
	Band 9 (B9) – Cirrus	1.36-1.38	30
TIRS (Thermal-Infrared Sensor)	Band 10 (B10) – TIRS 1	10.60-11.19	100
	Band 11 (B11) – TIRS 2	11.50-12.51	100

Table 2.2: Sentinel 2 bands and its characteristics (Toming et al., 2016; Vanhellemont and Ruddick, 2014)

Band	**Central Wavelength (nm)**	**Bandwidth (nm)**	**Spatial Resolution (m)**
Band 1 (B1) – Coastal aerosol	443	20	60
Band 2 (B2) – Blue	490	65	10
Band 3 (B3) – Green	560	35	10
Band 4 (B4) – Red	665	30	10
Band 5 (B5) – Vegetation red edge	705	15	20
Band 6 (B6) – Vegetation red edge	740	15	20
Band 7 (B7) – Vegetation red edge	775	20	20
Band 8 (B8) – NIR	842	115	10
Band 8a (B8a) – Vegetation red edge	865	20	20
Band 9 (B9) – Water vapour	940	20	60
Band 10 (B10) – SWIR – Cirrus	1375	30	60
Band 11 (B11) – SWIR	1610	90	20
Band 12 (B12) – SWIR	2190	180	20

2.3. Satellite image pre-processing methods for retrieving water quality parameters

Satellite imagery used in water quality studies often undergo pre-processing in the form of atmospheric and radiometric corrections (Sharaf El Din, 2020; Elangovan and Murali, 2020; Malahlela et al., 2018; Laili et al., 2015; Patra et al., 2017; Chen et al., 2020b; Kim, Ko and Nam, 2016; Wu et al., 2015). Atmospheric corrections include the removal of gaseous and aerosols effects (Bonansea et al., 2019a; Buma and Lee, 2020; Chen et al., 2019; Keith et al., 2018). Radiometric corrections are performed to convert Digital Numbers (DN) to radiance or top of the atmosphere (TOA) reflectance, which is necessary as DN are unitless and must be converted into meaningful quantitative values, enabling information to be obtained from features (Humboldt State University, nd; Shippert, 2013).

2.3.1. Atmospheric corrections

Various atmospheric correction methods are used in water quality studies (Table 2.3); however, there is much disagreement as to which is the best (Molkov et al., 2019; Ansper and Alikas, 2018). A few studies have attempted to compare the accuracy of atmospheric correction models, and the results vary among the studies. For example, Ansper and Alikas (2018) tested ACOLITE, Sen2Cor, C2RCC and POLYMER on Sentinel 2 imagery and found C2RCC to be the most effective method for smaller lakes, while Molkov et al. (2019) found ACOLITE to be most accurate in representing reflectance spectra. Contrary to these two preceding studies Dörnhöfer et al. (2016) found MIP to be the most successful atmospheric correction method compared to Sen2Cor and ACOLITE.

Table 2.3: Atmospheric correction methods used on Landsat 8 and Sentinel 2 imagery.

Atmospheric correction method	Satellite used	Study
Second simulation of satellite signal in the solar spectrum (6S)	Landsat 8 / Sentinel 2	Zhang et al. (2016); Bonansea et al. (2019a); Bresciani et al. (2018); Cairo et al. (2020); Li et al. (2017); Chen et al. (2020b); Zhu et al. (2020); Li et al. (2018); Wang et al. (2021)
Second simulation of satellite signal in the solar spectrum-vector algorithm (6SV)	Landsat 8	Laili et al. (2015); Giardino et al. (2014); Ciancia et al. (2020)
ACOLITE	Landsat 8 / Sentinel 2	Lee et al. (2016); Ansper and Alikas (2018); Molkov et al. (2019); Ciancia et al. (2020); Wang et al. (2021); Pahlevan et al. (2020); Dörnhöfer et al. (2016)
Sen2Cor	Sentinel 2	Guo et al. (2021); Shang et al. (2021); Grendaitė et al. (2018); Peterson, Sagan and Sloan (2020); Chen et al. (2020a); Ansper and Alikas (2018); Bonansea et al. (2019b); Molkov et al. (2019); Huangfu et al. (2020); Li, Ding and Ilyas (2021); Al-Kharusi et al. (2020); Mansaray et al. (2021); Bande et al. (2018); Sòria-Perpinyà et al. (2020); Wang et al. (2021); Kutser et al. (2016b); Toming et al. (2016); Dörnhöfer et al. (2016)
Dark Object Subtraction (DOS)	Landsat 8	Markogianni et al. (2017); Yanti, Susilo and Wicaksono (2016); Boucher et al. (2018); Sharaf El Din, Zhang and Suliman (2017); Mushtaq and

		Nee Lala (2017); Masocha, Mungenge and Nhiwatiwa (2018); El Din and Zhang (2017); Pham et al. (2018); Yepez et al. (2018); El-Zeiny and El-Kafrawy (2017); González-Márquez et al. (2018)
Landsat-8 surface reflectance code (LaSRC)	Landsat 8	Chen et al. (2019); Prasad, Saluja and Garg (2020); Olmanson et al. (2020); Hu et al. (2021); Peterson, Sagan and Sloan (2020); Chen et al. (2020a); Mansaray et al. (2021); Pham et al. (2018); Yepez et al. (2018); Vinh et al. (2019); Pizani et al. (2020); Deutsch et al. (2021); He, Jin and Shang (2021); Wang et al. (2021)
Fast Line-of-Sight Atmospheric Analysis of Spectral Hypercubes (FLAASH)	Landsat 8 / Sentinel 2	Fadel, Faour and Slim (2016); Yadav et al. (2019); Pu et al. (2019); Chen et al. (2017a); Alcântara et al. (2016); Kurniadin and Jaelani (2016); Buma and Lee (2020); Larson et al. (2021); Kutser et al. (2016a); Ansari and Akhoondzadeh (2020); Pham et al. (2018); Yepez et al. (2018); Quang et al. (2017); Bande et al. (2018)
C2RCC	Sentinel 2	Soomets et al. (2020); Li et al. (2021); Ansper and Alikas (2018); Molkov et al. (2019)
Case-2 Extreme Cases (C2X)	Sentinel 2	Soomets et al. (2020)
Empirical Line Method (ELM)	Sentinel 2	Ha et al. (2017)
Modified Atmospheric Correction for Inland Waters (MAIN)	Landsat 8	Olmanson et al. (2020)
Quick Atmospheric Correction (QUAC)	Landsat 8 / Sentinel 2	Malahlela et al. (2018); Yang and Anderson (2016); Buma and Lee (2020); Kutser et al. (2016a)
Model-based empirical line method (MoB-ELM)	Landsat 8	Concha and Schott (2016)
Darkest Pixel (DP)	Landsat 8	Patra et al. (2017)
POLYMER	Sentinel 2	Ansper and Alikas (2018); Aptoula and Ariman (2021); Pahlevan et al. (2020)
iCOR	Sentinel 2	Molkov et al. (2019)
Atmospheric and Topographic Correction for Satellite Images (ATCOR23)	Landsat 8	Kutser et al. (2016a)
Geographic Resources	Landsat 8	Kutser et al. (2016a)

Analysis Support System (GRASS)		
SeaDAS	Landsat 8	Pham et al. (2018); Pahlevan et al. (2020)
MACCS ATCOR Joint Algorithm (MAJA)	Sentinel 2	Pizani et al. (2020)
MUMM	Landsat 8 / Sentinel 2	Wang et al. (2021)
ATCOR	Landsat 8	Kutser et al. (2016b)
MIP	Sentinel 2	Dörnhöfer et al. (2016)

Yepez et al. (2018) tested DOS, FLAASH and LaSRC on Landsat 8 imagery and found LaSRC to be the most suitable method for the study, however, they did indicate that more research should conducted to validate the accuracy of LaSRC in comparison to DOS and FLAASH for correcting atmospheric distortion of Landsat 8 imagery. On the contrary, Buma and Lee (2020) found FLAASH to be the most accurate in comparison to QUAC. Meanwhile, Wang et al. (2021) found MUMM to be the most accurate correction method in their study comparing 6S, ACOLITE, Sen2Cor, LaSRC, and MUMM.

In their own studies, Kuster et al. (2016a) compared FLAASH, QAC, GRASS and ATCOR23, while Pham et al. (2018) compared FLAASH, LaSRC, SeaDAS and DOS, and both studies found that none of the atmospheric correction methods worked well, elucidating the lack of agreement among authors as to which atmospheric correction method is best.

Table 2.3 reveals that 6S, Sen2Cor, DOS, LaSRC and FLAASH are the most popular atmospheric correction methods used in relation to monitoring water quality, with Sen2Cor used specifically for Sentinel 2 images and LaSRC for Landsat 8 images.

2.3.2. Radiometric corrections

Radiometric corrections are performed on Landsat 8 imagery, often using the metadata, by converting DN to surface reflectance (Sharaf El Din, 2020; Elangovan and Murali, 2020; Buma and Lee, 2020), TOA reflectance (Markogianni et al., 2017; Ouma, Noor and Herbert, 2020; Bonansea et al., 2019a) or radiance (Watanabe et al., 2015; Li et al., 2017; Li et al., 2018).

Sentinel 2 imagery are already radiometrically corrected and in TOA reflectance; therefore, no radiometric correction is required (Ha et al., 2017; Grendaitė et al., 2018; Shang et al., 2021).

2.4. Water quality algorithms

Water quality parameters can be derived quantitatively from satellite imagery using empirical methods, analytical models, semi-analytical models, and in more recent years, machine learning algorithms (Matthews, 2011; Ritchie, Zimba and Everitt, 2003; Gholizadeh, Melesse and Reddi, 2016). The empirical approach establishes relationships between spectral properties and water quality parameters using statistical relationships (Ritchie, Zimba and Everitt, 2003). The analytical approach models surface water reflectance by using the Inherent Optical Properties (IOP) and the Apparent Optical Properties (AOP) to obtain water quality parameters, while the semi-analytical approach uses simplified analytical models to estimate water constituents (Gholizadeh, Melesse and Reddi, 2016). Machine learning is a branch of artificial intelligence where algorithms can learn the behaviour of the targeted phenomenon from training data (Silveira Kupssinskü et al., 2020; Lary et al., 2016).

Among the four algorithm development methods mentioned in the preceding paragraph, the empirical approach is the simplest and easiest to use and implement, often producing robust results for the given study area; however, the algorithms developed are time and region-specific (Matthews, 2011; Gholizadeh, Melesse and Reddi, 2016). The analytical approach is more complex and time-consuming but can retrieve multiple water quality parameters simultaneously, provided enough information of the IOP's of the study area is available (Matthews, 2011; Gholizadeh, Melesse and Reddi, 2016). Machine learning methods can be trained to learn from data and model complex dynamics while accepting many types of input data to model non-linear relationships, which are limited when traditional empirical (regression) methods are used (Silveira Kupssinskü et al., 2020; Maxwell, Warner and Fang, 2018). However, they are very complex, and few studies have been conducted using machine learning methods (Peterson et al., 2018; Larson et al., 2021).

Table 2.4 displays the methods used by various studies to retrieve water quality parameters from Landsat 8 and Sentinel 2 imagery. The most favoured method is the empirical method, owing to the large number of studies which have used this method, most likely due to its simplicity and ability to produce reliable results. On the other hand, semi-analytical methods have been used to a far lesser extent, possibly owing to their complex nature, while the use of machine learning methods has been increasing in popularity due to its accuracy and reliability (Silveira Kupssinskü et al., 2020).

Table 2.4: Methods and algorithms used to estimate water quality parameters from Landsat 8 and Sentinel 2 imagery.

Algorithm Type	Study
Statistical/Empirical	Sharaf El Din (2020); Markogianni et al. (2017); Chen et al. (2019); Bonansea et al. (2019a); Prasad, Saluja and Garg (2020); Fadel, Faour and Slim (2016); Lim and Choi (2015); Soomets et al. (2020); Ha et al. (2017); Ledesma et al. (2019); Shang et al. (2021); Olmanson et al. (2020); Ouma, Noor and Herbert (2020); Grendaitė et al. (2018); Malahlela et al. (2018); Olmanson et al. (2016); Deutsch, Alameddine and El-Fadel (2014); Laili et al. (2015); Chen et al. (2017a); Chen et al. (2017b); Alcântara et al. (2016); Watanabe et al. (2015); Patra et al. (2017); Ansper and Alikas (2018); Bonansea et al. (2019b); Kurniadin and Jaelani (2016); Molkov et al. (2019); Kontopoulou, Kolokoussis and Karantzalos (2017); Yang and Anderson (2016); Elangovan and Murali (2020); Buma and Lee (2020); Pirasteh et al. (2020); Kutser et al. (2016a); Keith et al. (2018); Li et al. (2017); Al-Kharusi et al. (2020); Karaoui et al. (2019); Sòria-Perpinyà et al. (2021); Ciancia et al. (2020); Mansaray et al. (2021); Shen and Feng (2018); Mushtaq and Nee Lala (2017); El Din and Zhang (2017); Pham et al. (2018); Yepez et al. (2018); Quang et al. (2017); Vinh et al. (2019); Liu et al. (2017); Pizani et al. (2020); Chen et al. (2020b); Bande et al. (2018); Deutsch et al. (2021); El-Zeiny and El-Kafrawy (2017); González-Márquez et al. (2018); Al-Fahdawi, Rabee and Al-Hirmizy (2015); Sòria-Perpinyà et al. (2020); Zhu et al. (2020); He, Jin and Shang (2021); Wang et al. (2021); Toming et al. (2016); Watanabe et al. (2017); Kim, Ko and Nam (2016); Wu et al. (2015); Masocha et al. (2018)
Physical/Analytical	No known studies
Semi-analytical	Zhang et al. (2016); Lee et al. (2016); Bresciani et al. (2018); Giardino et al. (2014); Manuel et al. (2020); Rodrigues et al. (2017); Dörnhöfer et al. (2016)

Machine learning	Guo et al. (2021), Prasad, Saluja and Garg (2020); Soomets et al. (2020); Zhang, Huang and Wang (2020); Li et al. (2021); Pu et al. (2019); Peterson, Sagan and Sloan (2020); Peterson et al. (2018); Huangfu et al. (2020); Larson et al. (2021); Aptoula and Ariman (2021); Li, Ding and Ilyas (2021); Sharaf El Din, Zhang and Suliman (2017); Bayati and Danesh-Yazdi (2021); Ansari and Akhoondzadeh (2020); Qi, Huang and Wang (2020); Sòria-Perpinyà et al. (2021); Wagle, Acharya and Lee (2019); Pahlevan et al. (2020)

2.5. Water quality parameters measured using Landsat 8 and Sentinel 2 imagery

The remote monitoring of water quality parameters depends on constituents found in surface waters which can impact the spectral signature of water by changing the backscattering and absorption of light (Ritchie, Zimba and Everitt, 2003; Matthews, 2011). These parameters are called optically active parameters and include chlorophyll-a (chl-a), total suspended solids (TSS), coloured dissolved organic matter (CDOM), Turbidity, and secchi disk depth (SDD) (Gholizadeh, Melesse and Reddi, 2016). Optically active parameters are more commonly estimated from satellite imagery because satellites can pick up on the spectral changes caused by the optically active parameters. On the contrary, parameters such as total phosphorous (TP), total nitrogen (TN), ammonia and dissolved organic carbon (DOC) are classified as optically inactive parameters, as they are unable to change the spectral properties of water. Therefore, they can only be inferred indirectly from the measurement of optically active water quality parameters; hence fewer studies have looked at their retrieval from satellite imagery (Gholizadeh, Melesse and Reddi, 2016; Ritchie, Zimba and Everitt, 2003).

Studies indicate that the visible and NIR (400 – 1000 nm) portions of the EMS are often used for water quality applications (Matthews, 2011; Gholizadeh, Melesse and Reddi, 2016), meaning that Landsat 8 bands B1 to B8 and Sentinel 2 bands B1 to B9 should be capable of retrieving water quality parameters.

Sections 2.5.1 to 2.5.9 will take a closer look at the different water quality parameters that have been estimated using Landsat 8 and Sentinel 2 imagery, including the absorption and backscattering properties, the success and limitations of different bands/band ratios and algorithms used in the retrieval of water quality parameters. While most studies conducted have developed multiple algorithms, only the most successful and applicable algorithms are listed in the Tables presented in the subsequent sections.

2.5.1. Chlorophyll-a

Chl-a is a parameter that can be used to determine the trophic level of a water body, a proxy for phytoplankton, and an indicator of the eutrophication level and quality of a water body (Markogianni et al., 2017; Soomets et al., 2020; Ha et al., 2017; Zhang, Huang and Wang, 2020; Li et al., 2021). Chl-a has distinctive spectral characteristics, absorbing electro-magnetic energy between 450 nm to 475 nm (blue), at 670 nm (red), and reflectance peaks occurring at 500 nm (green) and 700 nm (NIR) (Gholizadeh, Melesse and Reddi, 2016; Markogianni et al., 2018). However, absorption by CDOM and scattering by TSS found in inland water bodies can interfere with the spectral signals of chl-a, therefore the NIR-Red band ratios are often used for chl-a retrieval, as opposed to the blue-green band ratios which are commonly used for ocean waters (Molkov et al., 2019). Research has also shown that the red edge of the visible spectrum (B5-B7 and B8a in Sentinel 2) can be used to estimate chl-a, even in waters that contain a high amount of TSS and CDOM (Ha et al., 2017; Yadav et al., 2019), and many studies make use of the 700:670 nm ratio for chl-a retrieval (Matthews, 2011). Based on this information, Landsat 8 B2, B3, B4, B5 and Sentinel 2 B2, B3, B4, B5, B6, B7, B8 and B8a can be used to estimate chl-a (Table 2.1 and Table 2.2). Table 2.5 below displays not only the algorithms and band/bands used to estimate chl-a from Landsat 8 and Sentinel 2 imagery but also shows that using two or more bands, as opposed to single bands, is predominately utilised when estimating chl-a from both imageries.

Table 2.5: Chl-a algorithms

Study	Study area	Algorithm Type	Band/Band combination	R^2	RMSE	Satellite Imagery
Markogianni et al. (2017)	Trichonis Lake, Greece	Empirical	B1, B2, B3	0.19	-	Landsat 8
Prasad, Saluja and Garg (2020)	Ganga River, India	Empirical	B2, B4	0.68	9.86 $\mu g/l^{-1}$	Landsat 8
Prasad, Saluja and Garg (2020)	Ganga River, India	Machine Learning	-	0.97	1.26 $\mu g/l^{-1}$	Landsat 8
Fadel, Faour and Slim (2016)	Karaoun Reservoir, Lebanon	Empirical	B2, B4, B5	0.72	-	Landsat 8
Lim and Choi (2015)	Nakdong River, South Korea	Empirical	B2, B3, B4, B5	0.77	6.32 mg/m^{-3}	Landsat 8
Soomets et al. (2020)	Razna, Lubans, Burtnieks (Latvia) and Vorysjarv (Estonia)	Various	B4, B8	0.84	10.5 mg/m^{-3}	Sentinel 2
Bresciani et al. (2018)	Lakes Maggiore, Como, Iseo, Idro, Garda in Italy	Semi-analytical (BOMBER)	-	0.82	0.43 mg/m^{-3}	Landsat 8 and Sentinel 2
Ha et al. (2017)	Lake Ba Be, Vietnam	Empirical	B3, B4	0.68	0.14 µg/l	Sentinel 2
Ledesma et al. (2019)	Cassaffousth reservoir, Argentina	Empirical	B2, B4, B6, B7, B8	0.87	0.18 $\mu g/l^{-1}$	Landsat 8
Ouma, Noor and Herbert (2020)	Chebara Dam, Kenya	Empirical	B3, B11	0.70	12.84 µg/l	Sentinel 2
Ouma, Noor and Herbert (2020)	Chebara Dam, Kenya	Empirical	B3	0.85	2.55 µg/l	Landsat 8

Zhang, Huang and Wang (2020)	Donghu Lake, China	Machine Learning	B1, B2, B3, B4	0.77	22.63 µg/l	Landsat 8
Li et al. (2021)	45 lakes in China	Machine learning	B4, B8	0.88	6.28 µg/l	Sentinel 2
Yadav et al. (2019)	Lake Biwa, Japan	Spectral Decomposition Algorithm	B2, B3, B4, B5	0.65	1.02 µg/l	Landsat 8
Yadav et al. (2019)	Lake Biwa, Japan	Spectral Decomposition Algorithm	B2, B3, B4, B8a	0.76	0.97 µg/l	Sentinel 2
Grendaitė et al. (2018)	Lakes Jieznas Širvys, Guostus, and Šventas Poland	Empirical	B4, B5	0.79	7 µg/l^{-1}	Sentinel 2 (TOA)
Grendaitė et al. (2018)	Lakes Jieznas Širvys, Guostus, and Šventas Poland	Empirical	B4, B5, B8a	0.77	7 µg/l^{-1}	Sentinel 2 (BOA)
Grendaitė et al. (2018)	Lakes Jieznas Širvys, Guostus, and Šventas Poland	Empirical (tested algorithm developed by Matthews, Bernard and Robertson (2012) and calibrated for it for Sentinel 2)	B4, B5, B8a	0.76	9 µg/l^{-1}	Sentinel 2 (BOA)
Grendaitė et al. (2018)	Lakes Jieznas Širvys, Guostus, and Šventas Poland	Empirical (tested algorithm developed by Hunter et al. (2008) and Jiao et al. (2006) and calibrated it for Sentinel 2)	B4, B5	0.8	21 – 53 µg/l^{-1}	Sentinel 2 (TOA)
Malahlela et al. (2018)	Vaal Dam, South Africa	Empirical	B4, B5	0.43	-	Landsat 8
Peterson, Sagan and Sloan (2020)	Midwestern United States	Machine Learning	-	0.88	7.56 µg/l	Landsat 8/

						Sentinel 2
Deutsch, Alameddine and El-Fadel (2014)	Qaraoun Reservoir, Lebanon	Empirical	B4, B5	0.70	-	Landsat 8
Laili et al. (2015)	Poteran Island water, Indonesia	Empirical	B2, B4	0.57	51.94 mg/mg^3	Landsat 8
Chen et al. (2017b)	Lake Huron, USA	Empirical	B4, B5	0.95	3.12 mg/m^3	Sentinel 2
Watanabe et al. (2015)	Barra Bonita Reservoir, Brazil	Empirical	B2, B3, B4, B5	0.19 – 0.34	-	Landsat 8
Patra et al. (2017)	Nalban Lake, India	Empirical	B4, B5	0.88	0.14 µg/l	Landsat 8
Ansper and Alikas (2018)	Estonian Lakes	Empirical	B7	0.26	-	Sentinel 2
Ansper and Alikas (2018)	Peipsi	Empirical	B4, B5	0.44	-	Sentinel 2
Ansper and Alikas (2018)	Võrts-järv	Empirical	B4, B5, B7	0.93	-	Sentinel 2
Ansper and Alikas (2018)	Betuwe	Empirical	B7	0.83	-	Sentinel 2
Ansper and Alikas (2018)	Finnish boreal lakes	Empirical	B7	0.87	-	Sentinel 2
Ansper and Alikas (2018)	Vesijärvi	Empirical	B4, B5	0.97	-	Sentinel 2
Ansper and Alikas (2018)	Garda	Empirical	B2, B3, B4	0.25	-	Sentinel 2
Ansper and Alikas (2018)	Mag-giore	Empirical	B1	0.31	-	Sentinel 2
Molkov et al. (2019)	Gorky Reservoir, Russia	Empirical	B4, B5	0.86	3.02 mg/m^3	Sentinel 2
Cairo et al. (2020)	Ibitinga Reservoir, Brazil	Tested already developed 3 band algorithm by Gitelson et	B2, B3, B4	0.78	5.34 mg/m^3	Sentinel 2

		al. (2011) for oligotrophic waters				
Cairo et al. (2020)	Ibitinga Reservoir, Brazil	Tested already developed slope algorithm by Mishra and Mishra (2010) for eutrophic waters	B4, B8	0.93	12.09 mg/m^3	Sentinel 2
Cairo et al. (2020)	Ibitinga Reservoir, Brazil	Empirical	B3, B6	0.98	58.90 mg/m^3	Sentinel 2
Yang and Anderson (2016)	Jordan Lake, USA	Empirical (July, summer)	B1, B3	0.72	1.2 µg/l	Landsat 8
Yang and Anderson (2016)	Jordan Lake, USA	Empirical (November, autumn)	B3, B5	0.47	1.3 µg/l	Landsat 8
Elangovan and Murali (2020)	Krishnagiri Reservoir, India	Empirical	B1, B3, B5, B6, B7,	0.63	0.01 µg/l	Landsat 8
Manuel et al. (2020)	Laguna de Bay, Philippines	Semi-analytical (WASI-2D)	-	0.32	2.28 µg/l	Landsat 8
Buma and Lee (2020)	Lake Chad	Empirical	B4, B5, B8a	0.95	2.8%	Sentinel 2
Buma and Lee (2020)	Lake Chad	Empirical	B2, B3, B4	0.89	5.1%	Landsat 8
Pirasteh et al. (2020)	Lake Erie, USA	Empirical	-	0.92	6.05 mg/m^3	Sentinel 2
Aptoula and Ariman (2021)	Lake Balik, Turkey	Machine learning	-	0.95	4.07 µg/l	Sentinel 2
Aptoula and Ariman (2021)	Lake Balik, Turkey	Machine learning	-	0.93	2.95 µg/l	Sentinel 2
Aptoula and Ariman (2021)	Lake Balik, Turkey	Machine learning	-	0.76	13.64 µg/l	Sentinel 2

Aptoula and Ariman (2021)	Lake Balik, Turkey	Machine learning	-	0.95	2.87 µg/l	Sentinel 2
Boucher et al. (2018)	Maine and New Hampshire, USA	Empirical	B1, B2, B3, B4	0.16	0.64 µg/l	Landsat 8
Boucher et al. (2018)	Maine, USA	Empirical	B1, B2, B3, B4	0.27	0.65 µg/l	Landsat 8
Keith et al. (2018)	Everett Jordan Lake, USA	Empirical	B1, B3, B5	0.66	8.9 µg/l	Landsat 8
Karaoui et al. (2019)	Bin El Ouidane Reservoir	Empirical	B3, B4, B5, B6	0.78	0.03 mg/l	Sentinel 2
Sòria-Perpinyà et al. (2021)	Two lakes and 50 reservoirs in Spain	Empirical/Semi-analytical (under 5mg/m^3)	B1, B2, B3	0.62	0.91 mg/m^3	Sentinel 2
Sòria-Perpinyà et al. (2021)	Two lakes and 50 reservoirs in Spain	Empirical/Semi-analytical (over 5mg/m^3)	B4, B5	0.90	35.68 mg/m^3	Sentinel 2
Mansaray et al. (2021)	13 reservoirs in Oklahoma, USA	Empirical	B4, B5, B6, B11, B12	0.83	1.4 µg/l	Sentinel 2
Mansaray et al. (2021)	13 reservoirs in Oklahoma, USA	Empirical	B5, B6, B7	0.69	2.4 µg/l	Landsat 8
Wagle, Acharya and Lee (2019)	Phewa Lake, Nepal	Machine learning	B2, B3, B4	0.81	0.60 mg/cu.cm	Landsat 8
Vinh et al. (2019)	Thac Ba Reservoir, Vietnam	Empirical	B3, B4	0.82	0.91 mg/m^3	Landsat 8
Pizani et al. (2020)	Trˆes Marias Reservoir, Brazil	Empirical	B2, B3, B4, B5	0.75	0.84 µg/l	Sentinel 2
Pizani et al. (2020)	Trˆes Marias Reservoir, Brazil	Empirical	B2, B3, B4,	0.67	1.03 µg/l	Landsat 8

Chen et al. (2020b)	Lake Donghu, China	Empirical (March 2018)	B1, B2	0.91	-	Landsat 8
Chen et al. (2020b)	Lake Donghu, China	Empirical (December 2017)	B1, B2	0.76	-	Landsat 8
Bande et al. (2018)	Vaal Dam, South Africa	Empirical	B1, B2, B3, B4, B5	0.68	1.11 µg/l	Landsat 8
Bande et al. (2018)	Vaal Dam, South Africa	Empirical	B1, B2, B4	0.86	1.01 µg/l	Sentinel 2
Al-Fahdawi, Rabee and Al-Hirmizy (2015)	Lake Al-Habbaniyah, Iraq	Empirical (autumn)	B2	0.81	0.02 µg/l	Landsat 8
Al-Fahdawi, Rabee and Al-Hirmizy (2015)	Lake Al-Habbaniyah, Iraq	Empirical (winter)	B5	0.90	0.01 µg/l	Landsat 8
Al-Fahdawi, Rabee and Al-Hirmizy (2015)	Lake Al-Habbaniyah, Iraq	Empirical (summer)	B3	0.89	0.07 µg/l	Landsat 8
Li et al. (2018)	Xin'anjiang Reservoir, China	Empirical	B2, B3, B4,	0.80	3.32 µg/l^{-1}	Landsat 8
He, Jin and Shang (2021)	Yangtze River, China	Empirical	B1, B2, B4	0.95	0.52 µg/l	Landsat 8
Pahlevan et al. (2020)	Various worldwide	Machine learning	-	0.87	30.31 mg/m^3	Sentinel 2
Toming et al. (2016)	Estonia	Empirical	B4, B5, B6	0.83	-	Sentinel 2
Watanabe et al. (2017)	Barra Bonita reservoir, Brazil	Empirical		0.02	84.95 mg/m^{-3}	Landsat 8
Watanabe et al. (2017)	Barra Bonita reservoir, Brazil	Empirical	B4, B8	0.84	80.21 mg/m^{-3}	Sentinel 2
Kim, Ko and Nam (2016)	Nakdong River, South Korea	Empirical	B2, B4, B5	0.89	-	Landsat 8

Masocha et al. (2018)	Lake Chivero, Zinbabwe	Empirical	B4	0.69	-	Landsat 8
Masocha et al. (2018)	Mazvikadei Dam, Zimbabwe	Empirical	B4, B5	0.84	-	Landsat 8

Most studies conducted using Landsat 8 have used B2, B3, B4 and B5 in various combinations, resulting in R^2-values ranging from 0.19 to 0.97 (Prasad, Saluja and Garg, 2020; Buma and Lee, 2020; Wagle, Acharya and Lee, 2019; Vinh et al., 2019; Chen et al., 2020b; Li et al., 2018; Kim, Ko and Nam, 2016). Ledesma et al. (2019), Zhang, Huang and Wang (2020), Yang and Anderson (2016), Chen et al. (2020b) and He, Jin and Shang (2021) also found varying successes using combinations of Landsat 8 B1 to B7 for chl-a retrieval. However, Ouma, Noor and Herbert (2020) and Al-Fahdawi, Rabee and Al-Hirmizy (2015) used Landsat 8 single bands B2, B3, B5, and Ansper and Alikas (2018) used Sentinel 2 B7 to retrieve chl-a with good results ($R^2 > 0.8$). In relation to band combinations, studies show that Sentinel 2 B4:B8 and Landsat 8 B4:B5 ratios can be successfully used to retrieve chl-a ($R^2 > 0.7$) (Soomets et al., 2020; Li et al., 2021; Cairo et al., 2020; Watanabe et al., 2017; Deutsch, Alameddine and El-Fadel, 2014; Patra et al., 2017; Masocha et al., 2018). Another commonly used ratio is the Sentinel 2 red edge bands B5:B4 ratio, which makes use of the reflectance peak at 700 nm and the absorption peak at 665 nm, to retrieve chl-a from Sentinel 2 imagery (Grendaitė et al., 2018; Chen et al., 2017b; Ansper and Alikas, 2018; Molkov et al., 2019; Sòria-Perpinyà et al., 2021).

Studies have employed various algorithms for chl-a retrieval, while others used existing algorithms calibrated for Landsat 8 and Sentinel 2 data. Grendaitė et al. (2018) tested 12 existing algorithms and found that the algorithm developed by Matthews, Bernard and Robertson (2012) was most successful for retrieving chl-a from bottom-of-atmosphere (BOA) Sentinel 2 images, whereas the algorithms developed by Hunter et al. (2008) and Jiao et al. (2006) yielded the best results with TOA Sentinel 2 images, however, the root-mean-square-error (RMSE) values were high. Cairo et al. (2020) tested a three-band algorithm developed by Gitelson et al. (2011) for retrieving chl-a from oligotrophic waters, and a slope algorithm for Sentinel 2 imagery developed by Mishra and Mishra (2010) to retrieve chl-a from eutrophic waters, yielding positive results. In addition, Cairo et al. (2020) successfully developed an empirical algorithm for retrieving chl-a from hypertrophic waters using Sentinel 2 data.

Prasad, Saluja and Garg (2020) compared empirical and machine learning algorithms and found that machine learning algorithms (yielding higher R^2 and lower RMSE values) outperformed empirical algorithms (producing lower R^2 and higher RMSE values) for chl-a retrieval from Landsat 8. Li et al. (2021) tested three different machine learning algorithms (linear regression, support vector machine (SVM) and catboost), and found SVM to be the most accurate. On the contrary, Aptoula and Ariman (2021) investigated 2D Convolutional Neural Networks (CNN), 3D CNN, Fourier Attribute Lineages, Mixture Density Network, and a NIR-Red ratio under four different protocols and found that CNN performed better than every other method in chl-a retrieval from Sentinel 2 imagery. Ansper and Alikas (2018) tested and adapted 28 empirical algorithms to Sentinel 2 bands for chl-a retrieval in various lakes and obtained varying results ($0.26 < R^2 < 0.97$). Molkov et al. (2019) tested two-band and three-band NIR-Red algorithms, Normalized Difference Chlorophyll Index (NDCI) and the reflectance peak of 705 nm on Sentinel 2 images and found the NDCI algorithm worked best. On the contrary, Buma and Lee (2020) tested a two-band algorithm, three-band algorithm, fluorescence line height algorithm, and NDCI and found that the three-band algorithm worked best for chl-a retrieval from both Landsat 8 and Sentinel 2 imagery. Keith et al. (2018) tested a three-band reflectance model developed by Dall'Olmo, Gitelson, and Rundquist (2003), a blue-green band reflectance model developed by Gordon and Morel (1983), a green-blue reflectance model developed by Turner (2010), and two four-band reflectance models (fluorescence line height (FLH) blue and violet models) developed by Beck et al. (2016), and found that the three-band reflectance model was the most successful with Landsat 8 imagery. Boucher et al. (2018) tested six different algorithms for chl-a retrieval, Surface Algal Bloom Index (SABI) by Alawadi (2010), the 3BDA-like (KIVU) by Brivio et al. (2001), the Normalized Difference Vegetation Index (NDVI) by Mishra and Mishra (2012), the 2BDA by Dall'Olmo and Gitelson (2006), and the Kab1 and Kab2 by Kabbara et al. (2008) and found the Kab 2 algorithm to be the most successful for retrieving chl-a from Landsat 8 imagery. Bresciani et al. (2018), Manuel et al. (2020), and Sòria-Perpinyà et al. (2021) used semi-analytical methods to retrieve chl-a from Landsat 8 and Sentinel 2 data and obtained varying results. The WASI-2D method used by Manuel et al. (2020) obtained a R^2-value of 0.32, but the BOMBER model used by Bresciani et al. (2018) obtained a R^2-value of 0.82, while R^2-values ranged from 0.62 to 0.92 for Sòria-Perpinyà et al. (2021). Most studies, however, sought to develop empirical algorithms using Landsat 8 and Sentinel 2 imagery with varying results (Prasad, Saluja and Garg, 2020; Ouma, Noor and Herbert, 2020; Mansaray et al., 2021) among others.

Overall, the bands found in the visible and NIR regions have proven to be the best for chl-a retrieval. Most studies preferred the use of empirical methods for estimating chl-a from Landsat 8 and Sentinel 2 images, however, there is a noticeable increase in the use of machine learning methods, while few studies have used semi-analytical methods. The results indicate that while it is possible to retrieve chl-a using empirical, semi-analytical and machine learning methods from Landsat 8 and Sentinel 2 imagery with a fair amount of accuracy, not all studies could accurately estimate chl-a, highlighting the need for more studies to be conducted worldwide to generate, test, and improve chl-a algorithms both technically and for various sites.

2.5.2. Total Suspended Solids

Total suspended solids (TSS) is an important water quality parameter, which includes organic and inorganic substances (Matthews, 2011). The monitoring of TSS can provide information on a water body's hydrological, geomorphological, and biological environment (Larson et al., 2021; Pham et al., 2018). Increased TSS can negatively impact an aquatic environment by affecting nutrient dynamics, preventing phytoplankton production, reducing water clarity, and degrading water bodies (Ciancia et al., 2020; Larson et al., 2021; Peterson et al., 2018; Pham et al., 2018; Wang et al., 2021). TSS, like chl-a, is an optically active parameter that can influence water's spectral signature. Studies have found that the reflectance peak near 700 nm and the wavelengths between 700 nm and 800 nm are most useful in TSS determination (Matthews, 2011; Ritchie, Zimba and Everitt, 2003), with the NIR and red regions capable of TSS estimation (Matthews, 2011; Liu et al., 2017). Table 2.6 below presents studies conducted in TSS retrieval, the algorithms and band/bands used to estimate TSS from Landsat 8 and Sentinel 2 imagery and provides clues to their successes or limitations.

Table 2.6: TSS algorithms

Study	Study area	Algorithm Type	Band/Band combination	R^2	RMSE	Satellite Imagery
Zhang et al. (2016)	Xin'anjiang Reservoir, China	Semi-analytical	B1, B2, B3	> 0.9	-	Landsat 8
Sharaf El Din (2020)	Saint John River, Canada	Empirical	B1, B5	> 0.8	-	Landsat 8

Lim and Choi (2015)	Nakdong River, South Korea	Empirical	B3, B4, B5	0.78	1.40 mg/l^{-1}	Landsat 8
Soomets et al. (2020)	Razna, Lubans, Burtnieks (Latvia) and Vorysjarv (Estonia)	Various	-	0.89	3.41 mg/l^{-1}	Sentinel 2
Ouma, Noor and Herbert (2020)	Chebara Dam, Kenya	Empirical	B4, B8	0.61	8.38 mg/l	Sentinel 2
Ouma, Noor and Herbert (2020)	Chebara Dam, Kenya	Empirical	B2, B3	0.92	0.03 mg/l	Landsat 8
Deutsch, Alameddine and El-Fadel (2014)	Qaraoun Reservoir, Lebanon	Empirical	B4	0.34	-	Landsat 8
Laili et al. (2015)	Poteran Island water, Indonesia	Empirical	B2, B4	0.70	1.70 g/m^3	Landsat 8
Peterson et al. (2018)	Missouri-Mississippi River, USA	Machine learning	-	0.93	39.7 mg/l	Landsat 8
Kurniadin and Jaelani (2016)	Gili Iyang's waters, Dungkek, Sumenep, East Java Province, Indonesia	Empirical	B3, B4	0.66	-	Landsat 8
Molkov et al. (2019)	Gorky Reservoir, Russia	Empirical	B4, B5	0.78	0.13 mg/l	Sentinel 2
Larson et al. (2021)	Lake Erie, USA	Machine learning (0-15cm)	-	0.81	3.21 mg/l^{-1}	Landsat 8
Larson et al. (2021)	Lake Erie, USA	Machine learning (0-61cm)	-	0.86	5.54 mg/l^{-1}	Landsat 8

Larson et al. (2021)	Lake Erie, USA	Machine learning (0-91cm)	-	0.86	7.94 mg/l^{-1}	Landsat 8
Larson et al. (2021)	Lake Erie, USA	Machine learning (0-182cm)	-	0.89	9.66 mg/l^{-1}	Landsat 8
Sharaf El Din, Zhang and Suliman (2017)	Saint John River, Canada	Machine learning	-	0.97	0.22 mg/l^{-1}	Landsat 8
Sòria-Perpinyà et al. (2021)	Two lakes and 50 reservoirs in Spain	Empirical/Semi-analytical (Low TSS (under 20mg/L))	B5	0.85	1.55 mg/l	Sentinel 2
Sòria-Perpinyà et al. (2021)	Two lakes and 50 reservoirs in Spain	Empirical/Semi-analytical (High TSS (over 20mg/L))	B2, B7	0.77	10.35 mg/l	Sentinel 2
Ciancia et al. (2020)	PL Reservoir, Italy	Empirical	B4	0.81	0.89 g/m^3	Sentinel 2
Mushtaq and Nee Lala (2017)	Wular Lake, India	Empirical	B4	0.66	-	Landsat 8
El Din and Zhang (2017)	Saint John River, USA and Canada	Empirical	B1, B2, B4	0.89	0.80 mg/l	Landsat 8
Pham et al. (2018)	Red River, Vietnam	Empirical	B3, B4	0.75	9.08 mg/l	Landsat 8
Yepez et al. (2018)	Orinoco basin, Colombia and Venezuela	Empirical	B5	0.91	11.64 mg/l^{-1}	Landsat 8
Liu et al. (2017)	Poyang Lake, China	Empirical	B7	0.93	16.06 mg/l	Sentinel 2
Al-Fahdawi, Rabee and Al-Hirmizy (2015)	Lake Al-Habbaniyah, Iraq	Empirical (autumn)	B2	0.96	0.06 mg/l	Landsat 8
Al-Fahdawi, Rabee and Al-Hirmizy (2015)	Lake Al-Habbaniyah, Iraq	Empirical (winter)	B2	0.87	0.04 mg/l	Landsat 8

Al-Fahdawi, Rabee and Al-Hirmizy (2015)	Lake Al-Habbaniyah, Iraq	Empirical (summer)	B3	0.88	0.09 mg/l	Landsat 8
Zhu et al. (2020)	West Lake, China	Empirical	B3, B4	0.81	2.12 m^{-1}	Landsat 8
Wang et al. (2021)	Shengjin Lake and Chaohu Lake, China	Empirical	B3, B6	0.88	25.86 mg/l	Sentinel 2
Wang et al. (2021)	Shengjin Lake and Chaohu Lake, China	Empirical	B3, B5	0.83	30.58 mg/l	Landsat 8
Wu et al. (2015)	Dongting Lake, China	Empirical	B4	0.91	4.41 mg/l^{-1}	Landsat 8

Most studies conducted to retrieve TSS from satellite images (Table 2.6) have used Landsat 8 imagery, employing single bands or band ratios utilizing Landsat 8 B1 to B5. The studies which made use of Sentinel 2 bands found B2 to B8 useful, either as single bands or band ratios. In relation to single bands, Al-Fahdawi, Rabee and Al-Hirmizy (2015) found that Landsat 8 B2 correlated with TSS in autumn and winter and Landsat 8 B3 correlated with TSS in summer, obtaining R^2-values greater than 0.8. On the contrary, Wu et al. (2015) and Mushtaq and Nee Lala (2017) found success with Landsat 8 B4, while Sharaf El Din (2020) successfully used Landsat B1 to estimate TSS. In their study, Yepez et al. (2018) instead used Landsat 8 B5, and Liu et al. (2017) used Landsat 8 B7 to estimate TSS, both obtaining R^2-values greater than 0.9.

In relation to Sentinel 2, Sòria-Perpinyà et al. (2021) used Sentinel 2 single band B5 to retrieve TSS in freshwater bodies which contained low amounts of TSS (under 20 mg/l), and Ciancia et al. (2020) used Sentinel 2 B4 to estimate TSS, both with good results ($R^2 > 0.8$). In comparison to Sentinel 2 single bands, studies using different combinations of Sentinel 2 band ratios to retrieve TSS produced varying results, with R^2 values ranging from 0.61 to 0.89 (Table 2.6).

Similar to chl-a, empirical algorithms are mainly used in TSS retrieval, with good results ($R^2 > 0.7$). Ouma, Noor and Herbert (2020), Zhu et al. (2020) and Wang et al. (2021), among others, all estimated TSS using empirical algorithms on Landsat 8 with R^2-values greater than 0.7. Molkov et al. (2019), Ciancia et al. (2020), Lui et al. (2017), and Wang et al. (2021) used empirical algorithms on Sentinel 2 imagery to determine TSS and obtained R^2 values greater than 0.7. Zhang et al. (2016) developed a semi-analytical model for TSS retrieval from Landsat 8 and obtained promising results for the Xin'anjiang Reservoir in China ($R^2 > 0.9$). Unlike the authors in the preceding sentences, Sòria-Perpinyà et al. (2021) used a combination of semi-analytical and empirical methods for TSS retrieval from Sentinel 2 images in freshwater systems with low (< 20 mg/l) and high (> 20 mg/l) TSS concentrations and obtained good results ($R^2 > 0.77$). Peterson et al. (2018), Larson et al. (2021), and Sharaf El Din, Zhang and Suliman (2017) instead used different machine learning algorithms to estimate TSS with varying results. For example, Peterson et al. (2018) tested Random Forest (RF), SVM, Extreme Learning Machine (ELM), Feef-forward Neural Network, and Cascade forward Neural Network to retrieve TSS from Landsat 8 imagery and found that ELM obtained the highest R^2 (0.93) and lowest RMSE values (39.7 mg/l) (Table 2.6). Larson et al. (2021) tested three machine learning methods (RF, support vector regression and model averaged neural network) and a linear regression model and found that all machine learning methods outperformed linear regressions but also that RF and model averaged neural network outperformed support vector regression in TSS retrieval at multiple depths from Landsat 8. Sharaf El Din, Zhang and Suliman (2017) used a back propagation neural network machine learning method and retrieved TSS with high accuracy ($R^2 = 0.97$) from Landsat 8 imagery.

2.5.3. Coloured Dissolved Organic Matter

Coloured Dissolved Organic Matter (CDOM), also referred to as gelbstoff and gilvin, is comprised of organic substances soluble in water and contributes to water colour by colouring water yellowish-brown (Matthews, 2011; Gholizadeh, Melesse and Reddi, 2016). Monitoring CDOM is vital for gathering information about the photosynthetic activity, aquatic ecosystem functioning, potable water, and the transport of contaminants (Shang et al., 2021; Olmanson et al., 2020; Chen et al., 2017b). CDOM, an optically active parameter, often affects the blue and green regions of the EMS, with absorption taking place at 440 nm (Matthews, 2011; Gholizadeh, Melesse and Reddi, 2016; Alcântara et al., 2016). Research has shown that using a ratio which includes the red, green, and blue parts of the EMS can obtain CDOM from satellite imagery (Alcântara et al., 2016) and that the CDOM signal is only significant at wavelengths less than 550 nm in Landsat 8 and Sentinel 2.

All studies conducted to retrieve CDOM have made use of B2 to B4 (the blue, green, and red regions), however, Olmanson et al. (2020), Chen et al. (2017b) and Shang et al. (2021) also made use of B5 for Landsat 8 and Sentinel 2 imagery, obtaining successful results ($R^2 > 0.7$). While no band ratio is used more frequently than another, all studies have used band ratios including B2 to B5 for Landsat 8 and Sentinel 2 imagery (Table 2.7). For example, Chen et al. (2019) and Alcântara et al. (2016) used Landsat 8 B2 and B4 and obtained R^2-values of 0.78 and 0.70, respectively, while Sòria-Perpinyà et al. (2021) used the same band ratio for Sentinel 2 imagery and obtained a R^2-value of 0.52. Chen et al. (2017a) and Kutser et al. (2016a) used a Landsat 8 B3 and B4 combination, while Al-Kharusi et al. (2020) and Toming et al. (2016) used a Sentinel 2 B3 and B4 combination in CDOM retrieval and achieved R^2-values ranging from 0.63 to 0.82. Markogianni et al. (2017) and Soomets et al. (2020) used a combination of B2, B3, and B4 for Landsat 8 and Sentinel 2 imagery respectively and obtained different results. For example, Markogianni et al. (2017) obtained a R^2-value of 0.23 while Soomets et al. (2020) obtained a R^2-value of 0.93, possibly due to the difference in locations and satellite imagery used. Olmanson et al. (2020) and Olmanson et al. (2016) used a Landsat 8 B3, B4, and B5 combination and obtained a good correlation of 0.8 and above with in-situ CDOM, indicating the ability of this band combination for CDOM retrieval. The studies conducted suggest that while CDOM can be estimated from Landsat 8 and Sentinel 2 B2, B4, B3 and B5, the results vary from study to study, with some studies finding success with Landsat 8 and Sentinel 2, while other studies have not been as successful. This indicates the need for more research to be conducted to determine which band/band ratio is the most successful in determining CDOM for both satellites.

Table 2.7: CDOM algorithms

Study	Study area	Algorithm Type	Band/Band combination	R^2	RMSE	Satellite Imagery
Markogianni et al. (2017)	Trichonis Lake, Greece	Empirical	B2, B3, B4	0.23	-	Landsat 8
Chen et al. (2019)	Sacramento River, Northern San Francisco,	Empirical	B2, B4	0.78	-	Landsat 8

	and Lake Erie, North America					
Soomets et al. (2020)	Razna, Lubans, Burtnieks (Latvia) and Vorysjarv (Estonia)	Various	B2, B3, B4	0.93	0.88 m^{-1}	Sentinel 2
Shang et al. (2021)	93 reservoirs across China	Empirical	B2, B5	> 0.7	-	Sentinel 2
Olmanson et al. (2020)	Minnesota, United States of America	Empirical	B3, B4, B5	0.85	0.49 m^{-1}	Landsat 8
Olmanson et al. (2020)	Minnesota, United States of America	Empirical	B3, B4, B5	0.83	0.52 m^{-1}	Landsat 8
Olmanson et al. (2016)	Minnesota, Wisconsin, USA	Empirical	B3, B4, B5	0.82	-	Landsat 8
Chen et al. (2017a)	Lake Huron, USA	Empirical	B3, B4	0.82	0.86	Landsat 8
Chen et al. (2017b)	Lake Huron, USA	Empirical	B3, B5	0.91	0.60 m^{-1}	Sentinel 2
Alcântara et al. (2016)	Barra Bonita Reservoir, Brazil	Empirical	B2, B4	0.70	10.65%	Landsat 8
Kutser et al. (2016a)	Lake Peipsi and Võrtsjärv in Estonia. Três Marias Reservoir and Curuai Floodplain Lake in Brazil	Empirical	B3, B4	0.63	-	Landsat 8
Al-Kharusi et al. (2020)	Sweden	Empirical	B3, B4	0.64	3.48 m^{-1}	Sentinel 2
Sòria-Perpinyà et al. (2021)	Spain	Empirical/Semi-analytical	B2, B4	0.52	0.88 µg/L QSE	Sentinel 2

Toming et al. (2016)	Estonia	Empirical	B3, B4	0.72	-	Sentinel 2

In relation to algorithm methods, almost all studies used an empirical method, apart from Soomets et al. (2020) and Sòria-Perpinyà et al. (2021), who used a combination of algorithm methods (empirical, semi-analytical and machine learning). The results show that despite its simplicity, the empirical method is capable of CDOM estimation with an adequate level of accuracy; however, studies conducted in CDOM retrieval from Landsat 8 and Sentinel 2 imagery are limited, indicating the need for more studies to be conducted worldwide, using various algorithm methods.

2.5.4. SDD

SDD refers to the depth at which a circular white disk can no longer be seen by the human eye when dropped into a water body (Matthews, 2011). It is an optical measurement of water clarity that is influenced by organic and inorganic materials in a water body, making it an important water quality parameter as it relates to trophic conditions and lake productivity (Matthews, 2011; Bonansea et al., 2019b; Gholizadeh, Melesse and Reddi, 2016). Many studies have used empirical methods to retrieve SDD from different Landsat imagery using the red band or band ratio, taking advantage of SDD correlation with the red band (Matthews, 2011; Gholizadeh, Melesse and Reddi, 2016). Studies also indicate that as water clarity decreases, the red band's brightness increases (Matthews, 2011). Table 2.8 below presents the algorithms developed using Landsat 8 and Sentinel 2 imagery for SDD retrieval.

Table 2.8: SDD algorithms

Study	Study area	Algorithm Type	Band/Band combination	R^2	RMSE	Satellite Imagery
Lee et al. (2016)	Jiulongjiang River, China	Semi-analytical	-	0.96	-	Landsat 8
Bonansea et al. (2019a)	Cassaffousth Reservoir, Argentina	Empirical	B2, B3, B5	0.89	-	Landsat 8
Bonansea et al. (2019a)	Cassaffousth Reservoir, Argentina	Empirical	B2, B3, B8	0.88	-	Sentinel 2
Soomets et al. (2020)	Razna, Lubans, Burtnieks (Latvia) and Vorysjarv (Estonia)	Various	-	0.97	0.36 m	Sentinel 2
Olmanson et al. (2016)	Minnesota, Wisconsin, USA	Empirical	B2, B4	0.82	0.33 m	Landsat 8
Deutsch, Alameddine and El-Fadel (2014)	Qaraoun Reservoir, Lebanon	Empirical	B2, B4	0.47	-	Landsat 8

Bonansea et al. (2019b)	Río Tercero reservoir, Argentina	Empirical	B5, B7, B8	0.81	0.38 m	Sentinel 2
Sòria-Perpinyà et al. (2021)	Spain	Empirical/Semi-analytical	B3, B5	0.69	1.14 m	Sentinel 2
Mansaray et al. (2021)	Oklahoma, USA	Empirical	B3, B4, B7, B12	0.78	1.4 cm	Sentinel 2
Mansaray et al. (2021)	Oklahoma, USA	Empirical	B3, B4, B5	0.53	2.4 cm	Landsat 8
Pizani et al. (2020)	Trˆes Marias Reservoir, Brazil	Empirical	B1, B3	0.84	49.48 cm	Sentinel 2
Pizani et al. (2020)	Trˆes Marias Reservoir, Brazil	Empirical	B1, B3	0.81	54.15 cm	Landsat 8
Deutsch et al. (2021)	Canada	Empirical	B2, B4	> 0.45	< 2 m	Landsat 8
González-Márquez et al. (2018)	El Guajaro reservoir, Colombia	Empirical	B1, B3, B4	0.92	0.21 m	Landsat 8
Sòria-Perpinyà et al. (2020)	Albufera of València, Spain	Empirical	B2, B5	0.74	0.07 m	Sentinel 2
Masocha et al. (2018)	Lake Chivero, Zinbabwe	Empirical	B2, B3	0.75	-	Landsat 8
Masocha et al. (2018)	Mazvikadei Dam, Zimbabwe	Empirical	B2, B4	0.77	-	Landsat 8

The results in Table 2.8 indicate that the bands/band ratios from the visible spectrum were most often used to retrieve SDD; however, some studies used the NIR band (Bonansea et al., 2019a; Bonansea et al., 2019b; Mansaray et al., 2021). The Sentinel 2 vegetation red edge bands were also successfully used for SDD retrieval (Bonansea et al., 2019b; Sòria-Perpinyà et al., 2021; Mansaray et al., 2021; Sòria-Perpinyà et al., 2020), highlighting the sensitivity of the red edge region for the estimation of SDD. In addition, many studies have made use of Landsat 8 and Sentinel 2 B1 to B4 in various combinations, highlighting the ability of the visible spectrum to estimate SDD (Bonansea et al., 2019a; Olmanson et al., 2016; Pizani et al., 2020; González-Márquez et al., 2018; Sòria-Perpinyà et al., 2020; Sòria-Perpinyà et al., 2021; Masocha et al., 2018).

Most studies used empirical methods to retrieve SDD (Bonansea et al., 2019a; Olmanson et al., 2016; Deutsch, Alameddine and El-Fadel, 2014; Bonansea et al., 2019b; Mansaray et al., 2021; Pizani et al., 2020; Deutsch et al., 2021; González-Márquez et al., 2018; Sòria-Perpinyà et al., 2020; Masocha et al.,

2018) , agreeing with the research conducted by Matthews (2011), who found that empirical methods were mainly used when SDD was estimated from other satellites. An exception is Lee et al. (2016), who developed a semi-analytical model to retrieve SDD with an accuracy of 96%. Rodrigues et al. (2017) also used a semi-analytical model developed by Lee et al. (2015) on a reservoir in Brazil and found that a modification to this model allowed for the retrieval of SDD from both Landsat 8 and Sentinel 2 images. Overall, not many studies have been conducted in retrieving SDD using Landsat 8 and Sentinel 2, and the studies favoured empirical methods over analytical or machine learning methods, highlighting the possibilities for further research to be conducted in this area of water quality.

2.5.5. Turbidity

Turbidity is an optically active parameter closely linked to water clarity and TSS (Gholizadeh, Melesse and Reddi, 2016; Matthews, 2011). Turbidity is dependent on the number of suspended particles found in a water body, and the more suspended particles there are, the greater the turbidity of the water body (Gholizadeh, Melesse and Reddi, 2016). Turbidity both scatters and absorbs light, with suspended sediments scattering light and chl-a and CDOM absorbing light (Gholizadeh, Melesse and Reddi, 2016). Research indicates that the visible region of the EMS, especially the red band, can be used to measure turbidity (Gholizadeh, Melesse and Reddi, 2016; Matthews, 2011). Table 2.9 below shows studies and methods that have been used to retrieve turbidity from Landsat 8 and Sentinel 2 imagery.

Table 2.9: Turbidity algorithms

Study	Study area	Algorithm Type	Band combination	R^2	RMSE	Satellite Imagery
Sharaf El Din (2020)	Saint John River, Canada	Empirical	B1, B4, B5	> 0.8	-	Landsat 8
Ouma, Noor and Herbert (2020)	Chebara Dam, Kenya	Empirical	B2, B3	0.80	0.32 NTU	Sentinel 2
Ouma, Noor and Herbert (2020)	Chebara Dam, Kenya	Empirical	B2, B3	0.81	0.40 NTU	Landsat 8
Peterson, Sagan and Sloan (2020)	Midwestern United States	Machine Learning	-	0.83	5.19 FNU	Landsat 8/ Sentinel 2
Liu and Wang (2019)	Tseng-Wen reservoir and Nan-Hwa reservoir, Taiwan	Empirical (gene-expression programming (GEP))	B2, B3, B4, B5	0.82	0.58 NTU	Landsat 8

Liu and Wang (2019)	Tseng-Wen reservoir and Nan-Hwa reservoir, Taiwan	Empirical (GEP for critical turbidity conditions)	B2, B3, B4, B5	0.98	0.77 NTU	Landsat 8
Sharaf El Din, Zhang and Suliman (2017)	Saint John River, Canada	Machine learning	-	0.97	0.07 NTU	Landsat 8
Mansaray et al. (2021)	Oklahoma, USA	Empirical	B2, B4, B8, B12	0.75	1.6 NTU	Sentinel 2
Mansaray et al. (2021)	Oklahoma, USA	Empirical	B3, B4, B5, B7	0.51	1.8 NTU	Landsat 8
Shen and Feng (2018)	Hanjiang River, China	Empirical	B1, B2, B3	0.93	7.36 NTU	Landsat 8
Mushtaq and Nee Lala (2017)	Wular Lake, India	Empirical	B4	0.5	-	Landsat 8
Quang et al. (2017)	Cam Ranh Bay and Thuy Trieu Lagoon, Vietnam	Empirical	B4	0.84	-	Landsat 8
Pizani et al. (2020)	Trˆes Marias Reservoir, Brazil	Empirical	B1, B3	0.80	0.16 NTU	Sentinel 2
Pizani et al. (2020)	Trˆes Marias Reservoir, Brazil	Empirical	B1, B3	0.80	0.16 NTU	Landsat 8
Bande et al. (2018)	Vaal Dam, South Africa	Empirical	B1, B2, B4	0.50	167.9 NTU	Landsat 8
Bande et al. (2018)	Vaal Dam, South Africa	Empirical	B1, B2, B3, B4, B6, B9	0.59	147.69 NTU	Sentinel 2
González-Márquez et al. (2018)	El Guajaro reservoir, Colombia	Empirical	B4, B5	0.64	0.11 NTU	Landsat 8
Al-Fahdawi, Rabee and Al-Hirmizy (2015)	Lake Al-Habbaniyah, Iraq	Empirical	B3 (autumn)	0.96	0.02 NTU	Landsat 8

Al-Fahdawi, Rabee and Al-Hirmizy (2015)	Lake Al-Habbaniyah, Iraq	Empirical	B5 (winter)	0.96	0.01 NTU	Landsat 8
Al-Fahdawi, Rabee and Al-Hirmizy (2015)	Lake Al-Habbaniyah, Iraq	Empirical	B4 (summer)	0.80	0.07 NTU	Landsat 8
Masocha et al. (2018)	Lake Chivero, Zinbabwe	Empirical	B4, B2	0.81	-	Landsat 8
Masocha et al. (2018)	Mazvikadei Dam, Zimbabwe	Empirical	B4, B2	0.65	-	Landsat 8

As with chl-a, TSS, CDOM and SDD, mostly bands in the visible spectrum have been used to retrieve turbidity, with a few studies using the NIR and SWIR bands. For example, Shen and Fang (2018), Mushtaq and Nee Lala (2017), Quang et al. (2017), Pizani et al. (2020), Al-Fahdawi, Rabee and Al-Hirmizy (2015) and Masocha et al. (2018) all used Landsat 8 and/or Sentinel 2 B1 to B4. However, Sharaf El Din (2020), Liu and Wang (2019), Mansaray et al. (2021) and González-Márquez et al. (2018) used the NIR and/or SWIR bands in combination with the visible spectrum with viable results (Table 2.9).

Similar to other parameters reviewed in the previous sections of this article, the empirical methods have been mainly used to retrieve turbidity, often with good results ($R^2 > 0.7$); however, Peterson, Sagan and Sloan (2020) and Sharaf El Din, Zhang and Suliman (2017) used machine learning methods and both studies obtained R^2-values greater than 0.8. Lui and Wang (2019) developed a simulation to retrieve turbidity using two empirical methods (multiple linear regression and GEP) and found that GEP outperformed multiple linear regressions in both standard and critically turbid conditions. Overall, both empirical and machine learning methods retrieved turbidity from both Landsat 8 and Sentinel 2 imagery ($R^2 > 0.7$). However, Bande et al. (2018), González-Márquez et al. (2018), and Masocha et al. (2018), obtained R^2 values of less than 0.7, suggesting the need for more studies be conducted on the use of algorithm methods, particularly semi-analytical algorithms, to estimate turbidity.

2.5.6. Total Phosphorous

Total phosphorous (TP) consists of all forms of available phosphorous measurements (organic, inorganic, and dissolved) and is a challenging water parameter to estimate remotely because it is optically inactive and unable to influence the spectral properties of water directly, hence, it must be inferred from other water quality parameters (Gholizadeh, Melesse and Reddi, 2016; Guo et al., 2021). However, past studies have used the blue, green, and red regions of the visible spectrum to estimate TP from Landsat 8 and Sentinel 2 images (Table 2.10).

Table 2.10: TP algorithms

Study	Study area	Algorithm Type	Band/Band combination	R^2	RMSE	Satellite Imagery
Guo et al. (2021)	Tianjin, China	Machine Learning	B3, B4, B5, B6, B7, B8	0.94	-	Sentinel 2
Lim and Choi (2015)	Nakdong River, South Korea	Empirical	B2, B3, B4, B5	0.57	0.01 mg/l^{-1}	Landsat 8
Huangfu et al. (2020)	Huaihe River Basin, China	Machine Learning	B1, B4	0.60	0.03 mg/l	Sentinel 2
Li et al. (2017)	Xin'anjiang Reservoir, China	Empirical	B1, B2, B3, B4	0.46	0.007 mg/l	Landsat 8
Karaoui et al. (2019)	Bin El Ouidane Reservoir	Empirical	B2, B4, B7	0.52	0.001 mg/l	Sentinel 2
El-Zeiny and El-Kafrawy (2017)	Burullus lake, Egypt	Empirical (tested already developed algorithm by Wang and Ma (2001))	B2, B3	-	-	Landsat 8
He, Jin and Shang (2021)	Yangtze River, China	Empirical	B4, B6, B7	0.87	0.008 mg/l	Landsat 8
Karaoui et al. (2019)	Bin El Ouidane Reservoir	Empirical	B1, B3, B4, B5, B8a, B10	0.54	1.02 mg/l	Sentinel 2
Mushtaq and Nee Lala (2017)	Wular Lake, India	Empirical	-	0.72	-	Landsat 8

The results displayed in Table 2.10 above reveal that the estimation of TP from Landsat 8 and Sentinel 2 images vary greatly. Guo et al. (2021) used machine learning methods and a combination of Sentinel 2 B3 to B8 to estimate TP with an accuracy of 94%. He, Jin and Shang (2021) used empirical methods and Landsat 8 B4, B6, and B7 to retrieve TP with a correlation of 0.87. However, Lim and Choi (2015) used Landsat 8 B2 to B5 and Li et al. (2017) used empirical methods on Landsat 8 B1 to B4 and obtained lower R^2-values, 0.57 and 0.46, respectively. In their study, Huangfu et al. (2020) used machine learning methods on Sentinel 2 B1 and B4, resulting in an accuracy of 60%. These studies yielding lower accuracies mostly used the visible spectrum to estimate TP, except for Lim and Choi (2015) and He, Jin and Shang (2021) who also used the NIR and SWIR regions for Landsat 8. Studies on TP retrieval are limited, with no specific algorithm method or band/band ratio performing better than the others do. The non-optical nature of TP makes it challenging to estimate remotely; however, the highly accurate results obtained by Guo et al. (2021) (94%) and He, Jin and Shang (2021) (87%), using machine learning and empirical methods indicate that it is possible.

2.5.7. Total Nitrogen

Total Nitrogen (TN) is a measure of all the nitrogen in a water body and, like TP, it is an optically inactive parameter (Lim and Choi, 2015; Li et al., 2017). Studies conducted on the retrieval of TN from satellite images are limited (Table 2.11), however, TN can be correlated with optically active parameters such as chl-a, TSS and CDOM (Li et al., 2017); hence the visible spectrum can help determine TN remotely.

Table 2.11: TN algorithms

Study	Study area	Algorithm Type	Band/Band combination	R^2	RMSE	Satellite Imagery
Guo et al. (2021)	Tianjin, China	Machine Learning	B3, B4, B5, B6, B7, B8	0.88	-	Sentinel 2
Lim and Choi (2015)	Nakdong River, South Korea	Empirical	B3, B4, B5	0.55	0.49 mg/l^{-1}	Landsat 8
Li et al. (2017)	Xin'anjiang Reservoir, China	Empirical	B2, B4, B5	0.15	0.11 mg/l	Landsat 8
El-Zeiny and El-Kafrawy (2017)	Burullus lake, Egypt	Empirical (tested already developed algorithm Wang and Ma (2001))	B2, B3	-	-	Landsat 8
He, Jin and Shang (2021)	Yangtze River, China	Empirical	B5, B7	0.80	0.09 mg/l	Landsat 8
Karaoui et al. (2019)	Bin El Ouidane Reservoir	Empirical	B1, B2, B3, B9	0.67	0.61 mg/l	Sentinel 2

Table 2.11 shows varying results from studies using different algorithms for retrieving TN from satellite images. For example, Li et al. (2017) and Lim and Choi (2015) used empirical methods and Landsat 8 visible and NIR bands to retrieve TN with R^2-values of 0.15 and 0.55, respectively, while Karaoui et al. (2019) employed empirical methods on Sentinel 2 B1, B2, B3 and B9, resulting in a R^2 value of 0.67. Despite the lower accuracy realized in these two studies, Guo et al. (2021) used machine learning algorithms on Sentinel 2 while He, Jin and Shang (2021) used empirical methods on Landsat 8, resulting in higher R^2 values of 0.8 and more. The limited nature of studies on the retrieval of TN from satellite images (Table 2.11) points to the need for more studies to be conducted in this domain.

2.5.8. Dissolved Oxygen (DO)

Dissolved oxygen is an optically inactive water parameter, which plays a key role in the lives of all aquatic organisms that need oxygen for survival (Peterson, Sagan and Sloan, 2020; Gholizadeh, Melesse and Reddi, 2016). Like TP and TN, DO is a complex parameter to retrieve remotely, and studies on its retrieval from Landsat 8 and Sentinel 2 images are limited (Table 2.12).

Table 2.12: DO algorithms

Study	Study area	Algorithm Type	Band/Band combination	R^2	RMSE	Satellite Imagery
Peterson, Sagan and Sloan (2020)	Midwestern United States	Machine Learning	-	0.89	1.80 mg/l	Landsat 8/ Sentinel 2
Sharaf El Din, Zhang and Suliman (2017)	Saint John River, Canada	Machine learning	-	0.94	0.18 mg/l^{-1}	Landsat 8
Karaoui et al. (2019)	Bin El Ouidane Reservoir	Empirical	B8, B9, B10, B11	0.74	0.20 mg/l	Sentinel 2
Qi, Huang and Wang (2020)	Taihu Lake, China	Machine learning	-	0.84	1.68	Landsat 8
Mushtaq and Nee Lala (2017)	Wular Lake, India	Empirical	-	0.43	-	Landsat 8
Wagle, Acharya and Lee (2019)	Phewa Lake, Nepal	Machine learning	B2, B3, B4, B5	0.88	0.10 mg/cu.cm	Landsat 8
El Din and Zhang (2017)	Saint John River, USA and Canada	Empirical	B1, B2, B3, B6	0.90	0.73 mg/l	Landsat 8
Pizani et al. (2020)	Trˆes Marias Reservoir, Brazil	Empirical	B2, B4, B6, B11	0.83	0.08 mg/l	Sentinel 2
Pizani et al. (2020)	Trˆes Marias Reservoir, Brazil	Empirical	B2, B4, B6, B7	0.69	0.11 mg/l	Landsat 8
González-Márquez et al. (2018)	El Guajaro reservoir, Colombia	Empirical	B1, B3, B4, B5, B7	0.93	0.08 mg/l	Landsat 8

Studies conducted to retrieve DO from remotely sensed data have used empirical and machine learning algorithms on the visible, NIR and SWIR bands in different combinations. The successful retrieval of DO from satellites images is illustrated by Peterson, Sagan and Sloan (2020), Sharaf El Din, Zhang and Suliman (2017), Qi, Huang and Wang (2020) and Wagle, Acharya and Lee (2019), who used machine learning on Landsat 8 and Sentinel 2 to estimate DO with accuracies greater than 80% (Table 2.12). El Din and Zhang (2017) and González-Márquez et al. (2018) both used empirical methods on Landsat 8 and obtained a R^2-value of greater than 0.9; while Mushtaq and Nee Lala (2017) used the same methods and images in their studies and obtained a lower R^2-value of 0.43. Karaoui et al. (2019) instead based their study on Sentinel 2 B8 to B11, employing empirical methods and obtained a R^2 value of 0.74. In a comparative study, Pizani et al. (2020) used empirical methods on both Landsat 8 and Sentinel 2 images and found that Sentinel 2 produced a better result (R^2 = 0.83) in DO retrieval than Landsat 8 (R^2 = 0.69). The results obtained for DO retrieval are promising; however, more research needs to be conducted due to the limited number of studies carried out thus far.

2.5.9. Other parameters

Most of the water quality parameters listed in Table 2.13 are optically inactive and have been studied to a lesser extent using Landsat 8 and Sentinel 2 than chl-a, TSS, CDOM, SDD, TP, TN, and DO. These water quality parameters include chemical oxygen demand (COD), ammonia, fluorescent dissolved organic matter (fDOM), specific conductance, blue-green algae, DOC, biological oxygen demand (BOD), salinity, pH, ammonia-nitrogen, phycocyanin (PC), pondus hydrogenii, alkalinity, hardness, chloride, total dissolved solids (TDS), electrical conductivity (EC), oxidation reduction potential (ORP), organic carbon (OC), total carbon (TC), conductivity and water colour (Table 2.13). While employing the visible and NIR bands, most of these studies also made use of empirical algorithms and machine learning methods, as opposed to analytical methods. The results of this review indicates that machine learning methods were the most successful (R^2 > 0.7) in retrieving many water quality parameters such as COD, ammonia-nitrogen, fDOM, specific conductance, blue-green algae, pondus hydrogenii, salinity, and BOD (Table 2.13) from both Landsat 8 and Sentinel 2 imagery. Although empirical methods were also used to retrieve some water quality parameters, such as COD, ammonia, alkalinity, chloride, hardness, pH, EC, ORP, OC and TC from Landsat 8 and Sentinel 2, with limited success (many R^2 < 0.7), DOC and TDS were successfully retrieved (R^2 > 0.7) (Chen et al., 2020a; Toming et al., 2016; Al-Fahdawi, Rabee and Al-Hirmizy, 2015). Overall machine learning methods with the use of the visible and NIR bands produced more successful results than empirical methods in estimating the water quality parameters found in Table 2.13. Existing research on the retrieval of these water quality parameters is limited, motivating for more studies to be conducted on their retrieval from Landsat 8 and Sentinel 2.

Table 2.13: Algorithms developed for a variety of water quality parameters

Parameter	**Study**	**Study area**	**Algorithm Type**	**Band/Band combination**	**R^2**	**RMSE**	**Satellite Imagery**
COD	Guo et al. (2021)	Tianjin, China	Machine Learning	B2, B3, B5, B6, B7, B8	0.86	-	Sentinel 2
	Huangfu et al. (2020)	Huaihe River Basin, China	Machine learning	B2, B3, B4, B5, B8a	0.53	0.54 mg/l	Sentinel 2

	Sharaf El Din, Zhang and Suliman (2017)	Saint John River, Canada	Machine learning	-	0.91	0.15 mg/l^{-1}	Landsat 8
	Qi, Huang and Wang (2020)	Taihu Lake, China	Machine learning	-	0.84	0.55	Landsat 8
	Mushtaq and Nee Lala (2017)	Wular Lake, India	Empirical	B2	0.49	-	Landsat 8
Ammonia	Markogianni et al. (2017)	Trichonis Lake, Greece	Empirical	B1, B3, B4	0.07	-	Landsat 8
	Huangfu et al. (2020)	Huaihe River Basin, China	Machine learning	B5, B8	0.67	0.16 mg/l	Sentinel 2
fDOM	Peterson, Sagan and Sloan (2020)	Midwestern United States	Machine Learning	-	0.92	14.49 QSU	Landsat 8/ Sentinel 2
Specific conductance	Peterson, Sagan and Sloan (2020)	Midwestern United States	Machine Learning	-	0.87	48.46 Us	Landsat 8/ Sentinel 2
Blue-green algae	Peterson, Sagan and Sloan (2020)	Midwestern United States	Machine Learning	-	0.91	0.86 µg/l	Landsat 8/ Sentinel 2
DOC	Chen et al. (2020a)	Lake Huron, USA	Empirical (tested already developed algorithm by Chen at al. (2017a))	-	0.86	1.13 mg/l	Landsat 8
	Chen et al. (2020a)	Lake Huron, USA	Empirical (tested already developed algorithm by Chen at al. (2017b))	-	0.78	1.41 mg/l	Sentinel 2

	Toming et al. (2016)	Estonia	Empirical	B3, B4	0.92	-	Sentinel 2
BOD	Sharaf El Din, Zhang and Suliman (2017)	Saint John River, Canada	Machine learning	-	0.94	0.04 mg/l^{-1}	Landsat 8
	El-Zeiny and El-Kafrawy (2017)	Burullus lake, Egypt	Empirical (tested already developed algorithm by Wang and Ma (2001))	B2, B3	-	-	Landsat 8
Salinity	Bayati and Danesh-Yazdi (2021)	Lake Urmia, Iran	Machine learning	B2, B3, B4	0.95	5.33%	Landsat 8
	Bayati and Danesh-Yazdi (2021)	Lake Urmia, Iran	Machine learning	B2, B3, B4	0.95	5.37%	Sentinel 2
	Ansari and Akhoondzadeh (2020)	Karun Basin, Iran	Machine learning	B1, B2, B3	0.78	363 $\mu s\ cm^{-1}$	Landsat 8
Pondus Hydrogenii	Qi, Huang and Wang (2020)	Taihu Lake, China	Machine learning	-	0.72	0.49	Landsat 8
Ammonia Nitrogen	Qi, Huang and Wang (2020)	Taihu Lake, China	Machine learning	-	0.88	0.09	Landsat 8
PC	Sòria-Perpinyà et al. (2021)	Spain	Empirical/Semi-analytical	B4, B5	0.79	44.48 mg/m^3	Sentinel 2
pH	Mushtaq and Nee Lala (2017)	Wular Lake, India	Empirical	-	0.613	-	Landsat 8
	Pizani et al. (2020)	Trˆes Marias Reservoir, Brazil	Empirical	B1, B3, B6, B8	0.79	0.06	Sentinel 2
	Pizani et al. (2020)	Trˆes Marias Reservoir, Brazil	Empirical	B1, B3, B5	0.43	0.10	Landsat 8

	González-Márquez et al. (2018)	El Guajaro reservoir, Colombia	Empirical	B3, B4, B5, B6	0.81	0.08	Landsat 8
Alkalinity	Mushtaq and Nee Lala (2017)	Wular Lake, India	Empirical	B2	0.45	-	Landsat 8
Hardness	Mushtaq and Nee Lala (2017)	Wular Lake, India	Empirical	-	0.35	-	Landsat 8
Chloride	Mushtaq and Nee Lala (2017)	Wular Lake, India	Empirical	-	0.48	-	Landsat 8
TDS	Mushtaq and Nee Lala (2017)	Wular Lake, India	Empirical	B4	0.61	-	Landsat 8
	Al-Fahdawi, Rabee and Al-Hirmizy (2015)	Lake Al-Habbaniyah, Iraq	Empirical (autumn)	B2	0.97	0.03 mg/l	Landsat 8
	Al-Fahdawi, Rabee and Al-Hirmizy (2015)	Lake Al-Habbaniyah, Iraq	Empirical (winter)	B5	0.83	0.09 mg/l	Landsat 8
	Al-Fahdawi, Rabee and Al-Hirmizy (2015)	Lake Al-Habbaniyah, Iraq	Empirical (summer)	B3	0.91	0.05 mg/l	Landsat 8
EC	Mushtaq and Nee Lala (2017)	Wular Lake, India	Empirical	B4	0.61	-	Landsat 8
	González-Márquez et al. (2018)	El Guajaro reservoir, Colombia	Empirical	B2, B3, B4, B6	0.69	0.22 mS/cm	Landsat 8
ORP	Pizani et al. (2020)	Trˆes Marias Reservoir, Brazil	Empirical	B1, B4, B6	0.62	6.78 mV	Sentinel 2
	Pizani et al. (2020)	Trˆes Marias Reservoir, Brazil	Empirical	B1, B4, B5	0.43	8.32 mV	Landsat 8
OC	Pizani et al. (2020)	Trˆes Marias	Empirical	B4, B8	0.45	9.33 mg/l	Sentinel 2

		Reservoir, Brazil					
	Pizani et al. (2020)	Tr^es Marias Reservoir, Brazil	Empirical	B4, B5	0.54	8.51 mg/l	Landsat 8
TC	Pizani et al. (2020)	Tr^es Marias Reservoir, Brazil	Empirical	B2, B3, B5, B8	0.49	9.11 mg/l	Sentinel 2
	Pizani et al. (2020)	Tr^es Marias Reservoir, Brazil	Empirical	B2, B3, B5	0.62	7.81 mg/l	Landsat 8
Conductivity	Pizani et al. (2020)	Tr^es Marias Reservoir, Brazil	Empirical	B1, B2, B3, B8	0.76	4.87 mV	Sentinel 2
	Pizani et al. (2020)	Tr^es Marias Reservoir, Brazil	Empirical	B1, B2, B3, B5	0.69	5.59 mV	Landsat 8
Water Colour	Toming et al. (2016)	Estonia	Empirical	B3, B4	0.52	-	Sentinel 2

2.6. Discussion

Since the launch of Landsat 8 and Sentinel 2, many studies have been conducted to estimate various water quality parameters from these imageries. However, considering Sentinel 2 was launched relatively recently, very few studies have attempted to compare Landsat 8 and Sentinel 2 images for retrieving water quality parameters. Optically active parameters such as chl-a, TSS, CDOM, SDD and turbidity are frequently studied due to their ability to influence the spectral signature of water, and thus able to be picked up by satellites sensors (Guo et al., 2021). Optically inactive parameters such as TP, TN, DO, ammonia, DOC, COD, and many others are incapable of influencing the spectral signature of water and must therefore be inferred from optically active parameters such as chl-a, TSS, CDOM and SDD (Guo et al., 2021; Li et al., 2017). The literature review conducted in this paper indicated that the visible and NIR bands of both Landsat 8 and Sentinel 2 have been used predominately in the retrieval of the various water quality parameters globally (Pizani et al., 2020; Wagle, Acharya and Lee, 2019; Al-Fahdawi, Rabee and Al-Hirmizy, 2015; Prasad, Saluja and Garg, 2020; Grendaitė et al., 2018; Chen et al., 2017b; Liu and Wang, 2019; Olmanson et al., 2016).

Studies on chl-a retrieval mostly used Landsat 8 B2 to B5 and Sentinel 2 B4, B5, B7 and B8 in various band combinations (Table 2.5). Chl-a influences the EMS between 450 nm to 475 nm (absorption), at 500 nm (reflectance), 670 nm (absorption) and 700nm (reflectance), however CDOM and TSS can interfere with chl-a's spectral signatures (Gholizadeh, Melesse and Reddi, 2016; Markogianni et al., 2018; Molkov et al., 2019). Hence, NIR-Red band ratios can be used for chl-a retrieval from inland water bodies, contrary to the blue-green band ratios that are generally used for ocean waters (Molkov et al., 2019). This has been corroborated by research completed by Fadel, Faour and Slim (2016), Lim and Choi (2015), Soomets et al. (2020), Li et al. (2021), Yadav et al. (2019), Deutsch, Alameddine and El-Fadel (2014), Watanabe et al. (2015), Patra et al. (2017), Bande et al. (2018), Watanabe et al. (2017), Kim, Ko and Nam (2016) and Masocha et al. (2018), who all used the red and NIR bands, either as band ratios or in combination with other bands to retrieve chl-a from Landsat 8 and Sentinel 2. The literature review conducted by Matthews (2011) found some studies made use of a 700:670 nm ratio in chl-a estimations, however Landsat 8 does not have bands positioned at these wavelengths, hence this ratio cannot be applied to Landsat 8 imagery. Sentinel 2, however, has B5 and B4 positioned closely to 700nm and 670nm respectively, and studies conducted by Grendaitė et al. (2018), Sòria-Perpinyà et al. (2021), Chen et al. (2017b), Ansper and Alikas (2018) and Molkov et al. (2019) have used this band ratio for chl-a retrieval with successful results ($R^2 > 0.7$). The red edge bands of Sentinel 2 (B5, B6, B7, B8a) can also be used for chl-a estimations (Ha et al., 2017; Yadav et al., 2019), often in combination with other bands (Grendaitė et al., 2018; Ansper and Alikas, 2018; Cairo et al., 2020; Buma and Lee, 2020; Karaoui et al., 2019; Mansaray et al., 2021; Toming et al., 2016). Many studies conducted on chl-a retrieval from Landsat 8 and Sentinel 2 using different bands and band combinations, achieved varying results demonstrating that there is no agreement as to which bands should be used for the remote estimation of chl-a.

Studies conducted on TSS retrieval found Landsat 8 B1 to B5 and Sentinel 2 B2 to B8 capable of estimating TSS, with many studies making use of Landsat 8 B4 and B5, and Sentinel 2 B4 and B8. This highlights the capabilities of the red and NIR regions for TSS retrieval as corroborated by Matthews (2011) and Liu et al. (2017).

CDOM studies mainly used B2 to B4 from both Landsat 8 and Sentinel 2; these bands contain the blue and green regions, which has an absorption peak at 440 nm, and CDOM can only influence regions at wavelengths less than 550 nm (Alcântara et al., 2016; Matthews, 2011; Gholizadeh, Melesse and Reddi, 2016). However, some studies (Shang et al., 2021; Olmanson et al., 2020; Olmanson et al., 2016; Chen et al., 2017b) used Landsat 8 and Sentinel 2 B5, which falls at a wavelength greater than 550 nm, suggesting the possibilities of using these bands in future CDOM retrieval research.

Literature suggests that the use of the red band, either individually or as part of a band ratio, can be used to retrieve SDD (Matthews, 2011; Gholizadeh, Melesse and Reddi, 2016; Olmanson et al., 2016; Deutsch, Alameddine and El-Fadel, 2014; Mansaray et al., 2021; Deutsch et al., 2021; González-Márquez et al., 2018; Masocha et al., 2018). However, some studies used other bands in the visible, NIR, and red edge regions of the EMS (Bonansea et al., 2019a; Bonansea et al., 2019b; Sòria-Perpinyà et al., 2021; Pizani et al., 2020; Sòria-Perpinyà et al., 2020), suggesting that other bands can also be used to retrieve SDD.

Most studies on turbidity retrieval predominantly used the visible and NIR, but mostly the red band (e.g.: Sharaf El Din, 2020; Liu and Wang, 2019; Mansaray et al., 2021; Mushtaq and Nee Lala, 2017; Quang et al., 2017; Bande et al., 2018; González-Márquez et al., 2018; Masocha et al., 2018; Gholizadeh, Melesse and Reddi, 2016; Matthews, 2011).

Other water quality parameters such as TP, TN, DO, COD, ammonia, BOD, DOC, Salinity, EC, etc (Tables 2.10 – 2.13), have been estimated to a lesser extent than chl-a, TSS, CDOM, Turbidity and SDD, but have also made use of the visible and NIR regions. Various bands and band ratios have been used to retrieve these parameters, however studies conducted are limited and therefore trends in the band/band ratios used cannot be determined, suggesting the need for more research to be conducted in remote sensing estimation of these parameters.

Studies also reveal that empirical algorithms are most often used in water quality parameter estimation (Deutsch, Alameddine and El-Fadel, 2014; Laili et al., 2015; Chen et al., 2017a; Chen et al., 2017b; Alcântara et al., 2016; Watanabe et al., 2015; Patra et al., 2017; Ansper and Alikas, 2018; Bonansea et al., 2019b; Kurniadin and Jaelani, 2016; Molkov et al., 2019). However, there has been a steady increase in the use of machine learning algorithms recently (Table 2.4), with semi-analytical algorithms being the least favoured, possibly due to the complexity of developing such algorithms (Matthews, 2011; Gholizadeh, Melesse and Reddi, 2016).

2.7. Conclusion

This literature review focused on the retrieval of water quality parameters from Landsat 8 and Sentinel 2. The most retrieved parameter was chl-a, followed by TSS, and then CDOM, SDD and turbidity, all of which are optically active parameters. Parameters such as TP, TN, and DO were studied to a lesser extent, suggesting the need for more research to be conducted in the retrieval of these parameters. The visible and NIR bands were most often used in the retrieval of all water quality parameters for both Landsat 8 and Sentinel 2 images, generally as part of band ratios or combinations. Empirical algorithms were by far the most widely used in the retrieval of water quality parameters; however, there has been a steady increase in the use of machine learning in recent years. Although Landsat 8 and Sentinel 2 have played a great role in retrieving water quality parameters, the recent launch of Landsat 9, in tandem with the already orbiting Landsat 8, Sentinel 2A, and Sentinel 2B, provides water resource managers with an unparalleled free source of information, which can be used to supplement current water quality monitoring methods.

CHAPTER 3

CHLOROPHYLL-A AND TOTAL SUSPENDED SOLIDS ALGORITHMS FOR MONITORING WATER QUALITY IN THE INANDA DAM, KWA-ZULU NATAL, USING REMOTELY SENSED LANDSAT 8 AND SENTINEL 2 IMAGERY

This chapter is based on Moodley, V. and Ngetar, N.S. Chlorophyll-a and total suspended solids algorithms for monitoring water quality in the Inanda Dam, Kwa-Zulu Natal, using remotely sensed Landsat 8 and Sentinel 2 imagery. (Submitted to the *Journal of Spatial Science*)

Abstract

Freshwater resources, while crucial for the survival of all living organisms, only make up approximately two percent of all available water on earth and are subject to various anthropogenic and natural influences. It is therefore vital to monitor, conserve and sustain the current freshwater resources available to ensure the continued survival of humans, plant, and animal species. Traditional water quality monitoring methods are laborious, expensive, time-consuming, do not account for variations over large water bodies, and are almost impossible to conduct in inaccessible areas. The launch of Landsat 8 and Sentinel 2 satellites, with their improved specifications, provide a better alternative to traditional methods, and makes it possible to monitor water bodies of varying sizes. This study developed empirical algorithms to estimate chlorophyll-a and total suspended solids in the Inanda Dam using Landsat 8 and Sentinel 2. Radiance and reflectance values were extracted for bands and band ratios, and linear regression algorithms developed using in-situ concentrations, radiance, and reflectance values, to estimate chlorophyll-a and total suspended solids from satellite imagery. The results indicated that Landsat 8 and Sentinel 2 could be used to develop empirical algorithms to estimate chlorophyll-a and total suspended solids. The retrieval algorithms obtained R^2-values greater than 0.8, however the algorithms developed are both site and time specific, and therefore more research should be conducted on water quality and remote sensing.

Keywords: Landsat 8, Sentinel 2, algorithm development, water quality monitoring

3.1. Introduction

Freshwater resources, which are crucial in ensuring the survival of humankind and various living organisms, are also one of the most threatened resources (Mamun, Kim and An, 2021). A combination of stressors such as agricultural activities, industrialization, urbanization, and climate change severely impede the quality of inland water bodies globally (Ciancia et al., 2020; Mamun, Kim and An, 2021; Sharaf El Din, 2020). It has thus become vital to monitor the quality of lakes, rivers, dams, and reservoirs worldwide (Soomets et al., 2020; Mamun, Kim and An, 2021; Zhang, Huang and Wang, 2020). Water quality has traditionally been monitored using in-situ point sampling and laboratory analysis of the collected water samples. These methods, though accurate, are also time-consuming, expensive, labour intensive, and do not provide a complete overview of a water body's water quality (Guo et al., 2021; Prasad, Saluja and Garg, 2020; Ouma, Noor and Herbert, 2020; Grendaitė et al., 2018; Pu et al., 2019). The limitations of monitoring water quality using traditional water quality methods have provided an opportunity for the use of remote sensing as a tool for monitoring inland water quality (Guo et al., 2021; Markogianni et al., 2017; Bonansea et al., 2019a). The use of satellite remote sensing has made it possible to monitor various water quality parameters and water bodies cost-effectively, dynamically, and holistically (Markogianni et al., 2017; Ledesma et al., 2019; Pu et al., 2019).

In February 2013, the National Aeronautics and Space Administration (NASA) launched the eighth satellite in its Landsat series, Landsat 8. This satellite has an improved 12-bit radiometric resolution, good signal-to-noise ratio (SNR) and 11 bands with a spatial resolution of 30 m in the visible, near-infrared (NIR) and short-wave infrared (SWIR) regions. These developments in satellite remote sensing makes it possible to retrieve water quality parameters from smaller water bodies, which was previously unachievable (Roy et al., 2014; Bresciani et al., 2018; Loveland and Irons, 2016). Further to these developments, the European Space Agency (ESA) launched twin satellites, Sentinel 2A and Sentinel 2B, on 23 June 2015 and 7 March 2017, respectively (Bresciani et al., 2018; Bonansea et al., 2019b). These imageries also consist of a 12-bit radiometric resolution, a spatial resolution of between 10 m to 60 m for 13 bands, a temporal resolution of 5 days when both Sentinel 2 satellites are considered, and good SNR (Drusch et al., 2012; Bresciani et al., 2018; Chen et al., 2017b; Toming et al., 2016). While both satellites have not been designed for aquatic studies (Toming et al., 2016; Vanhellemont and Ruddick, 2016), these specifications make it possible to monitor inland water bodies (Bresciani et al., 2018; Gerace, Schott and Nevins, 2013; Vanhellemont and Ruddick, 2016), and when both Landsat 8 and Sentinel 2 are used in tandem, the temporal resolution decreases to three days (Pahlevan et al., 2019; Ouma, Noor and Herbert, 2020). The free dissemination of Landsat 8 and Sentinel 2 imagery, together with their suitable specifications, and good spatial and temporal resolutions, has increased their potential for monitoring water quality globally (Bresciani et al., 2018; Liu et al., 2017; Vanhellemont and Ruddick, 2016).

Studies conducted on monitoring water quality remotely have made use of algorithm development, in-situ water samples and satellite imagery to estimate water quality parameters (Chen et al., 2017b; Karaoui et al., 2019; Mushtaq and Nee Lala, 2017; Yepez et al., 2018; Bande et al., 2018). Due to their simplicity and ability to generate positive results, empirical methods are most used in developing algorithms for water quality research (Matthews, 2011).

Two water quality parameters commonly monitored using remote sensing are chlorophyll-a (chl-a) and total suspended solids (TSS), due to their abilities to influence the optical properties of water (Markogianni et al., 2017) and are vital in freshwater resource management (Elangovan and Murali, 2020; Manuel et al., 2020; Ciancia et al., 2020). Chl-a can be used to determine the trophic status of a water body (Matthews, 2011) and is a marker of possible eutrophication and algal blooms, which severely affects the quality of water (Li et al., 2021; Grendaitė et al., 2018; Markogianni et al., 2017; Soomets et al., 2020). Excess TSS can affect photosynthesis, dissolved oxygen levels, cause turbidity, increase siltation, and can be used as a proxy for pollutants entering a water body (Peterson et al., 2018; Soomets et al., 2020; Yanti, Susilo and Wicaksono, 2016).

This study developed empirical algorithms to estimate chl-a and TSS in the Inanda Dam, Kwa-Zulu Natal, South Africa, using Landsat 8 and Sentinel 2 imagery. The research aims were:

1) Develop empirical algorithms to monitor chl-a and TSS from Landsat 8 and Sentinel 2 imagery and generate maps displaying the surface distribution of chl-a and TSS over the Inanda Dam using the algorithms developed.

2) Compare the accuracy of Landsat 8 radiance, Landsat 8 reflectance, Sentinel 2 Top- of-Atmosphere (TOA) reflectance, and Sentinel 2 Bottom-of-Atmosphere (BOA) reflectance for developing algorithms.

3.2. Methodology

3.2.1. Study Area

This study was conducted in the Inanda Dam, situated in Kwangcolosi, Valley of a Thousand Hills, Kwa-Zulu Natal Province, South Africa (Figure 3.1). The dam has a depth of 50 m, a length of 23 km and a surface area of 14400000 m^2 with a total capacity of 256000000 m^3 (Agunbiade and Moodley, 2014). This dam is located on the uMgeni River, which forms part of the uMgeni catchment, and flows from the Drakensburg Mountains into the Indian Ocean north of the Durban city (Namugize, Jewitt and

Graham, 2018; Agunbiade and Moodley, 2014; Matongo et al., 2015; Tinmouth, 2009). The climate of this area, which influences the formation and concentrations of chl-a and TSS, is subtropical, with dry winters, wet summers, and an average rainfall of between 900 mm – 1000 mm (Ngetar, 2002; Namugize, Jewitt and Graham, 2018). The dam is surrounded by hilly, undulating landscapes in which rural communities practice agriculture (Nkoana, 2014; Rangeti, 2014) and is a vital source of drinking water for the surrounding communities and the people of Durban, South Africa (Fischer et al., 2019).

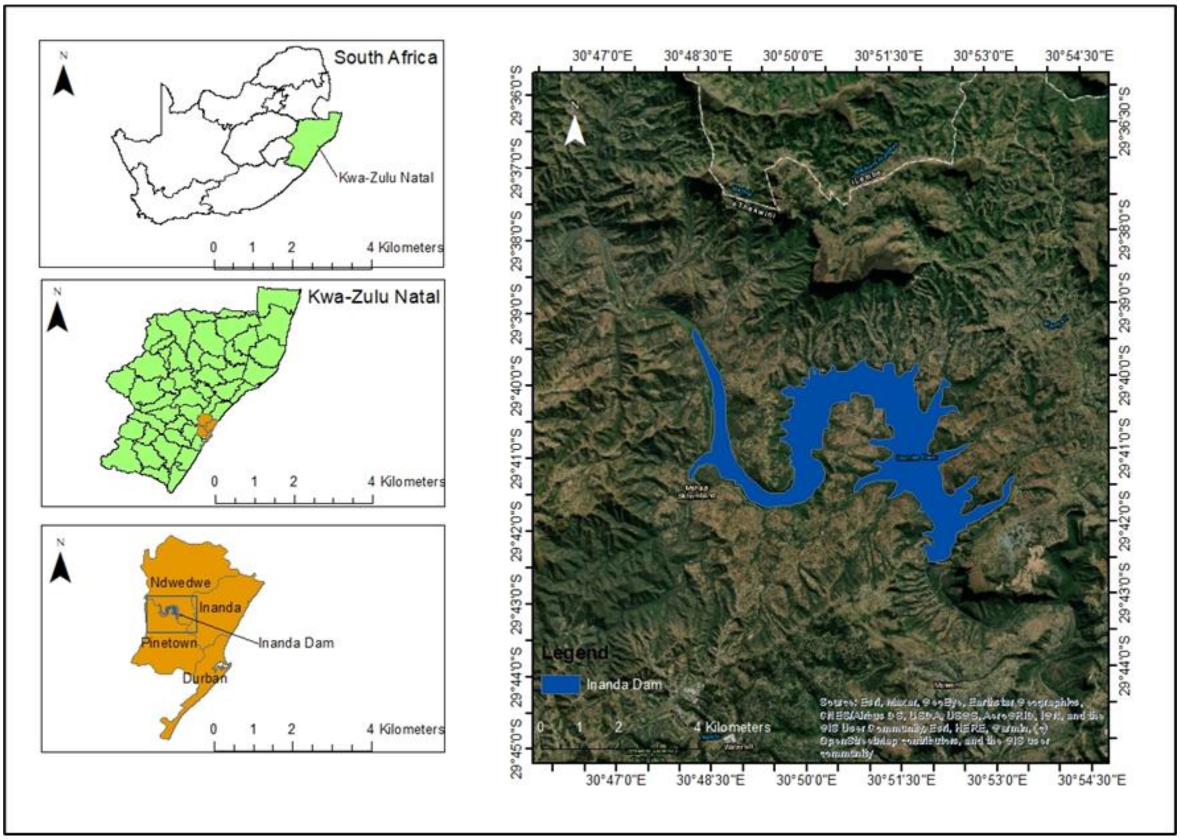

Figure 3.1: Map of Inanda Dam and its surrounding locations in Kwa-Zulu Natal, South Africa.

3.2.2. Fieldwork

Forty-five water samples were collected twice, on the 6th of March 2020 (wet season) and the 12th of May 2021 (dry season). Sample collection closely coincided with Landsat 8 (7th of March 2020 and the 12th of May 2021) and Sentinel 2 (4th of March 2020 and 13th of May 2021) overpass to obtain the most accurate results. At each point, two water samples and their GPS coordinates were collected, one for chl-a analysis and one for TSS analysis (Figure 3.2). A total of 90 samples were collected, but nine could not be used as either the chl-a or TSS concentration were outliers, and therefore the remaining 81 samples were used for the study. Figure 3.2 shows the distribution of sampling points for the wet and dry seasons.

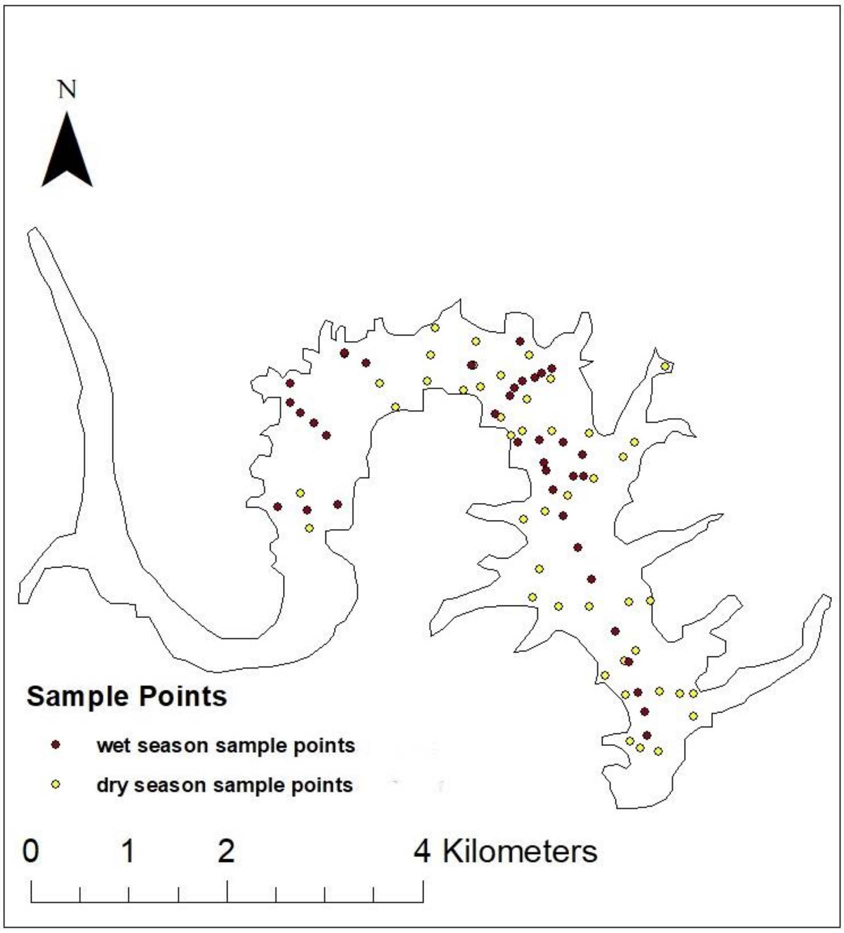

Figure 3.2: Location of wet and dry season sampling points in the Inanda Dam.

3.2.3. Laboratory Analysis

The concentration of chl-a in the water samples were measured using spectrophotometry, which filtered a water sample to obtain organisms consisting of chl-a. The chl-a was extracted using acetone after rupturing the cells of the organism and analyzed using the optical properties of chl-a. TSS concentrations were obtained using the filtration method, which included quantitatively filtering a portion of the sample through a glass fibre filter. The residue retained on the filter was gauged by gravimetric determination after drying the filter at 105 ± 2°C. Both procedures can be found in the Standard Methods for the Examination of Water and Wastewater (Prasad, Saluja and Garg, 2020; Sharaf El Din, 2020).

3.2.4. Pre-processing of Satellite Imagery

Landsat 8 and Sentinel 2 images were downloaded from the United States Geological Survey (USGS) and ESA Copernicus Hub, respectively. Landsat 8 images were atmospherically corrected to remove atmospheric effects such as gases and aerosols which impact the quality of satellite imagery and were also radiometrically corrected to convert Digital Numbers (DN) into radiance and reflectance (Bonansea et al., 2019a; Sharaf El Din, Zhang and Suliman, 2017; Kim, Ko and Nam, 2016). Both atmospheric and radiometric corrections were completed using FLAASH, an atmospheric correction module found in the ENVI software, to obtain radiance and reflectance values for bands one to seven of Landsat 8 satellite imagery (Fadel, Faour and Slim, 2016; Buma and Lee, 2020; Quang et al., 2017). Sentinel 2 images are already atmospherically corrected and available for download in two formats:

TOA and BOA reflectance, however, TOA reflectance images contain 13 bands with three different resolutions. Therefore, the bands of TOA reflectance images were resampled to one resolution (Sòria-Perpinyà et al., 2020), which was completed using the resampling function in SNAP (Ansper and Alikas, 2019). BOA reflectance images are already resampled to one resolution and therefore, no further processing was needed.

3.2.5. Algorithm development using band/band ratios and the mapping of chl-a and TSS

A Pearson correlation (as indicated by R in the upcoming sections) was used to determine the correlation between in-situ chl-a and TSS with bands/band ratios of satellite images. Landsat 8 band/band ratio radiance and reflectance of bands one to seven, and Sentinel 2 TOA and BOA band/band ratio reflectance of bands one to twelve were correlated with in-situ chl-a and TSS.

The bands/band ratios which obtained a correlation coefficient (R) of 0.8 and above with in-situ chl-a and TSS were used to maximise the accuracy of the algorithms developed. Fifty-seven data points were used to calibrate the algorithms, and the remaining 24 data points to validate the algorithms. Linear regression algorithms were developed in SPSS, using the form of $y = a+bx$, where a and b are statistically generated values, x represents the band/band ratios value, and y represents the estimated water quality parameter. The algorithms generated from Landsat 8 radiance, Landsat 8 reflectance, Sentinel 2 TOA reflectance, and Sentinel 2 BOA reflectance, which obtained the highest R^2-values, were further validated using a correlation analysis in SPSS, to determine the most accurate retrieval algorithms.

In ArcMap version 10.8.1, a geostatistical interpolation method was used to map and display the surface distribution of chl-a and TSS in the Inanda Dam using the developed algorithms.

3.3. Results

3.3.1. In-situ water quality concentrations

3.3.1.1. In-situ chl-a

During the wet and dry seasons, the overall concentration of in-situ chl-a in the Inanda Dam ranged from 0.6 µg/t to 29 µg/t (Figure 3.3(c)). In the wet season, the spatial distribution of chl-a varied from 5.7 µg/t to 29 µg/t (Figure 3.3(a)), while the dry season had a smaller variation of 0.6 µg/t to 5.7 µg/t (Figure 3.3(b)). Distribution patterns especially in the wet season show higher chl-a concentrations near the dam inlet, decreasing as water flows in the dam towards the dam wall. On the contrary, the concentration of chl-a varied in the dam during the dry season, with no specific pattern in the dam.

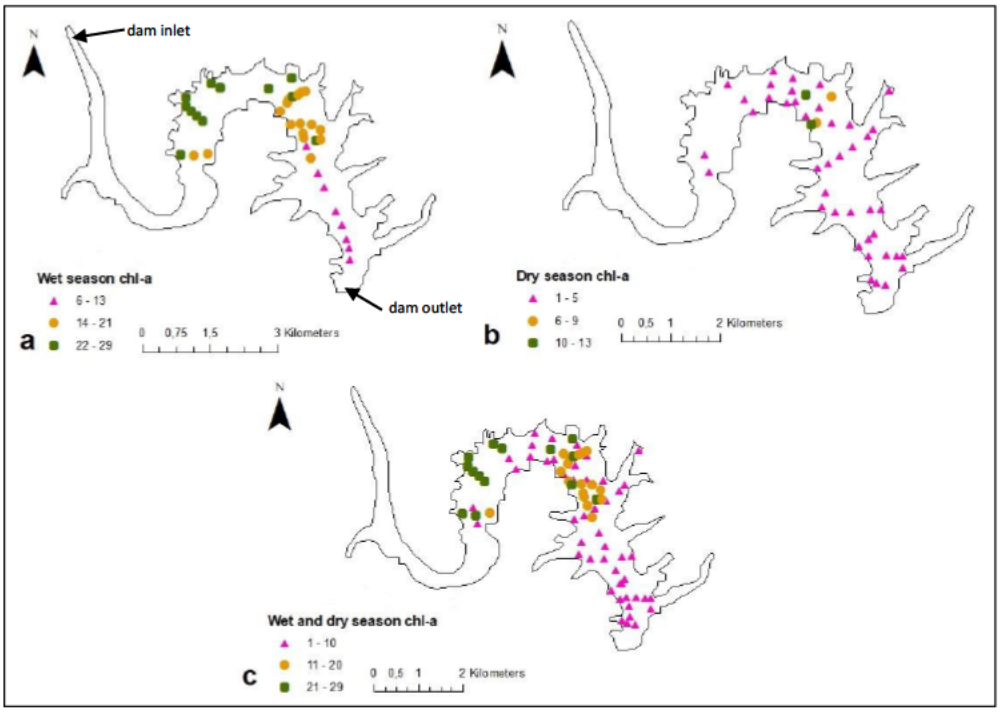

Figure 3.3: Distribution of in-situ chl-a for the (a) wet season, (b) dry season, and (c) wet and dry season.

3.3.1.2. In-situ TSS

The spatial distribution of in-situ TSS concentrations varied from 4 mg/ℓ to 10 mg/ℓ (Figure 3.4(a)) during the wet season and from 17.7 mg/ℓ to 18 mg/ℓ (Figure 3.4(b)) during the dry season. During the wet and dry seasons, an overall variation of 4 mg/ℓ to 18 mg/ℓ could be observed (Figure 3.4(c)). Generally, in the dry season, a higher TSS concentration with a limited variation was present while lower TSS concentrations with a wider variation was found in the wet season. There was no discernible trend in the pattern of TSS concentrations throughout the dam.

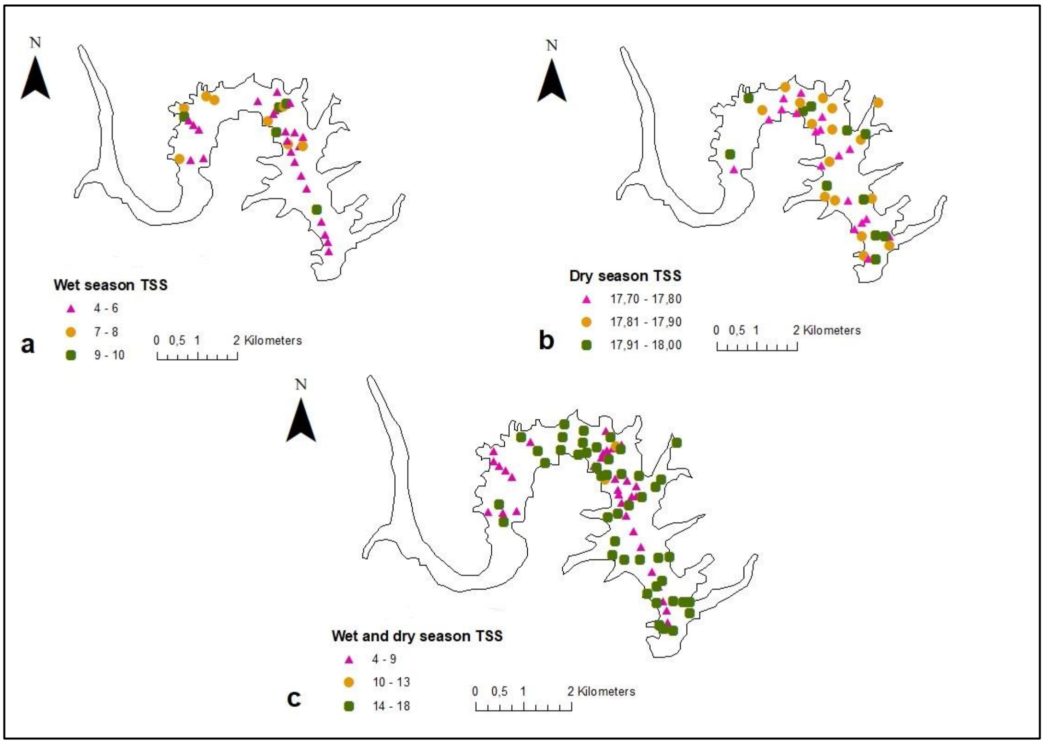

Figure 3.4: Distribution of in-situ TSS for the (a) wet season, (b) dry season, and (c) wet and dry season.

3.3.2. Correlations

3.3.2.1. Landsat 8

Table 3.1 displays the Pearson correlation R-values of 0.8 or more between Landsat 8 bands/band ratio radiance and reflectance values with in-situ chl-a and TSS, with the R^2-values indicated on the scatterplots (Figure 3.5 to Figure 3.8) displayed below. These are further analysed in sections 3.3.2.1.1 and 3.3.2.1.2.

Table 3.1: Correlations between Landsat 8 band/band ratio radiance and reflectance data, and in-situ chl-a and TSS

	Radiance		Reflectance	
Band/Band Ratio	Chl-a	TSS	Chl-a	TSS
B1	0.862	**-0.977**	-0.835	**0.983**
B2	0.882	-0.970	-0.822	0.983
B3	0.907	-0.947	-	-
B4	0.922	-0.928	-	-
B5	0.848	-0.806	-	-
B2:B1	0.902	-0.910	0.901	-0.886
B3:B1	0.917	-0.927	0.900	-0.952
B4:B1	0.931	-0.886	**0.917**	-0.935

	Radiance		Reflectance	
B6:B1	-	-	-	-0.841
B7:B1	-	-	-	-0.912
B1:B2	-0.900	0.914	-0.906	0.902
B3:B2	0.917	-0.933	0.889	-0.965
B4:B2	**0.932**	-0.882	0.912	-0.949
B7:B2	-	-	-	-0.888
B1:B3	-0.906	0.949	-0.871	0.975
B2:B3	-0.907	0.950	-0.867	0.977
B4:B3	-	-	-	0.900
B5:B3	-	0.907	-	
B1:B4	-0.923	0.917	-0.883	0.970
B2:B4	-0.926	0.908	-0.881	0.972
B3:B4	-	-0.803	-	-0.888
B5:B4	-	0.889	-	-
B1:B5	-	-	-0.815	0.885
B2:B5	-	-	-	0.847
B3:B5	-	-0.893	-	-0.885
B4:B5	-	-0.876	-	-0.854
B6:B5	-	-	-	-0.808
B7:B5	-	-	-	-0.815
B1:B6	-	-	-	0.895
B2:B6	-	-	-	0.878
B5:B6	-	-	-	0.822
B1:B7	-	-	-	0.898
B2:B7	-	-	-	0.885
B5:B7	-	-	-	0.831

3.3.2.1.1. Landsat 8 radiance

The correlation of bands B1, B2, and B5 radiance and in-situ chl-a was between 0.8 to 0.899, while B3, B4, B2:B1, B3:B1, B4:B1, B1:B2, B3:B2, B4:B2, B1:B3, B2:B3, B1:B4 and B2:B4 radiance obtained correlation values between 0.9 to 0.932 with in-situ chl-a. The most successful correlation was between the radiance of B4:B2 and in-situ chl-a, which obtained a correlation of 0.932 and a R^2-value of 0.869 (Figure 3.5).

In relation to TSS, the correlation between bands/band ratios B5, B4:B1, B4:B2, B3:B4, B5:B4, B3:B5 and B4:B5 radiance and in-situ TSS varied from 0.8 to 0.899. On the contrary, the correlation of bands B1, B2, B3, B4, B2:B1, B3:B1, B1:B2, B3:B2, B1:B3, B2:B3, B5:B3, B1:B4 and B2:B4 radiance with in-situ TSS was higher varying from 0.9 to 0.977. B1 radiance obtained the highest correlation and R^2-value with in-situ TSS (Figure 3.6), at a value of -0.977 and 0.955 respectively.

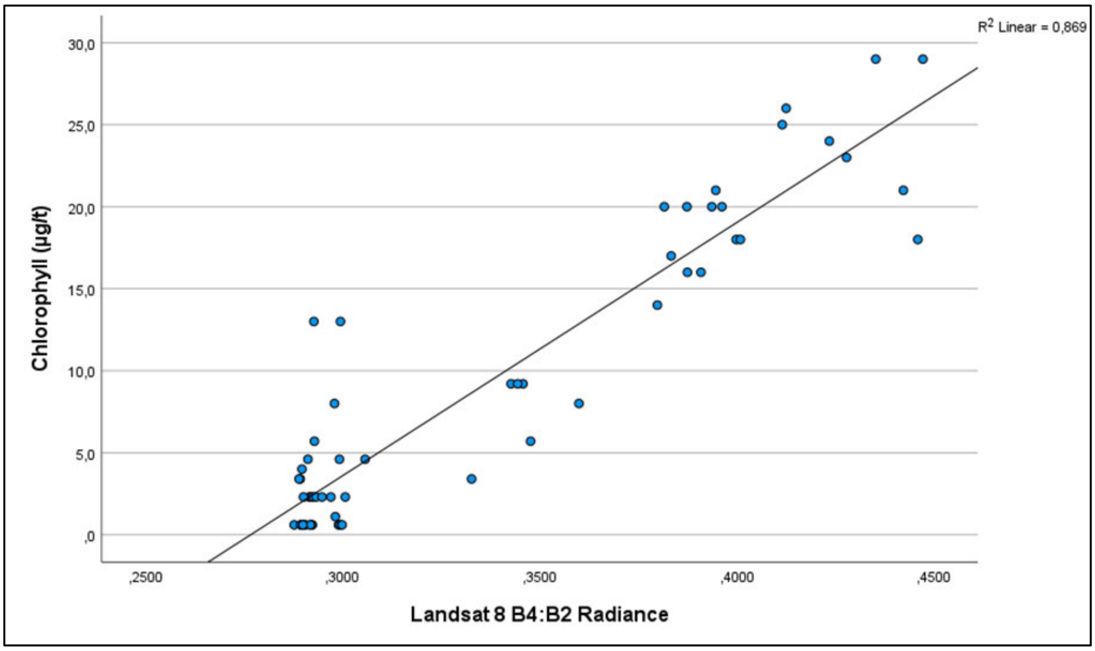

Figure 3.5: Correlation between in-situ chl-a and Landsat 8 B4:B2 Radiance.

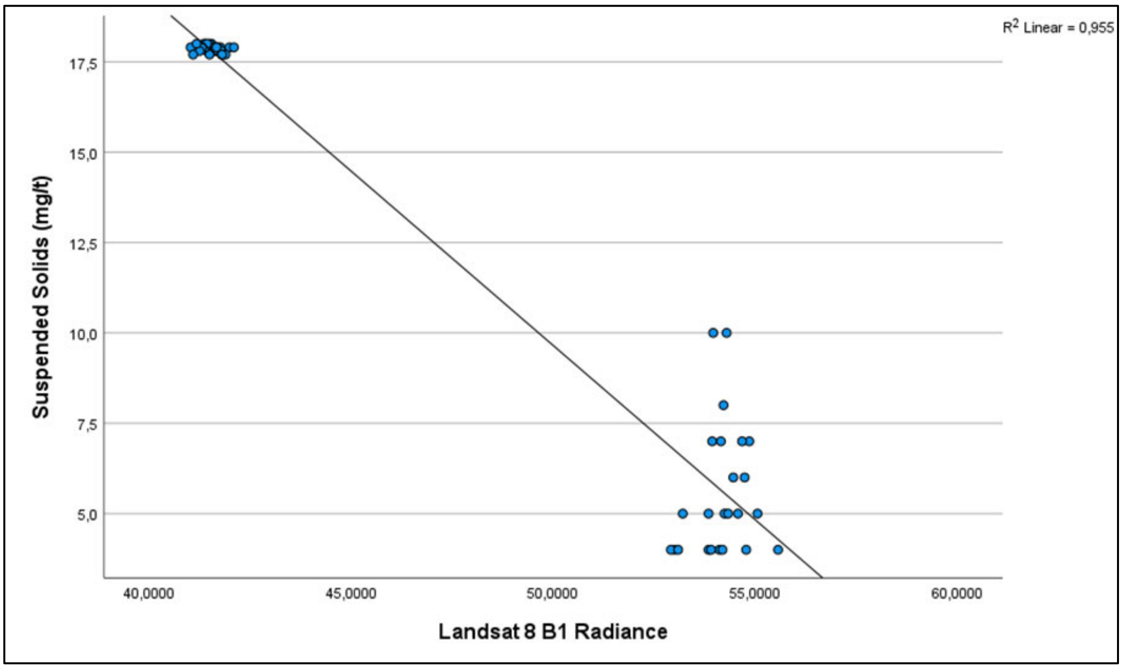

Figure 3.6: Correlation between in-situ TSS and Landsat 8 B1 Radiance.

3.3.2.1.2. Landsat 8 reflectance

A correlation of 0.8 to 0.899 was obtained between in-situ chl-a and B1, B2, B3:B2, B1:B3, B2:B3, B1:B4, B2:B4 and B1:B5 reflectance, while B2:B1, B3:B1, B4:B1, B1:B2 and B4:B2 reflectance obtained correlation values between 0.9 to 0.917 with in-situ chl-a. Figure 3.7 below displays the most successful correlation and R^2-value obtained between B4:B1 reflectance and in-situ chl-a (R = 0.917 and R^2 = 0.842).

In relation to TSS, B2:B1, B6:B1, B7:B2, B3:B4, B1:B5, B2:B5, B3:B5, B4:B5, B6:B5, B7:B5, B1:B6, B2:B6, B5:B6, B1:B7, B2:B7 and B5:B7 reflectance produced correlations between 0.8 to 0.899 with in-situ TSS. However, B1, B2, B3:B1, B4:B1, B7:B1, B1:B2, B3:B2, B4:B2, B1:B3, B2:B3, B4:B3, B1:B4 and B2:B4 reflectance yielded higher correlations ranging from 0.9 to 0.983 with in-situ TSS. The highest correlation was between B1 reflectance and in-situ TSS at 0.983, with a R^2-value of 0.966 (Figure 3.8).

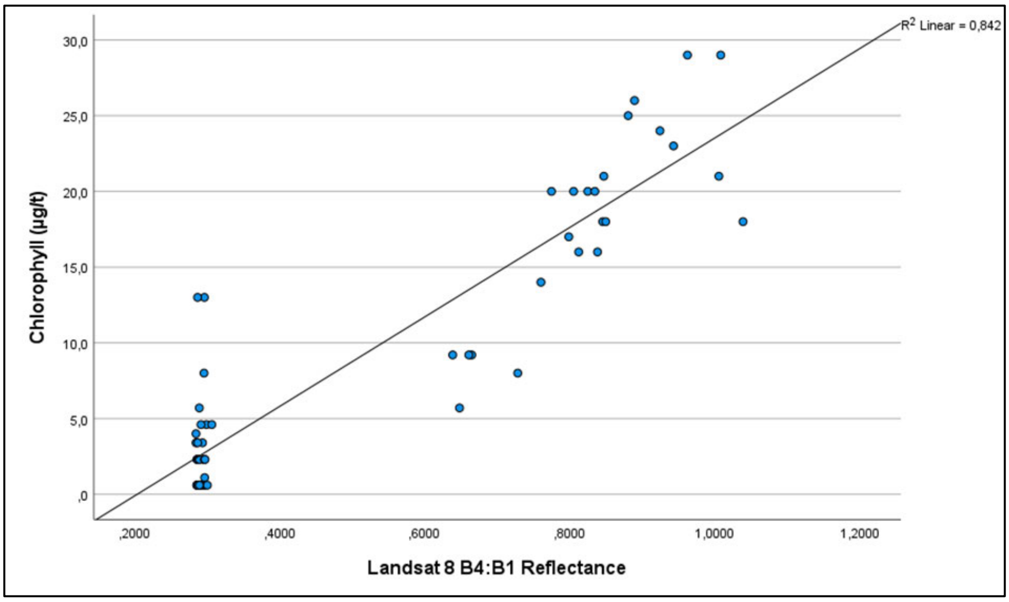

Figure 3.7: Correlation between in-situ chl-a and Landsat 8 B4:B1 Reflectance.

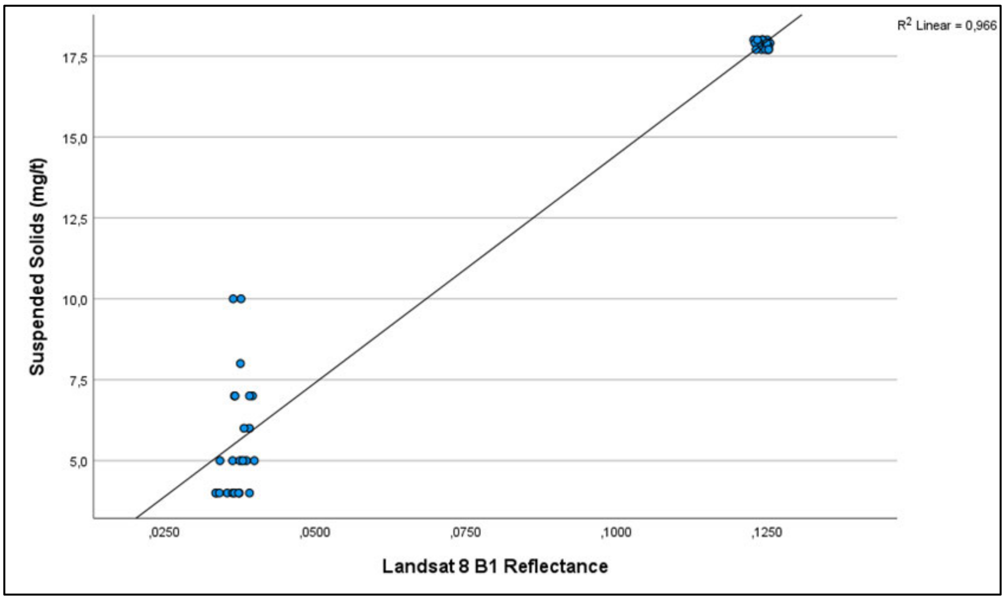

Figure 3.8: Correlation between in-situ TSS and Landsat 8 B1 Reflectance.

3.3.2.2. Sentinel 2

Table 3.2 displays the Pearson correlation R-values of 0.8 or more between Sentinel 2 bands/band ratio TOA and BOA reflectance values with in-situ chl-a and TSS, with the R^2-values indicated on the scatterplots (Figure 3.9 to 3.12) displayed below. These are further analysed in sections 3.3.2.2.1 and 3.3.2.2.2.

Table 3.2: Correlations between Sentinel 2 band/band ratio TOA and BOA reflectance, and in-situ chl-a and TSS

	TOA		BOA	
Band/Band Ratio	Chl-a	TSS	Chl-a	TSS
B1	-	-	**0.903**	**-0.950**
B3	**0.910**	-0.859	-	-
B4	0.902	-0.819	-	-
B5	0.807	-	0.843	-
B3:B2	-	-	0.865	-0.933
B4:B2	-	-	0.883	-0.913
B5:B2	-	-	0.828	-
B1:B3	-	**0.889**	-	0.852
B2:B3	-	-	-0.820	0.921
B10:B3	-0.825	0.897	-	-
B11:B3	-	-	-	0.805
B12:B3	-	-	-	0.809
B1:B4	-	0.867	-	0.811
B2:B4	-	-	-0.838	0.909
B10:B4	-0.828	0.891	-	-
B1:B5	-0.801	0.840	-0.848	-
B6:B5	-	0.853	-	-
B7:B5	-	-	-	0.811
B10:B5	-0.841	0.878	-	-
B11:B5	-	-	-	0.856
B5:B6	-	-0.834	-	-
B10:B6	-0.804	0.824	-	-
B5:B7	-	-	-	-0.837
B10:B7	-	0.821	-	-

B10:B8	-	0.817	-	-
B10:B8a	-	0.811	-	-
B3:B10	0.859	-0.876	-	-
B4:B10	0.857	-0.857	-	-
B5:B10	0.821	-	-	-
B5:B11	-	-	-	-0.844

3.3.2.2.1. Sentinel 2 TOA

The correlation of bands B5, B10:B3, B10:B4, B1:B5, B10:B5, B10:B6, B3:B10, B4:B10 and B5:B10 TOA reflectance and in-situ chl-a varied from 0.8 to 0.899, however B3 and B4 TOA reflectance obtained correlations greater than 0.9 with chl-a. The most successful correlation (R = 0.910) was between B3 TOA and in-situ chl-a, with a R^2-value of 0.831 (Figure 3.9).

In relation to TSS, B3, B4, B1:B3, B10:B3, B1:B4, B10:B4, B1:B5, B6:B5, B10:B5, B5:B6, B10:B6, B10:B7, B10:B8, B10:B8a, B3:B10 and B4:B10 TOA reflectance obtained correlations ranging from 0.8 to 0.889 with in-situ TSS. The highest correlation was found between B1:B3 TOA reflectance and in-situ TSS (R = 0.889), with a R^2-value of 0.799 (Figure 3.10).

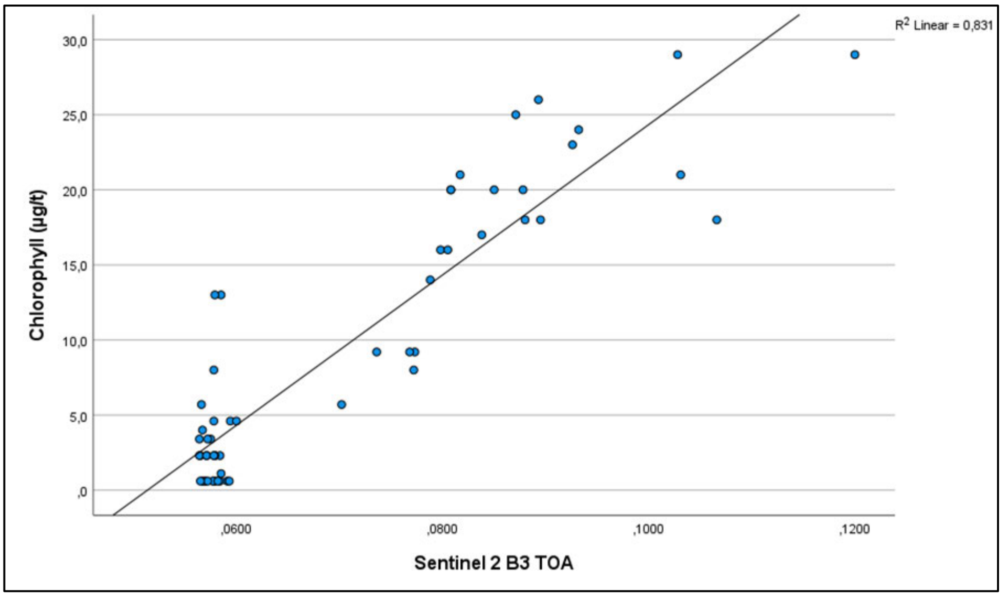

Figure 3.9: Correlations between in-situ chl-a and Sentinel 2 B3 TOA reflectance.

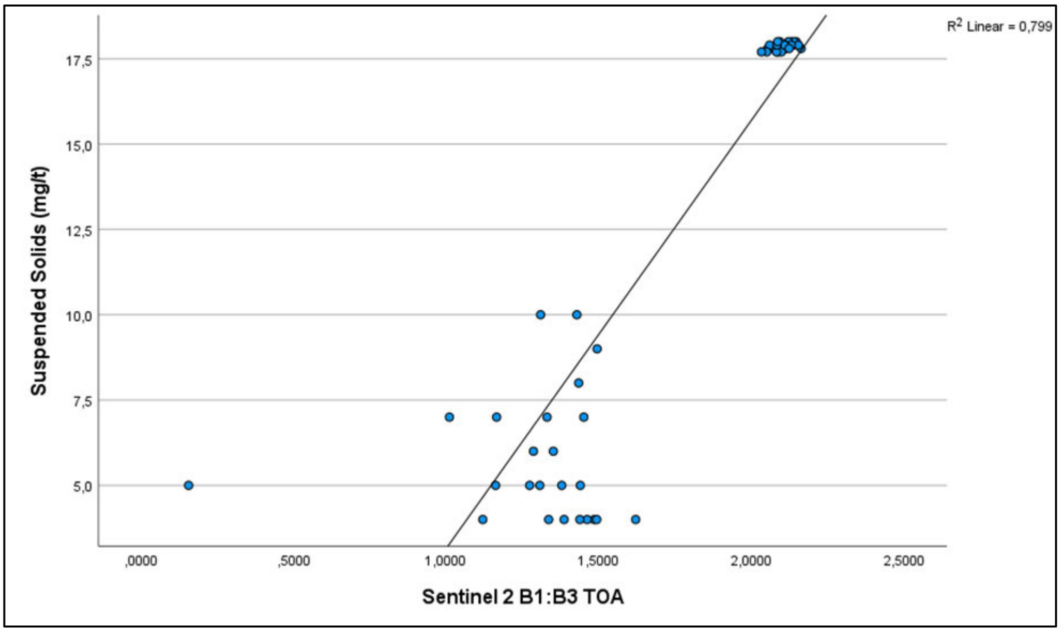

Figure 3.10: Correlations between in-situ TSS and Sentinel 2 B1:B3 TOA Reflectance.

3.3.2.2.2. Sentinel 2 BOA

The correlation of bands B5, B3:B2, B4:B2, B5:B2, B2:B3, B2:B4 and B1:B5 BOA reflectance and in-situ chl-a varied from 0.8 to 0.903, with the most successful correlation obtained between B1 BOA reflectance and in-situ chl-a at 0.903, with a R^2-value of 0.816 (Figure 3.11).

B1:B3, B11:B3, B12:B3, B1:B4, B7:B5, B11:B5, B5:B7 and B5:B11 BOA reflectance obtained correlations ranging from 0.8 to 0.899 with in-situ TSS, while B1, B3:B2, B4:B2, B2:B3 and B2:B4 BOA reflectance and in-situ TSS resulted in correlations varying from 0.9 to 0.950. Figure 3.12 below displays the highest correlation of -0.950 between B1 BOA reflectance and in-situ TSS, also obtaining a R^2-value of 0.902.

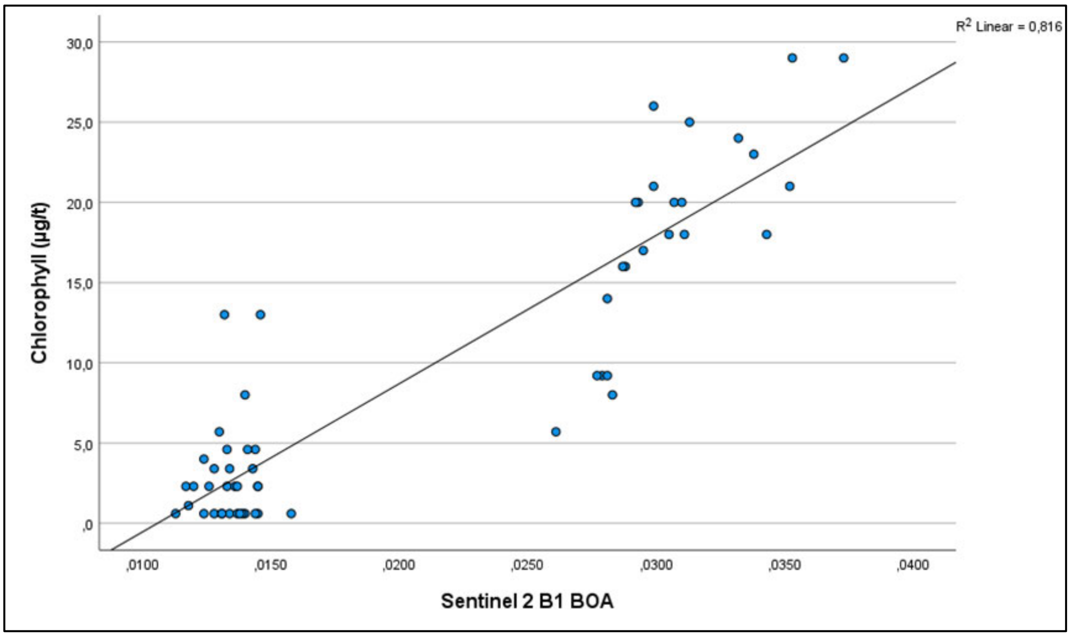

Figure 3.11: Correlations between in-situ chl-a and Sentinel 2 B1 BOA reflectance.

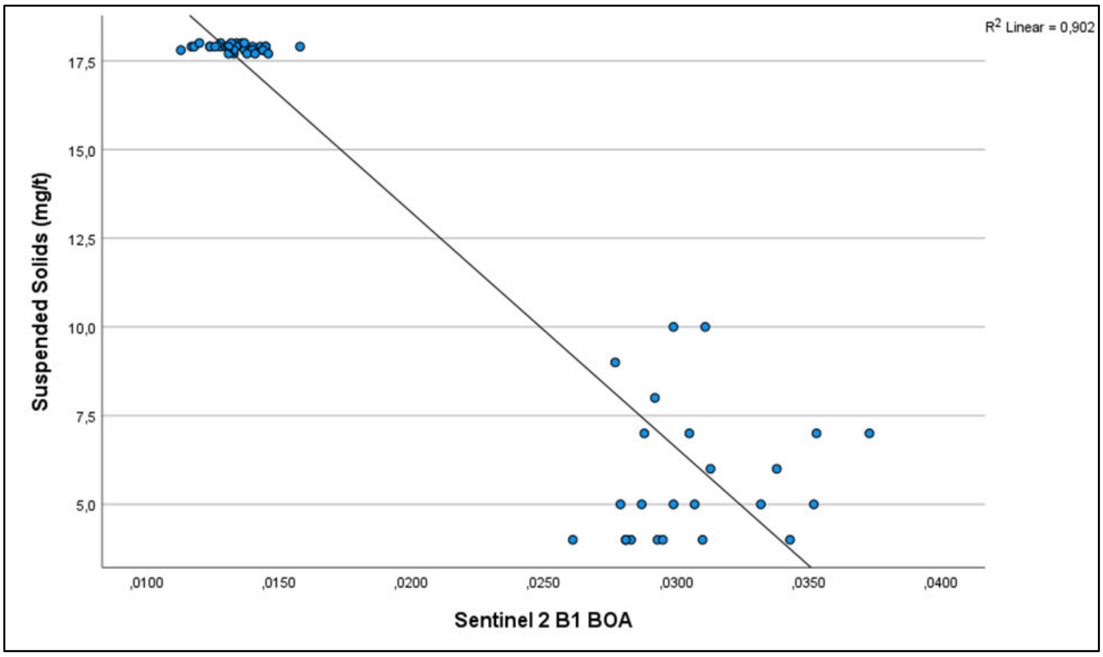

Figure 3.12: Correlations between in-situ TSS and Sentinel 2 B1 BOA Reflectance.

3.3.3. Algorithms

3.3.3.1. Chl-a

Several algorithms were generated in this study, however, only the most successful regression algorithms used to estimate chl-a from Landsat 8 and Sentinel 2 imagery are presented (Table 3.3). Landsat 8 B4:B2, B4:B1 and Sentinel 2 B3 and B1 displayed a strong correlation (R > 0.9) with in-situ chl-a and were used to develop chl-a retrieval algorithms. All the algorithms produced R^2-values greater than 0.8, however the Landsat 8 algorithms yielded slightly higher R^2-values and slightly lower standard errors (SE) than the Sentinel 2 algorithms, indicating that the Landsat 8 algorithms were marginally more accurate than the Sentinel 2 algorithms. Comparatively, the Landsat 8 radiance algorithm (R^2 = 0.869) performed better than the Landsat 8 reflectance algorithm (R^2 = 0.842), while the Sentinel 2 TOA algorithm (R^2 = 0.828) performed better than the Sentinel 2 BOA reflectance algorithm (R^2 = 0.816), by a small margin. When validated, all the algorithms produced a correlation value of greater than 0.9, indicating their strong capability to retrieve chl-a from both satellites.

Table 3.3: Most accurate chl-a algorithms generated using Landsat 8 radiance and reflectance values, and Sentinel 2 TOA and BOA reflectance values

Satellite	**Algorithm Type**	**Band/Band ratio**	**Algorithm**	**R**	**R^2**	**SE (µg/t)**	**Validated R**
Landsat 8	Radiance	B4:B2	*y= -42.730+ 154.423x*	0.932	0.869	3.2883	0.928
Landsat 8	Reflectance	B4:B1	*y= -6.037+29.579x*	0.917	0.842	3.6123	0.938
Sentinel 2	TOA reflectance	B3	*y= -25.925+ 502.455x*	0.910	0.828	3.7678	0.925

Sentinel 2	BOA reflectance	B1	*y= -9.799+ 924.677x*	0.903	0.816	3.896	0.916

3.3.3.2. TSS

In relation to TSS, of all the algorithms generated in this study, Table 3.4 represents the most accurate regression algorithms used to estimate TSS from Landsat 8 and Sentinel 2 imagery. Landsat 8 B1 displayed a strong correlation ($R > 0.95$) with in-situ TSS, and the resulting algorithms had R^2-values of greater than 0.95, indicating a statistically significant level of accuracy. The algorithms were further validated, resulting in a correlation greater than 0.95, with an SE of less than 1.5 mg/t. Sentinel 2 B1:B3 TOA reflectance and B1 BOA reflectance were most successful in developing TSS algorithms. Both bands (B1 and B3) displayed a strong correlation with TSS ($R > 0.85$), and the resulting algorithms had R^2-values of greater than 0.75 and SE less than 3 mg/t. The Landsat 8 reflectance algorithms ($R^2 = 0.966$) outperformed the Landsat 8 radiance algorithms ($R^2 = 0.955$) slightly, while the Sentinel 2 BOA algorithms performed significantly better than the TOA reflectance algorithms, obtaining a higher R^2-value ($R^2 = 0.902$) and lower SE (1.9429). After validating all four sets of algorithms, a correlation value greater than 0.9 was obtained. Overall, the Landsat 8 algorithms outperformed the Sentinel 2 algorithms; however, all four sets of algorithms can be used to retrieve TSS.

Table 3.4: Most accurate TSS algorithms generated using Landsat 8 radiance and reflectance values, and Sentinel 2 TOA and BOA reflectance values

Satellite	**Algorithm Type**	**Band/Band ratio**	**Algorithm**	**R**	R^2	**SE (mg/t)**	**Validated R**
Landsat 8	Radiance	B1	*y= 57.905-0.965x*	0.977	0.955	1.3335	0.970
Landsat 8	Reflectance	B1	*y= 0.350+140.827x*	0.983	0.966	1.1579	0.977
Sentinel 2	TOA reflectance	B1:B3	*y= -9.344+ 12.563x*	0.889	0.790	2.8363	0.926
Sentinel 2	BOA reflectance	B1	*y= 26.496- 663.317x*	0.950	0.902	1.9429	0.938

3.3.4. Surface distribution maps of chl-a and TSS in the Inanda dam

3.3.4.1. Surface distribution of chl-a in the Inanda Dam

The surface distribution of in-situ and estimated chl-a in the dam is shown in Figure 3.13. The in-situ distribution of chl-a varies from 0.6µg/t to 29µg/t, the highest occurring along the narrow dam inlet and decreasing as water flows downstream towards the dam wall as the dam widens. Despite the existence of this broad trend, there are some variations in the dam, as indicated by the letters x, y, and z in Figure 3.13. For example, there is a decrease in chl-a at point x, an increase at point y and a slight increase at point z. This general pattern of chl-a distribution is replicated to a varying degree by those mapped using the developed chl-a algorithms (Figures 3.13 (b) to (e)). A more detailed comparison shows that of all the algorithms, the Landsat 8 B4:B2 radiance algorithm more accurately mapped the distribution and concentrations of chl-a (Figure 3.13 (b)), than the Landsat 8 B4:B1 reflectance algorithm (Figure 13 (c)), Sentinel 2 B3 TOA reflectance algorithm (Figure 3.13 (d)), and

Sentinel 2 B1 BOA reflectance algorithm (Figure 3.13 (e)). The Landsat 8 B4:B1 reflectance algorithm (Figure 3.13 (c)) was unable to retrieve chl-a concentrations at the lowest and highest ends of the scale and the Sentinel 2 B3 TOA algorithm (Figure 3.13 (d)) overestimated chl-a concentrations. The Sentinel 2 B1 BOA algorithm (Figure 3.13 (e)) could not estimate high chl-a concentrations, however, could estimate lower chl-a concentrations found close to the dam wall.

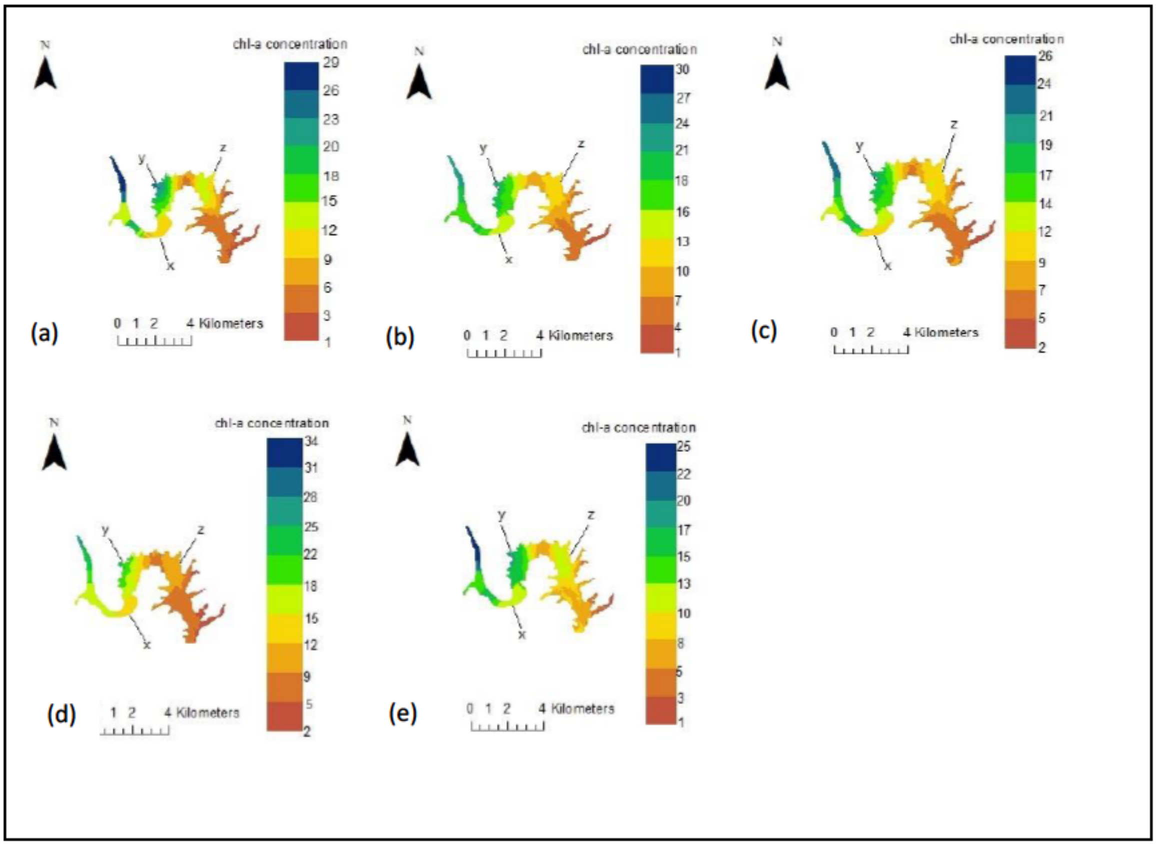

Figure 3.13: Surface distribution of chl-a according to (a) in-situ chl-a, (b) Landsat 8 B4:B2 radiance algorithm, (c) Landsat 8 B4:B1 reflectance algorithm, (d) Sentinel 2 B3 TOA reflectance algorithm, and (e) Sentinel 2 B1 BOA reflectance algorithm.

3.3.4.2. Surface distribution of TSS in the Inanda Dam

Unlike chl-a, the broad distribution of in-situ TSS concentrations in the Inanda Dam displayed a lower concentration near the dam inlet but higher concentrations along the edges of the dam and close to the dam wall downstream (Figures 3.14 (a) to 10 (e)). In-situ TSS concentrations ranged from 4mg/t to 18mg/t, similar to the concentrations extracted by the algorithms (Figures 3.14 (b) to (e)), except for some overestimations beyond this range by Landsat 8 B1 reflectance algorithm, Sentinel 2 B1:B3 TOA reflectance algorithm, and Sentinel 2 B1 BOA reflectance algorithm (Figures 3.14 (c) to (e)) respectively. The Landsat 8 B1 radiance algorithm estimated the exact range of TSS concentration in the dam as the in-situ TSS, with a quasi-similar spatial distribution pattern. In comparison with in-situ TSS, Landsat 8 B1 reflectance algorithm had difficulty estimating the lower limit of TSS concentrations but accurately estimated its upper limits as with in-situ TSS. Both Sentinel 2 algorithms estimated TSS concentrations beyond the lower limit of in-situ TSS (Figures 3.14 (d) and (e)).

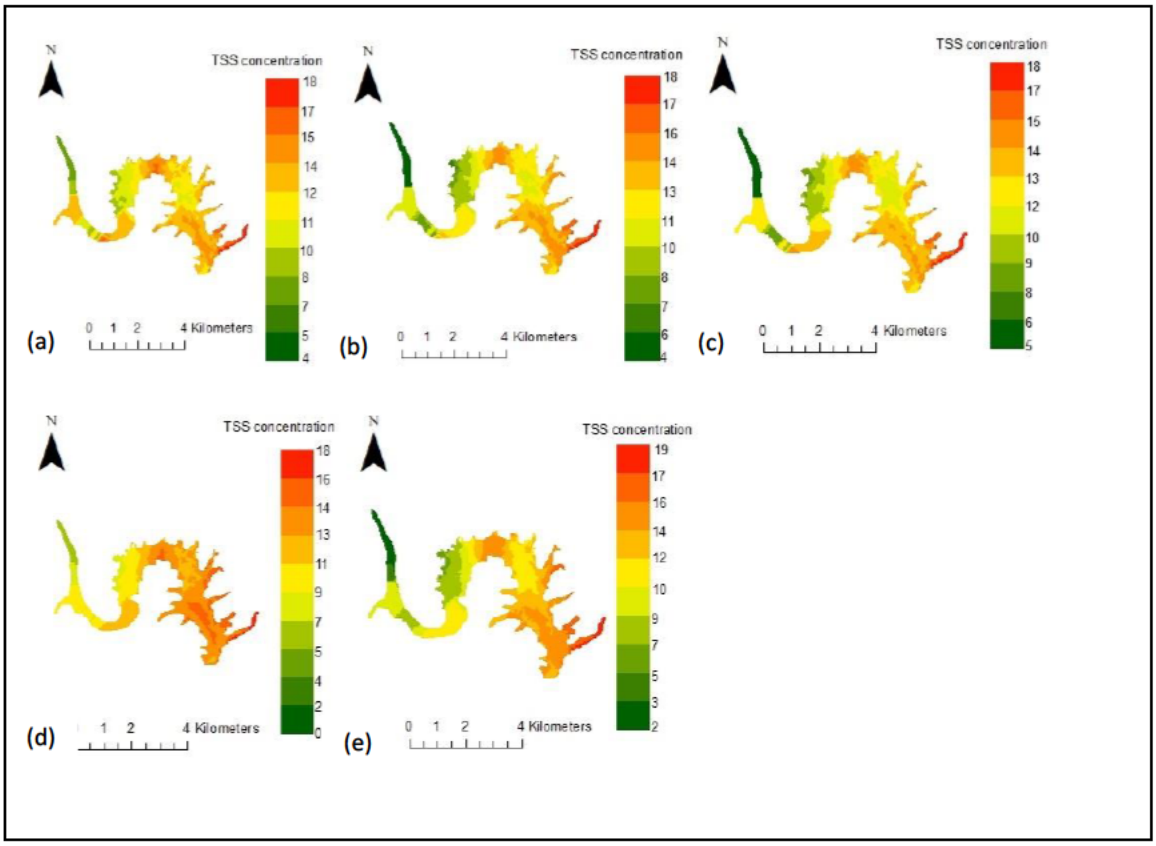

Figure 3.14: Surface distribution of TSS according to (a) in-situ data, (b) Landsat 8 B1 radiance algorithm, (c) Landsat 8 B1 reflectance algorithm, (d) Sentinel 2 B1:B3 TOA reflectance algorithm, and (e) Sentinel 2 B1 BOA reflectance algorithm.

3.4. Discussion

This study investigated the use of Landsat 8 and Sentinel 2 for chl-a and TSS retrieval. The results reveal that both satellites can successfully retrieve both water quality parameters from the Inanda Dam. These parameters were further mapped using geospatial tools to provide an overview of their surface distribution in the dam.

3.4.1. In-situ chl-a and TSS

The concentration of chl-a differed greatly between the wet and dry season, with higher concentrations and a wider variation in the wet season (0.6 µg/ℓ to 29 µg/ℓ) compared to the dry season (0.6 µg/ℓ to 5.7 µg/ℓ) (Figure 3.3). This could possibly be due to the higher temperatures and increased precipitation received during the wet season, which contributed to increased chl-a development (Matthews and Bernard, 2015; Ngetar, 2002; Namugize, Jewitt and Graham, 2018). The high concentration of chl-a at the dam inlet during the wet season could be attributed to pollution entering the dam due to upper catchment anthropogenic activities, the prevailing upstream wind direction which keeps phosphorus trapped upstream, and the meandering nature of the dam, which all contribute to the algal formation upstream (Graham, 2007; Simpson and Pillay, 2000). The likelihood of these factors contributing to higher upstream chl-a concentration offers an opportunity for further research to accurately determine their role in chl-a distribution in the Dam.

TSS concentrations also displayed a seasonal variation, where higher TSS concentrations were found in the dry season (17.7 mg/ℓ to 18 mg/ℓ) and lower concentrations in the wet season (4 mg/ℓ to 10 mg/ℓ) (Figure 3.4). Apparently, there is no existing study on TSS seasonal differences in the Inanda

Dam; however, an international study conducted by Sharaf El Din (2020) found high TSS concentrations during the wet season, but Ngabirano et al. (2016) found higher TSS concentrations during the dry season. Factors such as climate, pollution, pH changes and temperature changes may play a role in TSS concentrations (Sharaf El Din, 2020). This apparent disagreement among authors provides a gap for more research to determine the cause of seasonal variations of TSS in water bodies.

3.4.2. Band correlations with in-situ chl-a

Chl-a influences the blue, green, red and NIR regions of the EMS, with absorption occurring between 450 nm to 475 nm (blue), at 670 nm (red) and reflectance at 500 nm (green) and 700 nm (NIR) (Gholizadeh, Melesse and Reddi, 2016; Markogianni et al., 2018). However, in inland water bodies, the absorption by CDOM and scattering by TSS can affect chl-a spectral signatures, hence NIR-Red band ratios are often used (Molkov et al., 2019). B5, B7 and B8a of Sentinel 2, which comprises the red edge of the EMS, has been found useful in chl-a retrieval regardless of high levels of TSS and CDOM (Ha et al., 2017; Yadav et al., 2019). Matthews (2011) also found that many studies utilize the 700:670 nm ratio for chl-a retrieval, and based on this information it can be inferred that Landsat 8 B2, B3, B4, B5 and Sentinel 2 B2, B3, B4, B5, B6, B7, B8 and B8a can be used to estimate chl-a.

3.4.2.1. Landsat 8

Landsat 8 B1 to B5, single band or band ratios produced strong correlations with in-situ chl-a, for example B4:B2 radiance (R = 0.932) and B4:B1 reflectance (R = 0.917). These results corroborate studies conducted by Fadel, Faour and Slim (2016), Laili et al. (2015), Lim and Choi (2015), Watanabe et al. (2015), Al-Fahdawi, Rabee and Al-Hirmizy (2015), Patra et al. (2017), Prasad, Saluja and Garg (2020), Malahlela et al. (2018) and Elangovan and Murali (2020), who also found that chl-a can be retrieved from Landsat 8 visible and NIR bands (B1 – B5). Overall, stronger correlations were obtained between in-situ chl-a and Landsat 8 radiance compared to in-situ chl-a and Landsat 8 reflectance (Table 3.1), however further studies are needed to explore this reasoning.

3.4.2.2. Sentinel 2

Sentinel 2 B1 to B5 displayed the strongest correlations with in-situ chl-a, corroborating studies by Ha et al. (2017), Toming et al. (2016), Grendaitė et al. (2018), Molkov et al. (2019), Pirasteh et al. (2020), Sòria-Perpinyà et al. (2021) and Bande et al. (2018), however the results of this present study also indicate that B10 is sensitive to chl-a. The most successful correlations were B3 TOA reflectance (0.910) and B1 BOA (0.903) with in-situ chl-a, but in general, TOA reflectance produced stronger correlations than BOA reflectance overall, corroborating studies by Toming et al. (2016) and Grendaitė et al. (2018). The most successful band correlations in this study, however, differ from studies conducted elsewhere (Ansper and Alikas, 2019 and Chen et al., 2017b), which found that a B8:B4 ratio accurately estimated chl-a. Similarly, Ouma, Noor and Herbert (2020) used B3 and B11 and Buma and Lee (2020) found that a combination of B5 to B7 were also capable of chl-a retrieval. The variations apparent in these studies suggests the need for more studies to determine why these variations occur and which possible bands/band combinations under what conditions can best retrieve chl-a.

3.4.3. Band correlations with in-situ TSS

Research suggests that regions between 700 nm and 800 nm are most useful in estimating TSS remotely due to the reflectance peak found near 700 nm (Matthews, 2011; Ritchie, Zimba and Everitt, 2003), and the red and NIR regions of the EMS (Matthews, 2011; Liu et al., 2017). The red and NIR regions are Landsat 8 B4 and B5, and Sentinel 2 B4 and B8, respectively. Some studies have used these bands either individually, in combination with each other, or in combination with the visible, NIR and SWIR bands to retrieve TSS (Sharaf El Din, 2020; Lim and Choi, 2015; Ouma, Noor and Herbert, 2020; Deutsch, Alameddine and El-Fadel, 2014; Laili et al.,2015; Kurniadin and Jaelani, 2016; Molkov et al., 2019; Ciancia et al., 2020; Mushtaq and Nee Lala, 2017; El Din and Zhang, 2017; Yepez et al., 2018; Zhu et al., 2020; Wang et al., 2021; Wu et al., 2015).

3.4.3.1. Landsat 8

The results of this present study indicate that Landsat 8 B4 and B5 correlate well with in-situ TSS, however Landsat 8 B1 produced the best correlation overall, for both radiance (R = 0.977) and reflectance data (R = 0.983). These results, while different from the studies mentioned in the previous paragraph, corroborate Zhang et al. (2016), Sharaf El Din (2020) and El Din and Zhang (2017), who found that using Landsat 8 B1 as part of a band combination for TSS retrieval yielded the best TSS estimation results.

3.4.3.2. Sentinel 2

In relation to Sentinel 2, there were fewer positive correlations between Sentinel 2 bands and in-situ TSS, compared to correlations with in-situ chl-a. The most successful correlations were B1:B3 TOA reflectance (R = 0.889) and B1 BOA reflectance (R = 0.950) with in-situ TSS, different from previous studies which used the red and NIR bands to retrieve TSS (Ouma, Noor and Herbert, 2020; Molkov et al., 2019; Ciancia et al., 2020). However, B4 (red band) yielded significant correlations with in-situ TSS, either individually or as part of a band ratio (Table 3.2). Overall, in-situ TSS produced diverse relationships with bands/band ratios across the visible, NIR, and SWIR bands of Sentinel 2, as did most studies conducted on TSS retrieval from Sentinel 2 imagery (Sòria-Perpinyà et al., 2021; Liu et al., 2017; Wang et al., 2021), highlighting the need for more studies to be conducted in this field of research.

3.4.4. Algorithm development and mapping of chl-a and TSS

The algorithms developed for this study retrieved chl-a and TSS (R^2 > 0.8) and, after validation, produced R-values greater than 0.9; however, the SE values were slightly higher for chl-a than for TSS algorithms, indicating possible overestimation and underestimation of chl-a. Nonetheless, empirical methods are reliable for retrieving chl-a and TSS remotely from Landsat 8 and Sentinel 2, albeit with slight differences. In this present study, Landsat 8 algorithms slightly outperformed Sentinel 2 algorithms, obtaining slightly higher R^2-values and lower SE values, however both Landsat 8 and Sentinel 2 estimated and mapped the overall chl-a and TSS distribution in Inanda Dam. These results corroborate Ouma, Noor and Herbert (2020) who also found that Landsat 8 outperformed Sentinel 2 in TSS estimation but differ from those of Yadav et al. (2019), Buma and Lee (2020), Watanabe et al. (2017) and Bande et al. (2018) who found that Sentinel 2 outperforms Landsat in chl-a and TSS retrieval. These differences necessitate more comparative research on the retrieval of chl-a and TSS from Landsat 8 and Sentinel 2 imagery.

3.5. Conclusion

This study used Landsat 8 and Sentinel 2 imagery as a proxy to monitor chl-a and TSS in the Inanda Dam, South Africa. Linear regression algorithms were developed and validated to retrieve and map the spatial and surface distributions of chl-a and TSS in the Inanda Dam. Landsat 8 radiance and reflectance, and Sentinel 2 TOA and BOA reflectance values were correlated with in-situ chl-a and TSS to determine which bands/band ratio could best retrieve the above-mentioned parameters. Results showed Landsat 8 B4:B2 radiance (R = 0.932) and B4:B1 reflectance (R = 0.917), Sentinel 2 B3 TOA reflectance (R = 0.910) and B1 BOA reflectance (R = 0.903) most successfully correlated with in-situ chl-a. Landsat 8 B1 radiance (R = 0.977) and reflectance (R = 0.983), Sentinel 2 B1:B3 TOA reflectance (R = 0.889) and B1 BOA reflectance (R = 0.950) correlated the best with in-situ TSS. Although both Landsat 8 and Sentinel 2 could retrieve chl-a and TSS with R^2-values greater than 0.79, Landsat 8 algorithms performed slightly better than Sentinel 2 algorithms. Comparison of this present and past studies revealed both similarities and differences in bands/band ratios used to develop algorithms to retrieve chl-a and TSS from Landsat 8 and Sentinel 2 imagery, however most studies were successful with the visible and NIR bands. The apparent disagreements among authors, as revealed in this study motivate for further research on specific bands, or band combinations to develop empirical algorithms for monitoring chl-a and TSS globally using Landsat 8 and Sentinel 2 imagery.

CHAPTER 4

SYNTHESIS AND RECCOMENDATIONS

4.1. Introduction

Freshwater is a resource essential to the survival of all life and provides many services and functions, however anthropogenic factors have had negative impacts on the status of these water bodies. The need to monitor inland water bodies in a timeous and cost-effective manner is now imperative, particularly in South Africa, which is a water-scarce country. The Inanda Dam, which is situated in the Valley of a Thousand Hills in Kwa-Zulu Natal, is an important source of drinking water for the surrounding areas. Inland water bodies are monitored using in-situ point sampling which is an accurate but time-consuming, labour intensive and expensive endeavour. Advances in remote sensing technology and the free availability of satellite imagery have made it possible to frequently and inexpensively monitor water bodies remotely. Therefore, this study was aimed at monitoring chl-a and TSS in the Inanda Dam using algorithms developed from Landsat 8 and Sentinel 2 data. The objectives of this study were:

1. To develop algorithms for monitoring chl-a in the Inanda Dam using Landsat 8 and Sentinel 2 and produce maps showing the surface distribution of chl-a in the Inanda Dam.

2. To develop algorithms for monitoring TSS in the Inanda Dam using Landsat 8 and Sentinel 2 and produce maps showing the surface distribution of TSS in the Inanda Dam.

The summary of findings in relation to these four objectives are discussed in the sections that follow.

4.2. Objective 1: To develop algorithms for monitoring chl-a in the Inanda Dam using Landsat 8 and Sentinel 2 and produce maps showing the surface distribution of chl-a in the Inanda Dam.

Chl-a is a commonly monitored water quality parameter as it can inform managers and scientists on the status of an inland water body. Chl-a can be used to determine the trophic status of a water body and the possibility of eutrophication and algal blooms, which negatively affect water quality. The ability of chl-a to influence the spectral signature of water also makes it a viable parameter to retrieve using remote methods. In Chapter 2, a literature review was conducted to determine which band/band ratios and algorithms were capable of chl-a retrieval. The review revealed that bands in the visible and NIR regions of the EMS can estimate chl-a and most studies utilized empirical methods for chl-a retrieval. Consequently, in Chapter 3, this study made use of Landsat 8 and Sentinel 2 bands found in the visible and NIR regions of the EMS, as well as SWIR bands to develop empirical algorithms to retrieve chl-a. The results indicated that both Landsat 8 and Sentinel 2 can be used to estimate chl-a, with Landsat 8 algorithms slightly outperforming Sentinel 2 algorithms with higher R^2 and lower SE values. Also, the visible bands correlated most successfully with chl-a, as corroborated by many previous studies, however some bands and band combinations, particularly for Sentinel 2, that retrieved chl-a in this study, differ from studies conducted elsewhere, highlighting the need for further studies to be conducted.

In-situ sampling and analysis of water quality parameters, while accurate, are unable to provide an overview of the concentrations and distributions of a water quality parameter over a water body. With the algorithms developed in Chapter 3 for chl-a retrieval, maps displaying the surface distribution of chl-a over the Inanda Dam could be created. The results suggest the Landsat 8 B4:B2 radiance algorithm was most accurate in mapping chl-a concentrations, and the Landsat 8 B4:B1 reflectance algorithm had difficulty estimating the high and low chl-a concentrations. The Sentinel 2 B3 TOA reflectance algorithm overestimated chl-a concentrations and the Sentinel 2 B1 BOA reflectance algorithm could estimate lower chl-a concentrations but not higher chl-a concentrations.

4.3. Objective 2: To develop algorithms to monitor TSS in the Inanda Dam using Landsat 8 and Sentinel 2 and produce maps showing the surface distribution of TSS in the Inanda Dam.

Another important water quality parameter is TSS, which includes organic and inorganic substances from varying sources. TSS is often representative of the pollutants entering a water body, and a surplus of TSS can cause algal blooms, affect dissolved oxygen levels, and increase turbidity and siltation, which can harm the quality of dams. Much like chl-a, TSS can influence the spectral signature of water which makes it a suitable parameter to retrieve using remote sensing. The literature review conducted in Chapter 2 suggested that bands positioned near 700 and 800 nm, and NIR and red bands are capable of estimating TSS, however all the bands in the visible, NIR and SWIR regions of the EMS were tested in the retrieval of TSS. The results reveal that both Landsat 8 and Sentinel 2 can be used to estimate TSS, with Landsat 8 algorithms performing better than Sentinel 2 algorithms. The results also suggest that the NIR and red bands of Landsat 8 can be used to retrieve TSS, however the most successful correlation was with B1. In relation to Sentinel 2, the red band was capable of TSS estimation, however the most successful correlations were with B1 and B3. Many studies which sought to retrieve TSS from Landsat 8 and Sentinel 2 have obtained varying results with band sensitivity to TSS, demonstrating the need for more studies to be conducted in TSS retrieval using Landsat 8 and Sentinel 2.

As mentioned in 4.2, in-situ sampling can only determine the concentration of a water quality parameter at a specific point, hence the algorithms developed to estimate TSS were applied to Landsat 8 and Sentinel 2 imagery to produce a surface distribution map of TSS for the Inanda Dam. The Landsat 8 B1 reflectance algorithm could estimate upper TSS concentrations but struggled to retrieve lower TSS concentrations, while Sentinel 2 B1:B3 TOA reflectance and B1 BOA reflectance algorithm overestimated the lower limits of TSS concentrations, however the Landsat 8 B1 radiance algorithm estimated TSS concentrations over the dam with high accuracy.

4.4. Limitations

This study successfully achieved the aim and objectives laid out in Chapter 1, however this study is not without limitations. A major limitation when working with satellite data is cloud cover. Satellite imagery acquired on a cloudy day renders the image unusable as features on the Earth's surface cannot be seen. Another limitation is that the empirical algorithms developed in this study are site and time specific and cannot be used to retrieve chl-a and TSS from other water bodies in South Africa or globally. The algorithms are also not capable of estimating chl-a and TSS concentrations in the event of a major change to the system such as an oil spill or flooding. The algorithms developed in this study were calibrated with data collected during the wet and dry seasons in Kwa-Zulu Natal, and data collected more frequently throughout the year would have allowed for the development of more robust algorithms capable of estimating a larger range of chl-a and TSS concentrations. However, monetary limitations, time constraints, restricted capacity, and Covid-19 regulations did not allow for continual sample collection. There are also many water quality parameters such as CDOM, SDD, turbidity, etc that are routinely monitored which provide a holistic overview of the quality of a water body, however only chl-a and TSS were considered in this study due to budget and time constraints.

4.5. Recommendations and directions for future research

4.5.1. Recommendations

1. More research must be conducted on the use of remote sensing in water quality monitoring to improve the accuracy and reliability of these methods, and to allow for more integration of remotely sensed water quality monitoring in the overall monitoring of water quality in South Africa. Many water boards are situated throughout the country and resources should be invested in the remote and continuous monitoring of water resources, as water is a vital and scarce resource in South Africa.

2. There is a need to investigate the utilization of other sources of satellite imagery such as SPOT 6, SPOT 7, Sentinel 3 and Landsat 9 for monitoring water quality parameters, and efforts should be made to investigate the remote monitoring of parameters other than chl-a and TSS.
3. More funding should be provided in the field of water research using remote sensing applications considering the growing advancements in the field of remote sensing and algorithm development, and the importance of sustaining the current water resources available in South Africa.

4.5.2. Directions for future research

1. More water quality parameters, both optically active and optically inactive, should be researched to determine which band/band combinations are sensitive for their retrieval from satellite imagery.
2. Future research should attempt to develop algorithms that can be used nationwide or globally for various water quality parameters, independent of location or season.
3. The many advancements in technology have led to machine and deep learning becoming a promising field of study, and some studies have made use of machine learning algorithms to retrieve water quality parameters. However, there is still a need for more research in the use of machine and deep learning methods in estimating water quality parameters from satellite imagery.
4. One of the major challenges of monitoring water quality using remote sensing is the acquisition of satellite imagery without cloud cover. Recent technological advancements in unmanned aerial vehicles (UAV's) may be able to circumvent this issue by obtaining imagery that is unaffected by clouds and can therefore be used in the monitoring of water quality.

References

Agunbiade, F.O. and Moodley, B. 2014. Pharmaceuticals as emerging organic contaminants in Umgeni River water system, KwaZulu-Natal, South Africa. *Environmental Monitoring and Assessment*, *186*(11), pp.7273-7291.

Al-Fahdawi, A.A., Rabee, A.M. and Al-Hirmizy, S.M., 2015. Water quality monitoring of Al-Habbaniyah Lake using remote sensing and in situ measurements. *Environmental Monitoring and Assessment*, *187*(6), pp.1-11.

Alawadi, F., 2010. Detection of surface algal blooms using the newly developed algorithm surface algal bloom index (SABI). *Proceedings of the International Society for Optics and Photonics* 7825:1–14.

Alcântara, E., Bernardo, N., Watanabe, F., Rodrigues, T., Rotta, L., Carmo, A., Shimabukuro, M., Gonçalves, S. and Imai, N., 2016. Estimating the CDOM absorption coefficient in tropical inland waters using OLI/Landsat-8 images. *Remote Sensing Letters*, *7*(7), pp.661-670.

Al-Kharusi, E.S., Tenenbaum, D.E., Abdi, A.M., Kutser, T., Karlsson, J., Bergström, A.K. and Berggren, M., 2020. Large-scale retrieval of coloured dissolved organic matter in northern lakes using Sentinel-2 data. *Remote Sensing*, *12*(1), p.157.

Ansari, M. and Akhoondzadeh, M., 2020. Mapping water salinity using Landsat-8 OLI satellite images (Case study: Karun basin located in Iran). *Advances in Space Research*, *65*(5), pp.1490-1502.

Ansper, A. and Alikas, K., 2018. Retrieval of chlorophyll a from Sentinel-2 MSI data for the European Union water framework directive reporting purposes. *Remote Sensing*, *11*(1), p.64.

Aptoula, E. and Ariman, S., 2021. Chlorophyll-a retrieval from sentinel-2 images using convolutional neural network regression. *IEEE Geoscience and Remote Sensing Letters*, *19*, pp.1-5.

Bande, P., Adam, E., Elbasit, M.A.A. and Adelabu, S., 2018, July. Comparing landsat 8 and sentinel-2 in mapping water quality at vaal dam. In *Proceedings of the International Geoscience and Remote Sensing Symposium (IGARSS), Valencia, Spain* (pp. 22-27).

Bayati, M. and Danesh-Yazdi, M., 2021. Mapping the spatiotemporal variability of salinity in the hypersaline Lake Urmia using Sentinel-2 and Landsat-8 imagery. *Journal of Hydrology*, *595*, p.126032.

Beck, R., S. Zhan, H. Liu, S. Tong, B. Yang, M. Xu, Z. Ye, et al. 2016. Comparison of Satellite Reflectance Algorithms for Estimating Chlorophyll-A in a Temperate Reservoir Using Coincident Hyperspectral Aircraft Imagery and Dense Coincident Surface Observations. *Remote Sensing of Environment*, *178*, pp.15–30.

Bonansea, M., Ledesma, M., Rodriguez, C. and Pinotti, L., 2019a. Using new remote sensing satellites for assessing water quality in a reservoir. *Hydrological Sciences Journal*, *64*(1), pp.34-44.

Bonansea, M., Ledesma, M., Bazán, R., Ferral, A., German, A., O'Mill, P., Rodriguez, C. and Pinotti, L., 2019b. Evaluating the feasibility of using Sentinel-2 imagery for water clarity assessment in a reservoir. *Journal of South American Earth Sciences*, *95*, p.102265.

Boucher, J., Weathers, K.C., Norouzi, H. and Steele, B., 2018. Assessing the effectiveness of Landsat 8 chlorophyll a retrieval algorithms for regional freshwater monitoring. *Ecological Applications*, *28*(4), pp.1044-1054.

Bresciani, M., Cazzaniga, I., Austoni, M., Sforzi, T., Buzzi, F., Morabito, G. and Giardino, C., 2018. Mapping phytoplankton blooms in deep subalpine lakes from Sentinel-2A and Landsat-8. *Hydrobiologia*, *824*(1), pp.197-214.

Brivio, P. A., Giardino, C. and Zilioli E., 2001. Determination of chlorophyll concentration changes in Lake Garda using an image-based radiative transfer code for Landsat TM images. *International Journal of Remote Sensing*, *22*, pp.487–502.

Buma, W.G. and Lee, S.I., 2020. Evaluation of sentinel-2 and landsat 8 images for estimating chlorophyll-a concentrations in lake Chad, Africa. *Remote Sensing*, *12*(15), p.2437.

Cairo, C., Barbosa, C., Lobo, F., Novo, E., Carlos, F., Maciel, D., Flores Júnior, R., Silva, E. and Curtarelli, V., 2020. Hybrid chlorophyll-a algorithm for assessing trophic states of a tropical brazilian reservoir based on msi/sentinel-2 data. *Remote Sensing*, *12*(1), p.40.

Chen, J., Zhu, W., Tian, Y.Q. and Yu, Q., 2020a. Monitoring dissolved organic carbon by combining Landsat-8 and Sentinel-2 satellites: Case study in Saginaw River estuary, Lake Huron. *Science of the Total Environment*, *718*, p.137374.

Chen, Q., Huang, M., Bai, K. and Li, X., 2020b. An Optimal Two Bands Ratio Model to Monitor Chlorophyll-a in Urban Lake Using Landsat 8 Data. In *E3S Web of Conferences* (Vol. 143, p. 02003). EDP Sciences.

Chen, J., Zhu, W., Pang, S. and Cheng, Q., 2019. Applicability evaluation of Landsat-8 for estimating low concentration colored dissolved organic matter in inland water. *Geocarto International*, *37*(1), pp.1-15.

Chen, J., Zhu, W.N., Tian, Y.Q. and Yu, Q., 2017a. Estimation of colored dissolved organic matter from Landsat-8 imagery for complex inland water: case study of Lake Huron. *IEEE Transactions on Geoscience and Remote Sensing*, *55*(4), pp.2201-2212.

Chen, J., Zhu, W., Tian, Y.Q., Yu, Q., Zheng, Y. and Huang, L., 2017b. Remote estimation of colored dissolved organic matter and chlorophyll-a in Lake Huron using Sentinel-2 measurements. *Journal of Applied Remote Sensing*, *11*(3), p.036007.

Ciancia, E., Campanelli, A., Lacava, T., Palombo, A., Pascucci, S., Pergola, N., Pignatti, S., Satriano, V. and Tramutoli, V., 2020. Modeling and multi-temporal characterization of total suspended matter by the combined use of Sentinel 2-MSI and Landsat 8-OLI data: The Pertusillo Lake case study (Italy). *Remote Sensing*, *12*(13), p.2147.

Concha, J.A. and Schott, J.R., 2016. Retrieval of color producing agents in Case 2 waters using Landsat 8. *Remote sensing of Environment*, *185*, pp.95-107.

Dall'Olmo, G. and Gitelson, A.A., 2006. Effect of bio-optical parameter variability and uncertainties in reflectance measurements on the remote estimation of chlorophyll-a concentration in turbid productive waters: modeling results. *Applied Optics*, *45*, pp.3577–3592.

Dall'Olmo, G., Gitelson, A.A. and Rundquist, D.C., 2003. "Towards a Unified Approach for Remote Estimation of Chlorophyll-A in Both Terrestrial and Vegetation and Turbid Productive Waters." Geophysical Research Letters 30: 1038.

Deutsch, E.S., Cardille, J.A., Koll-Egyed, T. and Fortin, M.J., 2021. Landsat 8 lake water clarity empirical algorithms: large-scale calibration and validation using government and citizen science data from across Canada. *Remote Sensing*, *13*(7), p.1257.

Deutsch, E., Alameddine, I. and El-Fadel, M., 2014. Developing Landsat Based Algorithms to Augment in Situ Monitoring of Freshwater Lakes and Reservoirs. In *International Conference on Hydroinformatics.*

Dörnhöfer, K., Göritz, A., Gege, P., Pflug, B. and Oppelt, N., 2016. Water constituents and water depth retrieval from Sentinel-2A—A first evaluation in an oligotrophic lake. *Remote Sensing*, *8*(11), p.941.

Drusch, M., Del Bello, U., Carlier, S., Colin, O., Fernandez, V., Gascon, F., Hoersch, B., Isola, C., Laberinti, P., Martimort, P. and Meygret, A., 2012. Sentinel-2: ESA's optical high-resolution mission for GMES operational services. *Remote Sensing of Environment*, *120*, pp.25-36.

El Din, E.S. and Zhang, Y., 2017. Statistical estimation of the Saint John River surface water quality using Landsat-8 multi-spectral data. In *ASPRS Annual Conf. Proc. of Imaging and Geospatial Technology Forum (IGTF)*, Marriot Waterfront Baltimore, Maryland, United States of America.

El-Zeiny, A. and El-Kafrawy, S., 2017. Assessment of water pollution induced by human activities in Burullus Lake using Landsat 8 operational land imager and GIS. *The Egyptian Journal of Remote Sensing and Space Science*, *20*, pp.S49-S56.

Elangovan, A. and Murali, V., 2020. Mapping the chlorophyll-a concentrations in hypereutrophic Krishnagiri Reservoir (India) using Landsat 8 Operational Land Imager. *Lakes & Reservoirs: Research & Management*, *25*(4), pp.377-387.

Fadel, A., Faour, G. and Slim, K., 2016. Assessment of the trophic state and chlorophyll-a concentrations using Landsat OLI in Karaoun reservoir, Lebanon. *Lebanese Science Journal*, *17*(2), pp.130-145.

Fischer, F., Hamdan, Y., Hansson, A., Josefsson, E. and Sundström, L. 2019. Water quality modelling and quantitative microbial risk assessment of Msunduzi river. Bachelor's thesis. Department of Architecture and Civil Engineering, Chalmers University of Technology

Gerace, A.D., Schott, J.R. and Nevins, R., 2013. Increased potential to monitor water quality in the near-shore environment with Landsat's next-generation satellite. *Journal of Applied Remote Sensing*, *7*(1), p.073558.

Gholizadeh, M.H., Melesse, A.M. and Reddi, L., 2016. A comprehensive review on water quality parameters estimation using remote sensing techniques. *Sensors*, *16*(8), p.1298.

Giardino, C., Bresciani, M., Cazzaniga, I., Schenk, K., Rieger, P., Braga, F., Matta, E. and Brando, V.E., 2014. Evaluation of multi-resolution satellite sensors for assessing water quality and bottom depth of Lake Garda. *Sensors*, *14*(12), pp.24116-24131.

Gitelson, A.A., Gao, B.C., Li, R.R., Berdnikov, S. and Saprygin, V., 2011. Estimation of chlorophyll-a concentration in productive turbid waters using a Hyperspectral Imager for the Coastal Ocean—the Azov Sea case study. *Environmental Research Letters*, *6*(2), p.024023.

González-Márquez, L.C., Torres-Bejarano, F.M., Torregroza-Espinosa, A.C., Hansen-Rodríguez, I.R. and Rodríguez-Gallegos, H.B., 2018. Use of LANDSAT 8 images for depth and water quality assessment of El Guájaro reservoir, Colombia. *Journal of South American Earth Sciences*, *82*, pp.231-238.

Gordon, H. R., and Morel, A., 1983. Remote Assessment of Ocean Color for Interpretation of Satellite Visible Imagery: A Review. New York, NY: Springer-Verlag.

Graham, P.M., 2007. *Modelling the water quality in dams within the Umgeni Water operational area with emphasis on algal relations* (Doctoral dissertation, North-West University).

Grendaitė, D., Stonevičius, E., Karosienė, J., Savadova, K. and Kasperovičienė, J., 2018. Chlorophyll-a concentration retrieval in eutrophic lakes in Lithuania from Sentinel-2 data. *Geologija. Geografija*, *4*(1), pp. 15-28

Guo, H., Huang, J.J., Chen, B., Guo, X. and Singh, V.P., 2021. A machine learning-based strategy for estimating non-optically active water quality parameters using Sentinel-2 imagery. *International Journal of Remote Sensing*, *42*(5), pp.1841-1866.

Gurlin, D., Gitelson, A.A. and Moses, W.J., 2011. Remote estimation of chl-a concentration in turbid productive waters—Return to a simple two-band NIR-red model?. *Remote Sensing of Environment*, *115*(12), pp.3479-3490.

Ha, N.T.T., Thao, N.T.P., Koike, K. and Nhuan, M.T., 2017. Selecting the best band ratio to estimate chlorophyll-a concentration in a tropical freshwater lake using sentinel 2A images from a case study of Lake Ba Be (Northern Vietnam). *ISPRS International Journal of Geo-Information*, *6*(9), p.290.

Hart, R.C., 2011. Zooplankton biomass to chlorophyll ratios in relation to trophic status within and between ten South African reservoirs: Causal inferences, and implications for biomanipulation. *Water SA*, *37*(4), pp.513-522.

He, Y., Jin, S. and Shang, W., 2021. Water quality variability and related factors along the Yangtze River using Landsat-8. *Remote Sensing*, *13*(12), p.2241.

Hu, M., Ma, R., Cao, Z., Xiong, J. and Xue, K., 2021. Remote estimation of trophic state index for inland waters using Landsat-8 OLI imagery. *Remote Sensing*, *13*(10), p.1988.

Huangfu, K., Li, J., Zhang, X., Zhang, J., Cui, H. and Sun, Q., 2020. Remote estimation of water quality parameters of medium-and small-sized inland rivers using Sentinel-2 imagery. *Water*, *12*(11), p.3124.

Humboldt State University. nd. Available Online: http://gsp.humboldt.edu/olm_2015/Courses/GSP_216_Online/lesson4-1/radiometric.html [Accessed 05 May 2019].

Hunter, P., Tyler, A., Willby, N. and Gilvear, D., 2008. The spatial dynamics of vertical migration by Microcystis aeruginosa in a eutrophic shallow lake: A case study using high spatial resolution time-series airborne remote sensing. *Limnology and Oceanography*. 53(6): 2391–2406.

Jaiyeola, A.T., 2016. Estimation of suspended sediment yield flowing into Inanda Dam using genetic programming. Master of Engineering Thesis: Durban University of Technology.

Jiao, H., Zha, Y., Gao, J., Li, Y., Wei, Y. and Huang J., 2006. Estimation of chlorophyll-a concentration in Lake Tai, China using in situ hyperspectral data. *International Journal of Remote Sensing.* 27(19): 4267–4276.

Kabbara, N., Benkhelil, J., Awad, M. and Barale, V., 2008. Monitoring water quality in the coastal area of Tripoli (Lebanon) using high-resolution satellite data. *ISPRS Journal of Photogrammetry and Remote Sensing, 63,* pp.488–495.

Karaoui, I., Arioua, A., Boudhar, A., Hssaisoune, M., El Mouatassime, S., Ouhamchich, K.A., Elhamdouni, D., Idrissi, A.E.A. and Nouaim, W., 2019. Evaluating the potential of Sentinel-2 satellite images for water quality characterization of artificial reservoirs: The Bin El Ouidane Reservoir case study (Morocco). *Meteorology Hydrology and Water Management. Research and Operational Applications*, *7*(1), pp.31-39.

Keith, D., Rover, J., Green, J., Zalewsky, B., Charpentier, M., Thursby, G. and Bishop, J., 2018. Monitoring algal blooms in drinking water reservoirs using the Landsat-8 Operational Land Imager. *International Journal of Remote Sensing*, *39*(9), pp.2818-2846.

Kim, H.H., Ko, B.C. and Nam, J.Y., 2016. Predicting chlorophyll-a using Landsat 8 OLI sensor data and the non-linear RANSAC method–a case study of Nakdong River, South Korea. *International Journal of Remote Sensing*, *37*(14), pp.3255-3271.

Kontopoulou, E., Kolokoussis, P. and Karantzalos, K., 2017. Water quality estimation in Greek lakes from Landsat 8 multispectral satellite data. *European Water*, *58*, pp.191-196.

Kurniadin, N. and Jaelani, L.M., 2016. Empirical Algorithm Modeling for Estimating Total Suspended Solid Concentration Using In-situ Data and Atmospheric Corrected Landsat 8, Case Study: Gili Iyang â€ TM s Waters Empirical Algorithm Modeling for Estimating Total Suspended Solid Concentration Us. In *The 2nd Internasional Seminar on Science and Technology (ISST) for Sustainable Infrastructure Empowering Research and Technology for Sustainable Infrastructure* (pp. 379-380).

Kutser, T., Casal Pascual, G., Barbosa, C., Paavel, B., Ferreira, R., Carvalho, L. and Toming, K., 2016a. Mapping inland water carbon content with Landsat 8 data. *International Journal of Remote Sensing*, *37*(13), pp.2950-2961.

Kutser, T., Paavel, B., Verpoorter, C., Ligi, M., Soomets, T., Toming, K. and Casal, G., 2016b. Remote sensing of black lakes and using 810 nm reflectance peak for retrieving water quality parameters of optically complex waters. *Remote Sensing*, *8*(6), p.497.

Laili, N.L., Arafah, F., Jaelani, A. and Pamungkas, A.D., 2015. Development of water quality parameter retrieval algorithms for estimating total suspended solids and chlorophyll-A concentration using Landsat-8 imagery at Poteran island water. *Remote Sensing and Spatial Information Sciences*, *2*(2), pp.55-62

Lary, D.J., Alavi, A.H., Gandomi, A.H. and Walker, A.L., 2016. Machine learning in geosciences and remote sensing. *Geoscience Frontiers*, *7*(1), pp.3-10.

Larson, M.D., Simic Milas, A., Vincent, R.K. and Evans, J.E., 2021. Landsat 8 monitoring of multi-depth suspended sediment concentrations in Lake Erie's Maumee River using machine learning. *International Journal of Remote Sensing*, *42*(11), pp.4064-4086.

Ledesma, M.M., Bonansea, M., Ledesma, C.R., Rodríguez, C., Carreño, J. and Pinotti, L., 2019. Estimation of chlorophyll-a concentration using Landsat 8 in the Cassaffousth reservoir. *Water Supply*, *19*(7), pp.2021-2027.

Lee, Z., Shang, S., Qi, L., Yan, J. and Lin, G., 2016. A semi-analytical scheme to estimate Secchi-disk depth from Landsat-8 measurements. *Remote sensing of environment*, *177*, pp.101-106.

Lee, Z., Shang, S., Hu, C., Du, K., Weidemann, A., Hou, W., Lin, J., Lin, G., 2015. Secchi disk depth: a new theory and mechanistic model for underwater visibility. *Remote Sensing of Environment, 169*, pp.139–149.

Li, S., Song, K., Wang, S., Liu, G., Wen, Z., Shang, Y., Lyu, L., Chen, F., Xu, S., Tao, H. and Du, Y., 2021. Quantification of chlorophyll-a in typical lakes across China using Sentinel-2 MSI imagery with machine learning algorithm. *Science of the Total Environment*, *778*, p.146271.

Li, X., Ding, J. and Ilyas, N., 2021. Machine learning method for quick identification of water quality index (WQI) based on Sentinel-2 MSI data: Ebinur Lake case study. *Water Supply*, *21*(3), pp.1291-1312.

Li, Y., Zhang, Y., Shi, K., Zhou, Y., Zhang, Y., Liu, X. and Guo, Y., 2018. Spatiotemporal dynamics of chlorophyll-a in a large reservoir as derived from Landsat 8 OLI data: understanding its driving and restrictive factors. *Environmental Science and Pollution Research*, *25*(2), pp.1359-1374.

Li, Y., Zhang, Y., Shi, K., Zhu, G., Zhou, Y., Zhang, Y. and Guo, Y., 2017. Monitoring spatiotemporal variations in nutrients in a large drinking water reservoir and their relationships with hydrological and meteorological conditions based on Landsat 8 imagery. *Science of the Total Environment*, *599*, pp.1705-1717.

Lim, J. and Choi, M., 2015. Assessment of water quality based on Landsat 8 operational land imager associated with human activities in Korea. *Environmental Monitoring and Assessment*, *187*(6), pp.1-17.

Liu, L.W. and Wang, Y.M., 2019. Modelling reservoir turbidity using Landsat 8 satellite imagery by gene expression programming. *Water*, *11*(7), p.1479.

Liu, H., Li, Q., Shi, T., Hu, S., Wu, G. and Zhou, Q., 2017. Application of sentinel 2 MSI images to retrieve suspended particulate matter concentrations in Poyang Lake. *Remote Sensing*, *9*(7), p.761.

Loveland, T.R. and Irons, J.R., 2016. Landsat 8: The plans, the reality, and the legacy. *Remote Sensing of Environment*, *185*, pp.1-6.

Malahlela, O.E., Oliphant, T., Tsoeleng, L.T. and Mhangara, P., 2018. Mapping chlorophyll-a concentrations in a cyanobacteria-and algae-impacted Vaal Dam using Landsat 8 OLI data. *South African Journal of Science*, *114*(9-10), pp.1-9.

Mamun, M., Kim, J.Y. and An, K.G., 2021. Multivariate Statistical Analysis of Water Quality and Trophic State in an Artificial Dam Reservoir. *Water*, *13*(2), p.186.

Mansaray, A.S., Dzialowski, A.R., Martin, M.E., Wagner, K.L., Gholizadeh, H. and Stoodley, S.H., 2021. Comparing PlanetScope to Landsat-8 and Sentinel-2 for sensing water quality in reservoirs in agricultural watersheds. *Remote Sensing*, *13*(9), p.1847.

Manuel, A., Blanco, A.C., Tamondong, A.M., Jalbuena, R., Cabrera, O. and Gege, P., 2020. Optmization of bio-optical model parameters for turbid lake water quality estimation using Landsat 8 and wasi-2D. *The International Archives of Photogrammetry, Remote Sensing and Spatial Information Sciences*, *42*, pp.67-72.

Markogianni, V., Kalivas, D., Petropoulos, G.P. and Dimitriou, E., 2018. An appraisal of the potential of Landsat 8 in estimating chlorophyll-a, ammonium concentrations and other water quality indicators. *Remote Sensing*, *10*(7), p.1018.

Markogianni, V., Kalivas, D., Petropoulos, G. and Dimitriou, E., 2017. Analysis on the feasibility of Landsat 8 imagery for water quality parameters assessment in an oligotrophic Mediterranean Lake. *International Journal of Geological and Environmental Engineering*, *11*(9), pp.906-914.

Masocha, M., Mungenge, C. and Nhiwatiwa, T., 2018. Remote sensing of nutrients in a subtropical African reservoir: testing utility of Landsat 8. *Geocarto International*, *33*(5), pp.458-469.

Masocha, M., Dube, T., Nhiwatiwa, T. and Choruma, D., 2018. Testing utility of Landsat 8 for remote assessment of water quality in two subtropical African reservoirs with contrasting trophic states. *Geocarto international*, *33*(7), pp.667-680.

Matongo, S., Birungi, G., Moodley, B. and Ndungu, P., 2015. Occurrence of selected pharmaceuticals in water and sediment of Umgeni River, KwaZulu-Natal, South Africa. *Environmental Science and Pollution Research*, *22*(13), pp.10298-10308.

Matthews, M.W. and Bernard, S., 2015. Eutrophication and cyanobacteria in South Africa's standing water bodies: A view from space. *South African Journal of Science*, *111*(5), pp.1-8.

Matthews M. W., Bernard S., and Robertson L., 2012. An algorithm for detecting trophic status (chlorophyll-a), cyanobacterial-dominance, surface scums and floating vegetation in inland and coastal waters. *Remote Sensing of Environment*. 124: 637–652.

Matthews, M.W., 2011. A current review of empirical procedures of remote sensing in inland and near-coastal transitional waters. *International Journal of Remote Sensing*, *32*(21), pp.6855-6899.

Maxwell, A.E., Warner, T.A. and Fang, F., 2018. Implementation of machine-learning classification in remote sensing: An applied review. *International Journal of Remote Sensing*, *39*(9), pp.2784-2817.

Mishra, S. and Mishra, D.R., 2012. Normalized difference chlorophyll index: a novel model for remote estimation of chlorophyll-a concentration in turbid productive waters. *Remote Sensing of Environment, 117*, pp.394–406.

Mishra, D.R. and Mishra, S., 2010. Plume and bloom: effect of the Mississippi River diversion on the water quality of Lake Pontchartrain. *Geocarto international*, *25*(7), pp.555-568.

Molkov, A.A., Fedorov, S.V., Pelevin, V.V. and Korchemkina, E.N., 2019. Regional models for high-resolution retrieval of chlorophyll a and TSM concentrations in the Gorky Reservoir by Sentinel-2 imagery. *Remote Sensing*, *11*(10), p.1215.

Mushtaq, F. and Nee Lala, M.G., 2017. Remote estimation of water quality parameters of Himalayanlake (Kashmir) using Landsat 8 OLI imagery. *Geocarto international*, *32*(3), pp.274-285.

Namugize, J.N., Jewitt, G. and Graham, M., 2018. Effects of land use and land cover changes on water quality in the uMngeni river catchment, South Africa. *Physics and Chemistry of the Earth, Parts A/B/C*, *105*, pp.247-264.

Ngabirano, H., Byamugisha, D. and Ntambi, E., 2016. Effects of seasonal variations in physical parameters on quality of gravity flow water in Kyanamira Sub-County, Kabale District, Uganda. *Journal of Water Resource and Protection, 8*, pp.1297-1309

Ngetar, N.S., 2002. Post-dam sediment dynamics below the Inanda Dam at the Mgeni estuary, KwaZulu Natal (South Africa). Master of Science dissertation: University of Kwa-Zulu Natal.

Nkoana, M.A., 2014. Urban biodiversity management in the face of climate change: livelihood impacts and adaptation strategies in Inanda community of eThekwini Metropolitan Area, KwaZulu-Natal, South Africa. Master of Science dissertation: University of Kwa-Zulu Natal.

Olmanson, L.G., Page, B.P., Finlay, J.C., Brezonik, P.L., Bauer, M.E., Griffin, C.G. and Hozalski, R.M., 2020. Regional measurements and spatial/temporal analysis of CDOM in 10,000+ optically variable Minnesota lakes using Landsat 8 imagery. *Science of the Total Environment*, *724*, p.138141.

Olmanson, L.G., Brezonik, P.L., Finlay, J.C. and Bauer, M.E., 2016. Comparison of Landsat 8 and Landsat 7 for regional measurements of CDOM and water clarity in lakes. *Remote Sensing of Environment*, *185*, pp.119-128.

Ouma, Y.O., Noor, K. and Herbert, K., 2020. Modelling Reservoir Chlorophyll-a, TSS, and Turbidity Using Sentinel-2A MSI and Landsat-8 OLI Satellite Sensors with Empirical Multivariate Regression. *Journal of Sensors*, *2020*, pp.1-21.

Pahlevan, N., Smith, B., Schalles, J., Binding, C., Cao, Z., Ma, R., Alikas, K., Kangro, K., Gurlin, D., Hà, N. and Matsushita, B., Moses, W., Greb, S., Lehmann, M.K., Ondrusek, M., Oppelt, N. and Stumpf, R. 2020. Seamless retrievals of chlorophyll-a from Sentinel-2 (MSI) and Sentinel-3 (OLCI) in inland and coastal waters: A machine-learning approach. *Remote Sensing of Environment*, *240*, p.111604.

Pahlevan, N., Chittimalli, S.K., Balasubramanian, S.V. and Vellucci, V., 2019. Sentinel-2/Landsat-8 product consistency and implications for monitoring aquatic systems. *Remote sensing of Environment*, *220*, pp.19-29.

Palmer, S.C., Kutser, T. and Hunter, P.D., 2015. Remote sensing of inland waters: Challenges, progress and future directions. *Remote sensing of Environment*, *157*, pp.1-8.

Patra, P.P., Dubey, S.K., Trivedi, R.K., Sahu, S.K. and Rout, S.K., 2017. Estimation of chlorophyll-a concentration and trophic states in Nalban Lake of East Kolkata Wetland, India from Landsat 8 OLI data. *Spatial Information Research*, *25*(1), pp.75-87.

Peterson, K.T., Sagan, V. and Sloan, J.J., 2020. Deep learning-based water quality estimation and anomaly detection using Landsat-8/Sentinel-2 virtual constellation and cloud computing. *GIScience & Remote Sensing*, *57*(4), pp.510-525.

Peterson, K.T., Sagan, V., Sidike, P., Cox, A.L. and Martinez, M., 2018. Suspended sediment concentration estimation from landsat imagery along the lower missouri and middle Mississippi Rivers using an extreme learning machine. *Remote Sensing*, *10*(10), p.1503.

Pham, Q.V., Ha, N.T.T., Pahlevan, N., Oanh, L.T., Nguyen, T.B. and Nguyen, N.T., 2018. Using Landsat-8 images for quantifying suspended sediment concentration in Red River (Northern Vietnam). *Remote Sensing*, *10*(11), p.1841.

Pirasteh, S., Mollaee, S., Fatholahi, S.N. and Li, J., 2020. Estimation of phytoplankton chlorophyll-a concentrations in the Western Basin of Lake Erie using Sentinel-2 and Sentinel-3 data. *Canadian Journal of Remote Sensing*, *46*(5), pp.585-602.

Pizani, F.M., Maillard, P., Ferreira, A.F. and de Amorim, C.C., 2020. Estimation of water quality in a reservoir from Sentinel-2 MSI and Landsat-8 OLI sensors. *ISPRS Annals of Photogrammetry, Remote Sensing & Spatial Information Sciences*, *5*(3).

Prasad, S., Saluja, R. and Garg, J.K., 2020. Assessing the efficacy of Landsat-8 OLI imagery derived models for remotely estimating chlorophyll-a concentration in the Upper Ganga River, India. *International Journal of Remote Sensing*, *41*(7), pp.2439-2456.

Pu, F., Ding, C., Chao, Z., Yu, Y. and Xu, X., 2019. Water-quality classification of inland lakes using Landsat8 images by convolutional neural networks. *Remote Sensing*, *11*(14), p.1674.

Qi, C., Huang, S. and Wang, X., 2020. Monitoring water quality parameters of Taihu Lake based on remote sensing images and LSTM-RNN. *IEEE Access*, *8*, pp.188068-188081.

Quang, N.H., Sasaki, J., Higa, H. and Huan, N.H., 2017. Spatiotemporal variation of turbidity based on landsat 8 OLI in Cam Ranh Bay and Thuy Trieu Lagoon, Vietnam. *Water*, *9*(8), p.570.

Rangeti, I., 2014. Determinants of Key Drivers for Potable Water Treatment Cost in uMngeni Basin. Master of Technology Thesis. Environmental Health in the Faculty of Health Sciences, Durban University of Technology.

Ritchie, J.C., Zimba, P.V. and Everitt, J.H., 2003. Remote sensing techniques to assess water quality. *Photogrammetric Engineering & Remote Sensing*, *69*(6), pp.695-704.

Rodrigues, T., Alcântara, E., Watanabe, F. and Imai, N., 2017. Retrieval of Secchi disk depth from a reservoir using a semi-analytical scheme. *Remote Sensing of Environment*, *198*, pp.213-228.

Roy, D.P., Wulder, M.A., Loveland, T.R., Woodcock, C.E., Allen, R.G., Anderson, M.C., Helder, D., Irons, J.R., Johnson, D.M., Kennedy, R. and Scambos, T.A., 2014. Landsat-8: Science and product vision for terrestrial global change research. *Remote sensing of Environment*, *145*, pp.154-172.

Shang, Y., Liu, G., Wen, Z., Jacinthe, P.A., Song, K., Zhang, B., Lyu, L., Li, S., Wang, X. and Yu, X., 2021. Remote estimates of CDOM using Sentinel-2 remote sensing data in reservoirs with different trophic states across China. *Journal of Environmental Management*, *286*, p.112275.

Sharaf El Din, E., 2020. A novel approach for surface water quality modelling based on Landsat-8 tasselled cap transformation. *International Journal of Remote Sensing*, *41*(18), pp.7186-7201.

Sharaf El Din, E., Zhang, Y. and Suliman, A., 2017. Mapping concentrations of surface water quality parameters using a novel remote sensing and artificial intelligence framework. *International Journal of Remote Sensing*, *38*(4), pp.1023-1042.

Shen, X. and Feng, Q., 2018. Statistical model and estimation of inland riverine turbidity with Landsat 8 OLI images: A case study. *Environmental Engineering Science*, *35*(2), pp.132-140.

Shippert, P. 2013. Digital Number, Radiance and Reflectance. https://www.harrisgeospatial.com/Learn/Blogs/Blog-Details/ArtMID/10198/ArticleID/16278/Digital-Number-Radiance-and-Reflectance. [Accessed 13/07/2019].

Silveira Kupssinskü, L., Thomassim Guimarães, T., Menezes de Souza, E., C. Zanotta, D., Roberto Veronez, M., Gonzaga Jr, L. and Mauad, F.F., 2020. A method for chlorophyll-a and suspended solids prediction through remote sensing and machine learning. *Sensors*, *20*(7), p.2125.

Simpson, D. and Pillay, M., 2000. Quantifying externalities: Study of the impact of nutrient loading in the Msunduzi River on downstream users. In *WISA 2000 Biennial Conference, Sun City, South Africa* (pp. 2-4).

Soomets, T., Uudeberg, K., Jakovels, D., Brauns, A., Zagars, M. and Kutser, T., 2020. Validation and comparison of water quality products in baltic lakes using sentinel-2 msi and sentinel-3 OLCI data. *Sensors*, *20*(3), p.742.

Sòria-Perpinyà, X., Vicente, E., Urrego, P., Pereira-Sandoval, M., Tenjo, C., Ruíz-Verdú, A., Delegido, J., Soria, J.M., Peña, R. and Moreno, J., 2021. Validation of Water Quality Monitoring Algorithms for Sentinel-2 and Sentinel-3 in Mediterranean Inland Waters with In Situ Reflectance Data. *Water*, *13*(5), p.686.

Sòria-Perpinyà, X., Urrego, E.P., Pereira-Sandoval, M., Ruiz-Verdú, A., Soria, J.M., Delegido, J., Vicente, E. and Moreno, J., 2020. Monitoring water transparency of a hypertrophic lake (the Albufera of València) using multitemporal Sentinel-2 satellite images. *Limnetica*, *39*(1), pp.373-386.

Tinmouth, N., 2009. The Mgeni Estuary pre-and post Inanda Dam Estuarine dynamics. Master of Science dissertation: University of Kwa-Zulu Natal.

Toming, K., Kutser, T., Laas, A., Sepp, M., Paavel, B. and Nõges, T., 2016. First experiences in mapping lake water quality parameters with Sentinel-2 MSI imagery. *Remote Sensing*, *8*(8), p.640.

Turner, D. 2010. "Remote Sensing of Chlorophyll-A Concentrations to Support the Deschutes Basin Lake and Reservoir TMDLs." Report to the US Environmental Protection Agency for 104b3 2009 Grant, Component 4: 1–43.

Vanhellemont, Q. and Ruddick, K., 2016, May. Acolite for Sentinel-2: Aquatic applications of MSI imagery. In *Proceedings of the 2016 ESA Living Planet Symposium, Prague, Czech Republic* (pp. 9-13).

Vanhellemont, Q. and Ruddick, K., 2014. Landsat-8 as a precursor to Sentinel-2: Observations of human impacts in coastal waters. *ESA Special Publication*, *726*.

Vinh, P.Q., Ha, N.T.T., Binh, N.T., Thang, N.N., Oanh, L.T. and Thao, N.T.P., 2019. Developing algorithm for estimating chlorophyll-a concentration in the Thac Ba Reservoir surface water using Landsat 8 Imagery. *Vietnam Journal of Earth Sciences*, *41*, pp.10-20.

Wagle, N., Acharya, T.D. and Lee, D.H., 2019. Estimating Chlorophyll-a and Dissolved Oxygen Based on Landsat 8 Bands Using Support Vector Machine and Recursive Partitioning Tree Regressions. *Multidisciplinary Digital Publishing Institute Proceedings*, *42*(1), p.25.

Wang, H., Wang, J., Cui, Y. and Yan, S., 2021. Consistency of suspended particulate matter concentration in turbid water retrieved from Sentinel-2 MSI and Landsat-8 OLI sensors. *Sensors*, *21*(5), p.1662.

Wang, X.J. and Ma, T., 2001. Applications of remote sensing techniques in monitoring and assessing the water quality of Taihu Lake. *Bulletin of Environmental Contamination and Toxicology*. 67, pp.863–870.

Watanabe, F., Alcantara, E., Rodrigues, T., Rotta, L., Bernardo, N. and Imai, N., 2017. Remote sensing of the chlorophyll-a based on OLI/Landsat-8 and MSI/Sentinel-2A (Barra Bonita reservoir, Brazil). *Anais da Academia Brasileira de Ciências*, *90*, pp.1987-2000.

Watanabe, F.S.Y., Alcântara, E., Rodrigues, T.W.P., Imai, N.N., Barbosa, C.C.F. and Rotta, L.H.D.S., 2015. Estimation of chlorophyll-a concentration and the trophic state of the Barra Bonita hydroelectric reservoir using OLI/Landsat-8 images. *International Journal of Environmental Research and Public Health*, *12*(9), pp.10391-10417.

Wu, G., Cui, L., Liu, L., Chen, F., Fei, T. and Liu, Y., 2015. Statistical model development and estimation of suspended particulate matter concentrations with Landsat 8 OLI images of Dongting Lake, China. *International Journal of Remote Sensing*, *36*(1), pp.343-360.

Yadav, S., Yamashiki, Y., Susaki, J., Yamashita, Y. and Ishikawa, K., 2019. Chlorophyll estimation of lake water and coastal water using Landsat-8 and Sentinel-2A satellite. *International Archives of the Photogrammetry, Remote Sensing & Spatial Information Sciences*, *42*, pp.77-82

Yang, Z. and Anderson, Y., 2016. Estimating chlorophyll-A concentration in a freshwater lake using Landsat 8 imagery. *J. Environ. Earth Sci*, *6*(4), pp.134-142.

Yanti, A., Susilo, B. and Wicaksono, P., 2016, November. The aplication of Landsat 8 OLI for total suspended solid (TSS) mapping in Gajahmungkur reservoir Wonogiri regency 2016. In *IOP Conference Series: Earth and Environmental Science* (Vol. 47, No. 1, p. 012028). IOP Publishing.

Yepez, S., Laraque, A., Martinez, J.M., De Sa, J., Carrera, J.M., Castellanos, B., Gallay, M. and Lopez, J.L., 2018. Retrieval of suspended sediment concentrations using Landsat-8 OLI satellite images in the Orinoco River (Venezuela). *Comptes Rendus Geoscience*, *350*(1-2), pp.20-30.

Zhang, T., Huang, M. and Wang, Z., 2020. Estimation of chlorophyll-a Concentration of lakes based on SVM algorithm and Landsat 8 OLI images. *Environmental Science and Pollution Research*, *27*(13), pp.14977-14990.

Zhang, Y., Zhang, Y., Shi, K., Zha, Y., Zhou, Y. and Liu, M., 2016. A Landsat 8 OLI-based, semianalytical model for estimating the total suspended matter concentration in the slightly turbid Xin'anjiang Reservoir (China). *IEEE Journal of Selected Topics in Applied Earth Observations and Remote Sensing*, *9*(1), pp.398-413.

Zhu, W., Huang, L., Sun, N., Chen, J. and Pang, S., 2020. Landsat 8-observed water quality and its coupled environmental factors for urban scenery lakes: A case study of West Lake. *Water Environment Research*, *92*(2), pp.255-265.